INFORMATION TO USERS

This manuscript has been reproduced from the microfilm master. UMI films the text directly from the original or copy submitted. Thus, some thesis and dissertation copies are in typewriter face, while others may be from any type of computer printer.

The quality of this reproduction is dependent upon the quality of the copy submitted. Broken or indistinct print, colored or poor quality illustrations and photographs, print bleedthrough, substandard margins, and improper alignment can adversely affect reproduction.

In the unlikely event that the author did not send UMI a complete manuscript and there are missing pages, these will be noted. Also, if unauthorized copyright material had to be removed, a note will indicate the deletion.

Oversize materials (e.g., maps, drawings, charts) are reproduced by sectioning the original, beginning at the upper left-hand corner and continuing from left to right in equal sections with small overlaps.

ProQuest Information and Learning
300 North Zeeb Road, Ann Arbor, MI 48106-1346 USA
800-521-0600

UNIVERSITY OF CINCINNATI

June 12, 19 97

I, Susan E. Turbek,

hereby submit this as part of the requirements for the degree of:

Master of Science

in Geology

It is entitled

Topography-Dependent Glacial Deposition:

An Example from the Lake District of Chile

Approved by:

Glenn D. Caudle

John Grover

David Nash

TOPOGRAPHY-DEPENDENT GLACIAL DEPOSITION: AN EXAMPLE FROM THE LAKE DISTRICT OF CHILE

A thesis submitted to the

Division of Research and Advanced Studies
of the University of Cincinnati

in partial fulfillment of the
requirements for the degree of

MASTER OF SCIENCE

in the Department of Geology
of the College of Arts and Sciences

1997

by

Susan E. Turbek

A.B., Cornell University 1991

Committee Chair: Dr. Thomas V. Lowell

ProQuest Information and Learning Company
300 North Zeeb Road
P.O. Box 1346
Ann Arbor, MI 48106-1346

Abstract

There is a facies relationship between glacially-derived sediment deposits and structures and their topographic position, near the margin of temperate piedmont glaciers in the Southern Lake District, Chile, South America. Different glacial processes occurred on the slope from present water level to the moraine crest. Lower slope processes include glaciolacustrine sedimentation and large-scale thrusting. Middle slope processes include low-angle subglacial thrusting of thin, lacustrine-sediment slices. Upper slope processes include high-angle thrusting and deposition of lodgement and flow till.

Two different sets of glacial processes are represented by the sediments found in this region. One set of processes, varying over time as the glacier advances and retreats, occurs at the ice margin; this set explains the sections described on the lower slope. The second set of processes occurs in different topographic positions at the same time; this set explains the features described on the middle and upper slopes. Slope angle and porewater pressure may be involved in promoting subglacial thrusting. The topographic dependence of the model may result from changes in hydrologic conditions and groundwater behavior with topography. Further modeling of the effects of porewater pressure on subglacial processes must consider subglacial bed slope in an effort to generate a universal till-genesis model.

Acknowledgments

I wish to thank the people of the Southern Lake District of Chile, South America, who gave permission to study outcrops either on their property or under their jurisdiction, including: Sr. Alberto Hechenleitner, mayor of the town of Frutillar, who granted permission to study outcrops in the town of Frutillar, and Captain Roberto Avila, who assisted in gaining this permission.

I wish to thank my committee members, Dr. John Grover, Dr. David Nash, and especially my committee chair Dr. Tom Lowell, for their patience and good humor throughout this project. I also wish to thank Lisa Trump, who did an outstanding job of drafting to produce Plates I and II.

Financial support for this fieldwork was provided by a grant from the National Geographic Society.

I dedicate this thesis to John and Carol Turbek, Greg Reid, and Deanna and Gerald Reid, whose love and encouragement helped me to complete this research.

Table of Contents

List of Figures

Introduction

The basal dynamics of ice sheets are poorly understood because the basal zones of ice sheets are inaccessible. Dreimanis (1988) suggests that till deposition is affected by four end-member processes, represented by a till tetrahedron, which produce melt-out till, deformation till, lodgement till, and gravity flowtill. His model focuses on the vertical sequence that forms at a given location during a glacial cycle. This leads to the question, "for a given time slice, what is the lateral distribution of these facies?"

The purpose of this study was to investigate how topography affects the basal processes of flat-profile, temperate, piedmont glaciers. This was accomplished by mapping glacial sediments and structures, in relation to their topographic position, for the youngest glacial deposits in two basins, the Lago Llanquihue basin and the Seno Reloncaví basin in the southern Lake District of Chile, South America (Figure 1). The Lake District of Chile is a good location for this study because both the chronology of the deposits (Lowell *et al.*, 1995) and accompanying climate conditions (based on pollen records by Heusser *et al.*, 1996, in press), have been intensively investigated. At least four glacial expansions reached the edges of these basins between 27,000 and 14,000 radiocarbon years B.P.

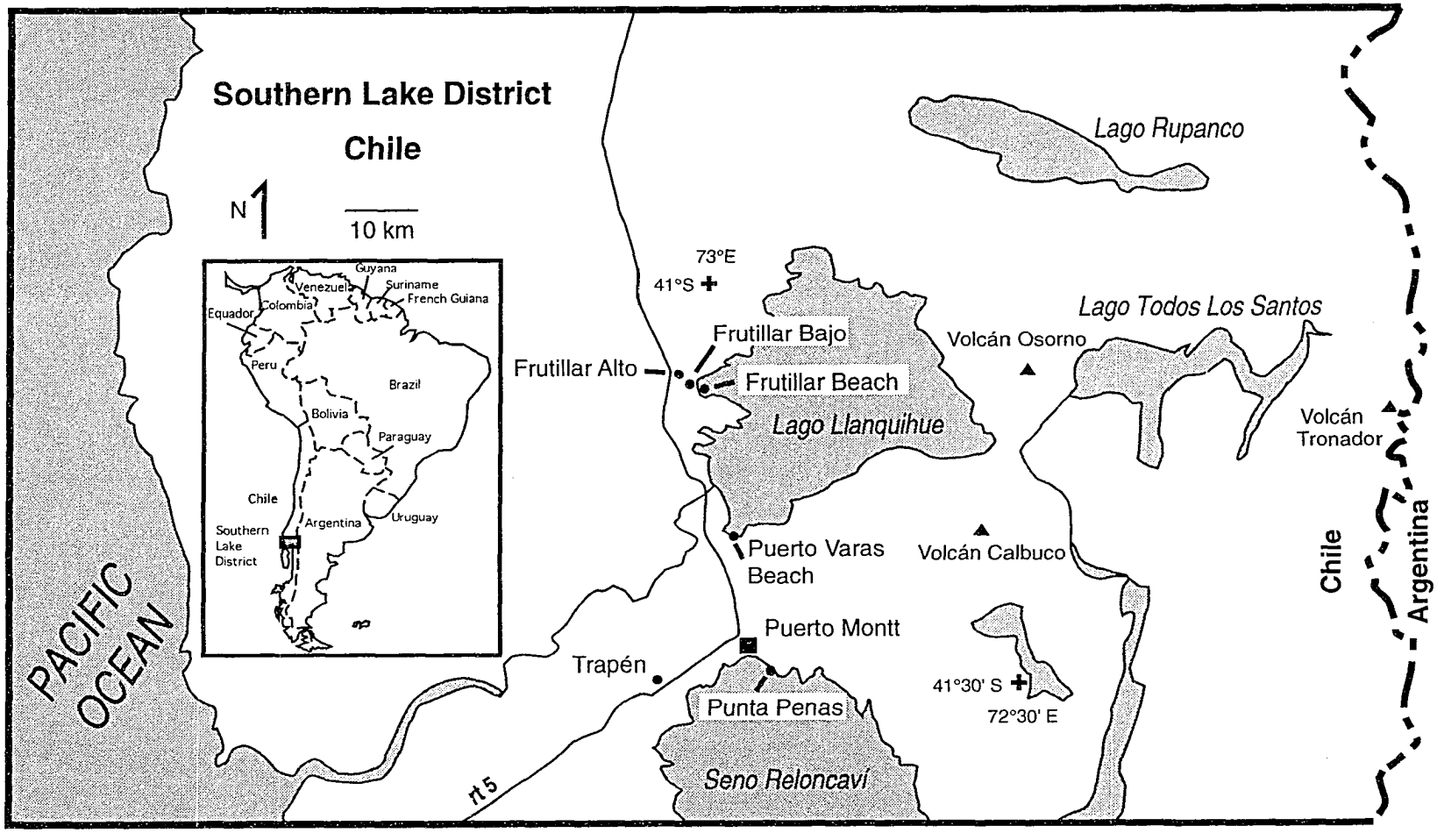

Figure 1. Geography of the Southern Lake District, Chile. Six key sites are indicated by solid circles, towns by squares, and volcanoes by triangles. The Andes mountain chain, which was the source of past glacier advances, runs along the Chile-Argentina border. Inset shows the location of the Southern Lake District in relationship to South America.

Background

Many studies investigate individual processes of glacier-related sedimentation and glaciotectonism. The following studies provide insights to some of the features we have observed in Chile.

In the subglacial, marginal zone of the Myrdalsjökul glacier in Iceland, thrusted till sheets stacked to form a moraine ridge (Krüger, 1993). Evidently, winter freeze-on of subglacial lodgement till allowed yearly glacier fluctuations of this stable ice margin to pick up and deposit till slices.

Some structures and sediments are thought to be indicative of a subglacial shear zone formed under either advancing glacier ice or a subglacial thrust sheet. Subglacial shear zones can be either brittle or ductile, depending on sediment properties in the glacier bed. Brittle shear zones result in the formation of Riedel shears or conjugate normal faults (beneath subglacial tills or thrust shear zones) and tensional fractures in sediments (Wateren, 1995). Ductile shear zones result in the formation of deformation till. Within a ductile shear zone, sediments show zero strain at the boundaries, increasing to the highest strain at the middle of the shear zone (Wateren, 1995). Attenuation and boudinage of sediment folds occurs at low strains, increasing at higher strains to produce a laminated till if different grain sizes or colors of sediments are present. Ultimately, a completely homogenized deformation till forms at very high strains (Hart and Boulton, 1991).

Hart and Boulton (1991) propose that lodgement of subglacial sediment occurs through the attenuation of stress with increasing depth in a soft deformable bed. This process of lodgement till deposition differs radically from that proposed by Dreimanis (1988), in which debris is lodged when friction overcomes the shear stress imparted by sliding glacier ice.

Glacier dynamics are influenced by the type of basal sediments (Menzies, 1989; Boulton and Dobbie, 1993), freezing conditions (Krüger, 1993; Boulton *et al.*, 1995; Boulton and Caban, 1995), and porewater pressure (Menzies, 1989; Boulton and Dobbie, 1993) at the glacier base. Many scientists now debate the assumption that frozen conditions are necessary for glacially-induced thrusting of unconsolidated sediments (Hart and Boulton, 1991; Wateren, 1995).

Boulton and Dobbie (1993) calculate that for a subglacial bed of low permeability sediment overlying high permeability sediment, the vertical passage of meltwater through the bed is hindered, causing low effective pressures at the glacier sole and allowing deformation. Boulton *et al.* (1995) model the effects of an ice sheet on groundwater flow. Boulton and Caban (1995) conclude that the presence of permafrost or of an aquiclude in the proglacial zone will drive up the porewater pressure in subglacial sediments below the base of the aquiclude. As porewater pressure increases, the effective pressure and the overburden pressure decrease. Consequently, cohesion of subglacial sediment is reduced to the point where lateral stresses fracture through the sediment and thrusting occurs.

Hydrofractures are also common in the subglacial zone and may contain clastic dikes pointing downwards into underlying lower-permeability sediments (Boulton and Caban, 1995). When basal meltwater drains vertically through a low-permeability layer into a higher-permeability layer below, a large porewater pressure gradient forms across the low-permeability layer. This pressure gradient forces water to fracture through the low-permeability layer, relieving the pressure gradient and depositing fluidized sediment. In the glacier-marginal zone, hydrofracturing can form clastic dikes pointing upwards by a similar mechanism.

Study Setting

The Southern Lake District of Chile is named for its many scenic lakes (Figure 1). The glaciers that formed these lake basins originated in the Andes mountains to the east and flowed west-northwest. Outcrops around two of these lake basins were studied- the Seno Reloncaví basin and the Lago Llanquihue basin.

Seno Reloncaví is a marine embayment of the coast of Chile at the present time. During glacial times, this embayment was cut off from the ocean by an ice lobe flowing northwest, as indicated by maximum glacial limits mapped on Isla Grande de Chiloé to the west of Seno Reloncaví (Porter, 1981).

Lago Llanquihue is ~45 km across and reaches a maximum depth of 320 meters at the center. Porter (1981) estimates the Llanquihue glacier to have

reached a length of 95 km at maximum extent. The Llanquihue glacier flowed through Lago Todos Los Santos and into Lago Llanquihue (Figure 1). Much of the construction of the volcano Osorno, which lies between these two lakes, ocurred post-glacially (Porter, 1981). Bahia Frutillar (Figure 2), located on the west side of Lago Llanquihue, is a typical topographic setting for the margin of these temperate piedmont glacier lobes. Ice flow here was almost directly westward, through the center of the bay towards the town of Frutillar.

Moraine complexes and ice-marginal channels ring the bay (Porter, 1981; Andersen, in press). These moraine ridges are compound moraines but have a short linear extent, making them hard to correlate around the bay. Overlain on the innermost moraine surface is a kame terrace at approximately 90 meters elevation. This terrace formed during the last ice advance of the Llanquihue lobe (Porter, 1981). Similar terraces presumably formed during prior glacier advances and provided material for thrusting or other glacial reworking. Extensive outwash plains were deposited outside the moraines when the glacier stood at the moraine crests.

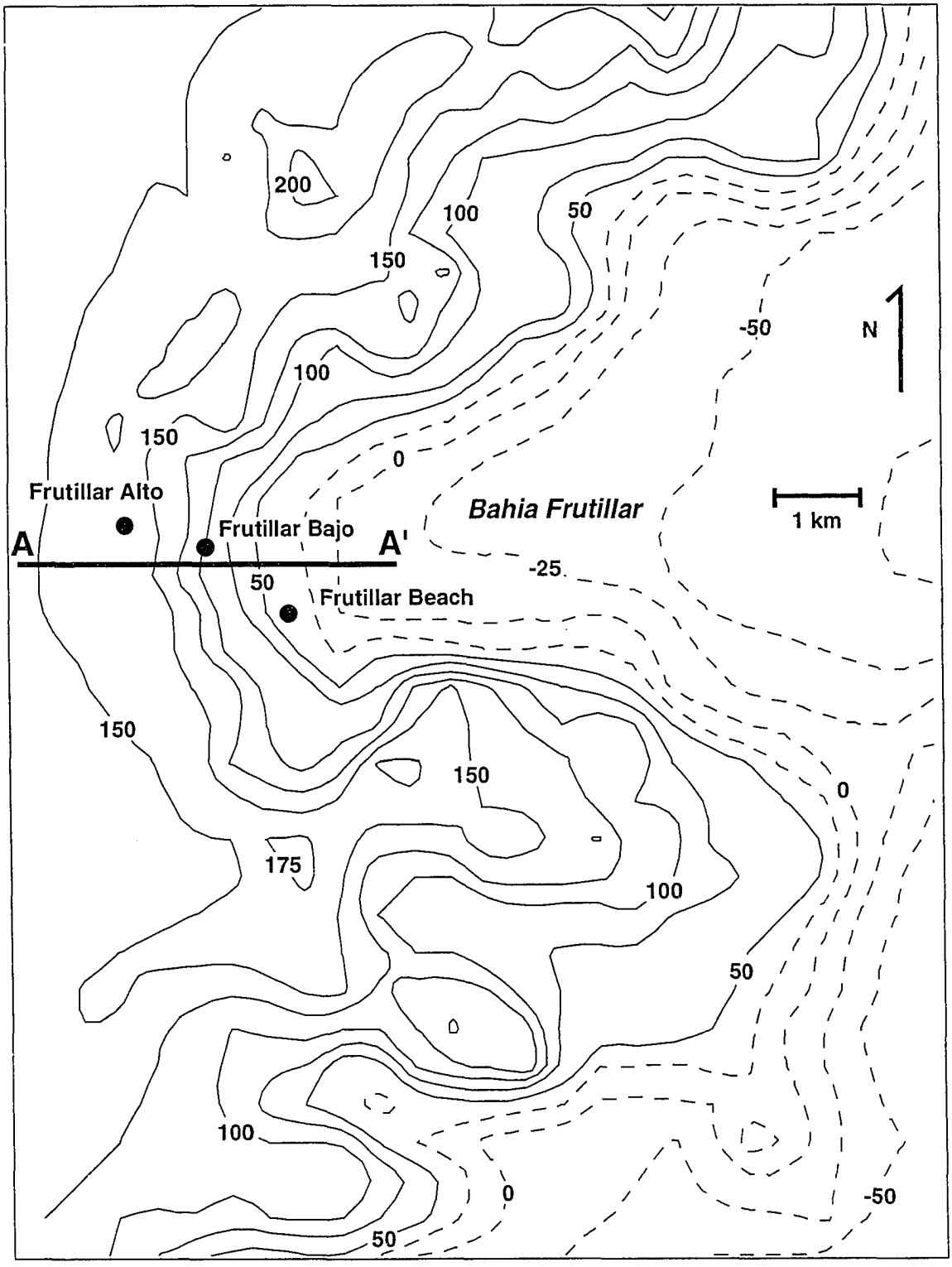

Figure 2. Topography in the Frutillar basin is representative of the ice-marginal topography of these temperate piedmont glaciers. Cross-section A-A' (Figure 3) is approximately along ice flowline. The sections within this basin are indicated by solid circles. Contour interval is 25 m, with elevations measured relative to mean annual sea level. Elevation contours are dashed below present lake level (51 m).

Site Descriptions

Because the glacial facies model we have developed is dependent on topography, the geology of six key sections will be described with respect to the position of the section on the topographic slope. Sites at present lake level are described first, followed by sites along the ice contact slope rising out of the basin, and then lastly by sites at the top of the slope (the moraine ridge). All sections described in this study are within 2-10 km of the maximum ice extent position for these temperate piedmont glacier systems. Four of the sites are located in the Llanquihue basin- one in Puerto Varas on the southern shore, and three in Frutillar on the western shore of Llago Llanquihue (Figures 1 and 2). Two sites are located near Puerto Montt, Chile, in territory glaciated by the Seno Reloncaví glacier lobe (Figure 1). These six sections and their relationship to basin topography are shown in Figure 3:

1. The Puerto Varas Beach and Frutillar Beach sections are located on the lower slope, at present lake level.
2. The Frutillar Bajo and Punta Penas sections are located along the middle slope above the present lake basin.
3. The Frutillar Alto and Trapén sections are located on the upper slope.

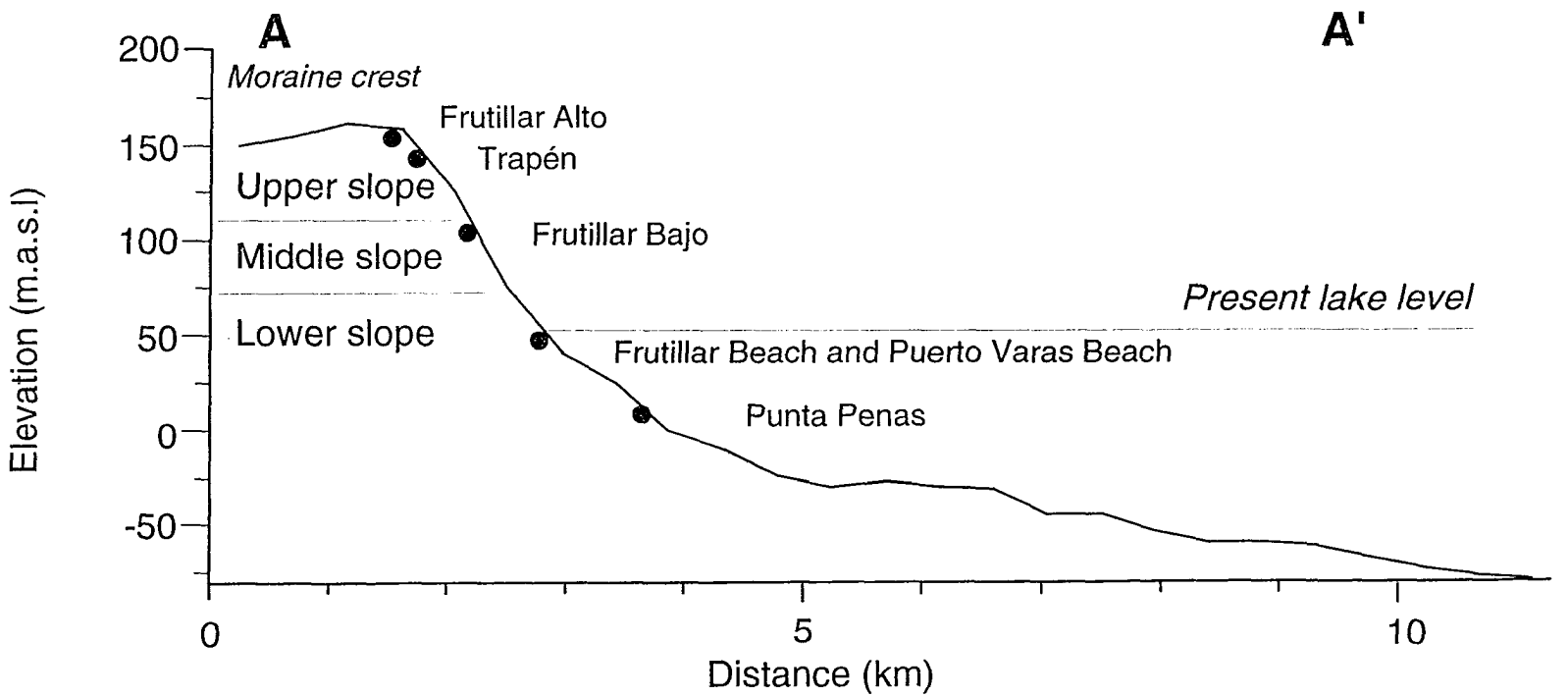

Figure 3. Topographic profile of the Frutillar basin, approximately along ice flowline, for the section A-A' (Figure 2). The middle slope position has a slope of 10°. The elevation ranges for the three topographic positions are valid for the Llanquihue sites only, and varied with different glaciations; the Trapén and Punta Penas sections (located on the upper and middle slope, respectively) are plotted to show the greater range of elevation spanned by the Seno Reloncaví glacier. The topographic positions of the Seno Reloncaví lobe span a greater range of topography and begin at much lower elevations than the Llanquihue lobe positions.

Lower Slope Position

The lower slope position (Figure 3) includes terrain with elevations up to approximately 20 meters above the present lake level (at 51 meters above sea level) for the Frutillar basin. Sediments found here are glaciolacustrine in origin and have been deformed as a result of ice-marginal stresses.

Puerto Varas Beach Section

The Puerto Varas Beach section occupies a lower slope position (Figure 3). Deformed sediments are exposed in a sub-basin along the southeastern shore of Lago Llanquihue at Puerto Varas, where ice flow was almost directly south (approximately towards 200° azimuth). The beach at Puerto Varas is 2 km inside the maximum ice position (Figure 4).

Exposed along the present shoreline are repeated sequences of three types of bedded sediments: (1) hard, semi-lithified, graded beds of clay, silt, and sand, (2) massive ash or silt beds, and (3) pebbly or sandy diamicton beds, often containing large cobbles. Many of the massive ash or silt beds contain highly deformed clay layers. This exposed section extends for at least 105 meters along the shoreline, and is a composite of seven different packages of sediments (Figure 6 and Appendix 2-Table 1).

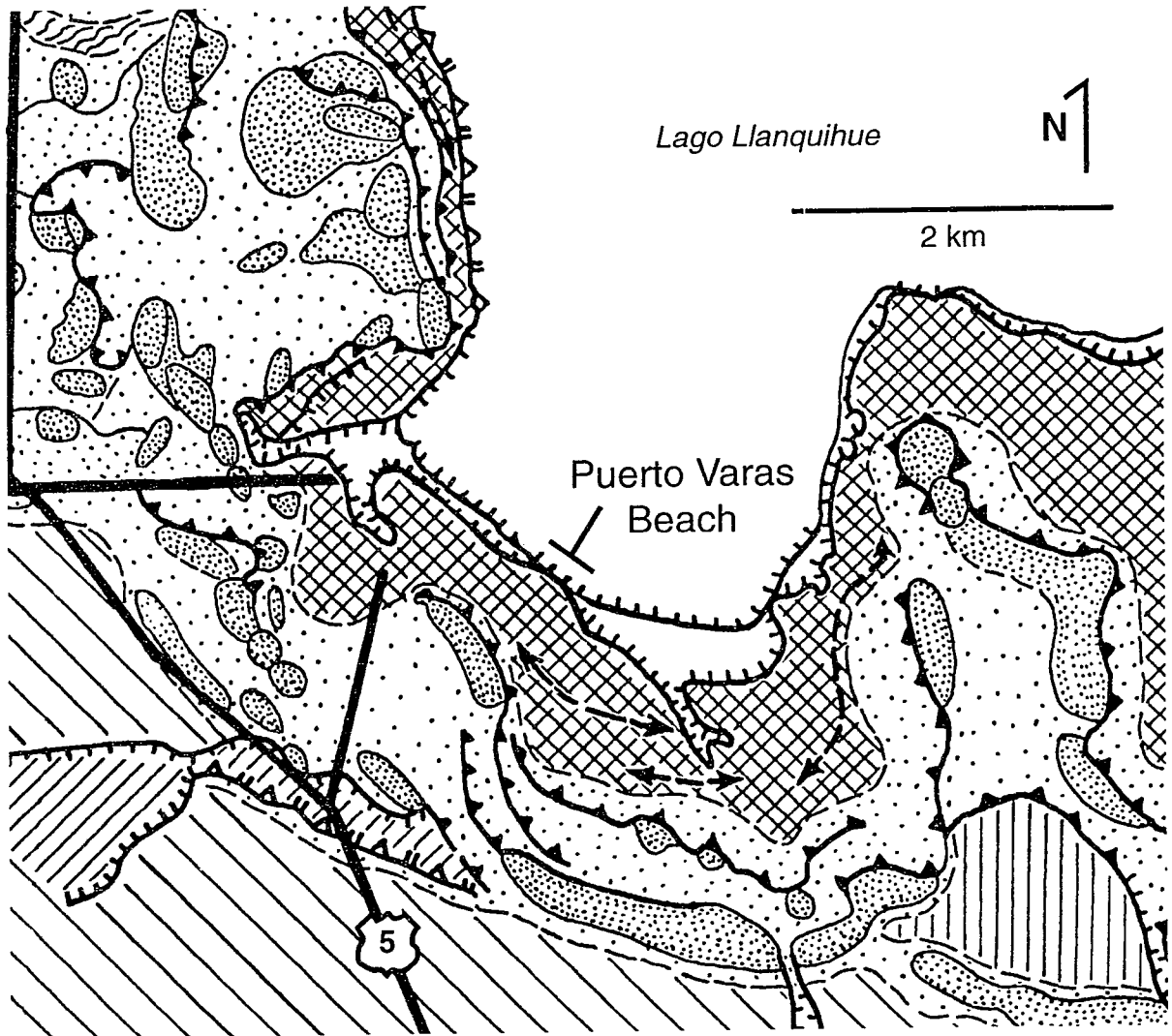

Figure 4. Map of the geomorphic landforms surrounding the Puerto Varas Beach section (from Andersen, in press). This section lies within two kilometers of the maximum ice position. The legend for the patterns is given in Figure 5.

Ice contact zone (generally break in well-preserved ice-contact slope or terrace)

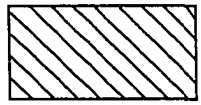

Main Llanquihue outwash plain

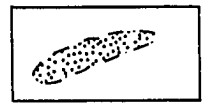

Indistinct Llanquihue moraine ridge

Ice-contact zone modified by post-depositional erosion

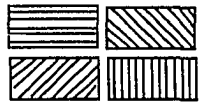

Subsidiary Llanquihue outwash plains (flat)

Distinct Llanquihue moraine hill

Terrace scarp

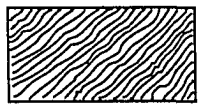

Subsidiary Llanquihue outwash plains (slightly hummocky)

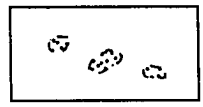

Indistinct Llanquihue moraine hill

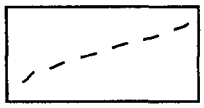

Proximal margin of terrace or moraine

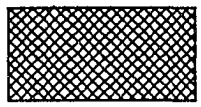

Llanquihue lake-margin ice-contact terrace

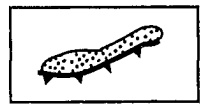

Llanquihue moraine ridge with well-preserved ice-contact slope

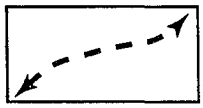

Ice-marginal meltwater channel (flow direction not determined)

Llanquihue drift, hummocky in places

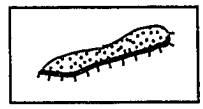

Llanquihue moraine ridge with erosional scarp

Ice-marginal meltwater channel (flow direction determined)

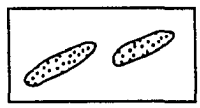

Distinct Llanquihue moraine ridge

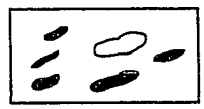

Flutes and drumlins

Figure 5. Legend for the geomorphic landforms maps (Figures 4, 11, and 27).

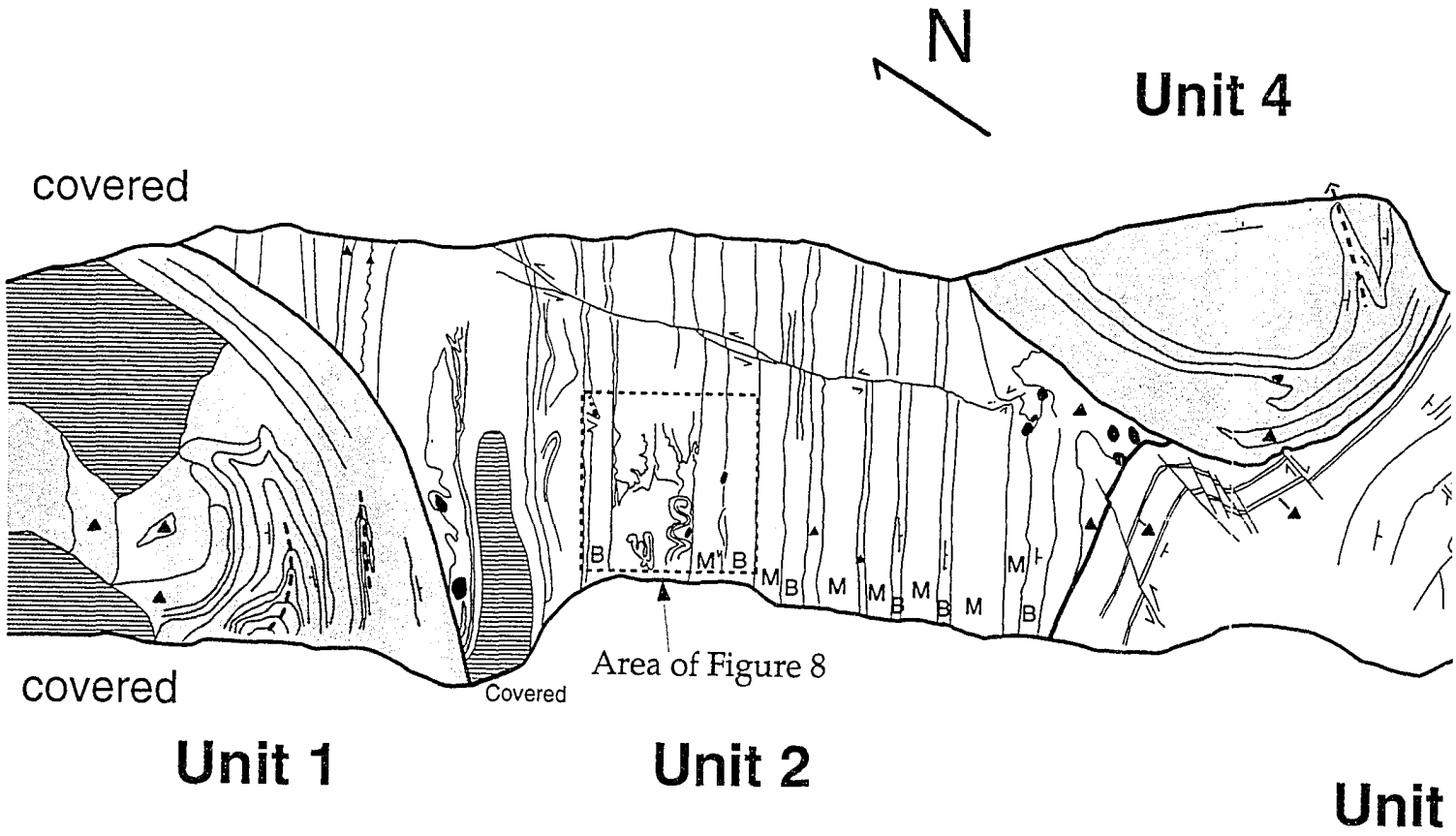

Figure 6. Map of the Puerto Varas Beach section (plan view). This section is divided into seven units. The shaded units have been thrusted, probably by past glacier activity at the ice margin.

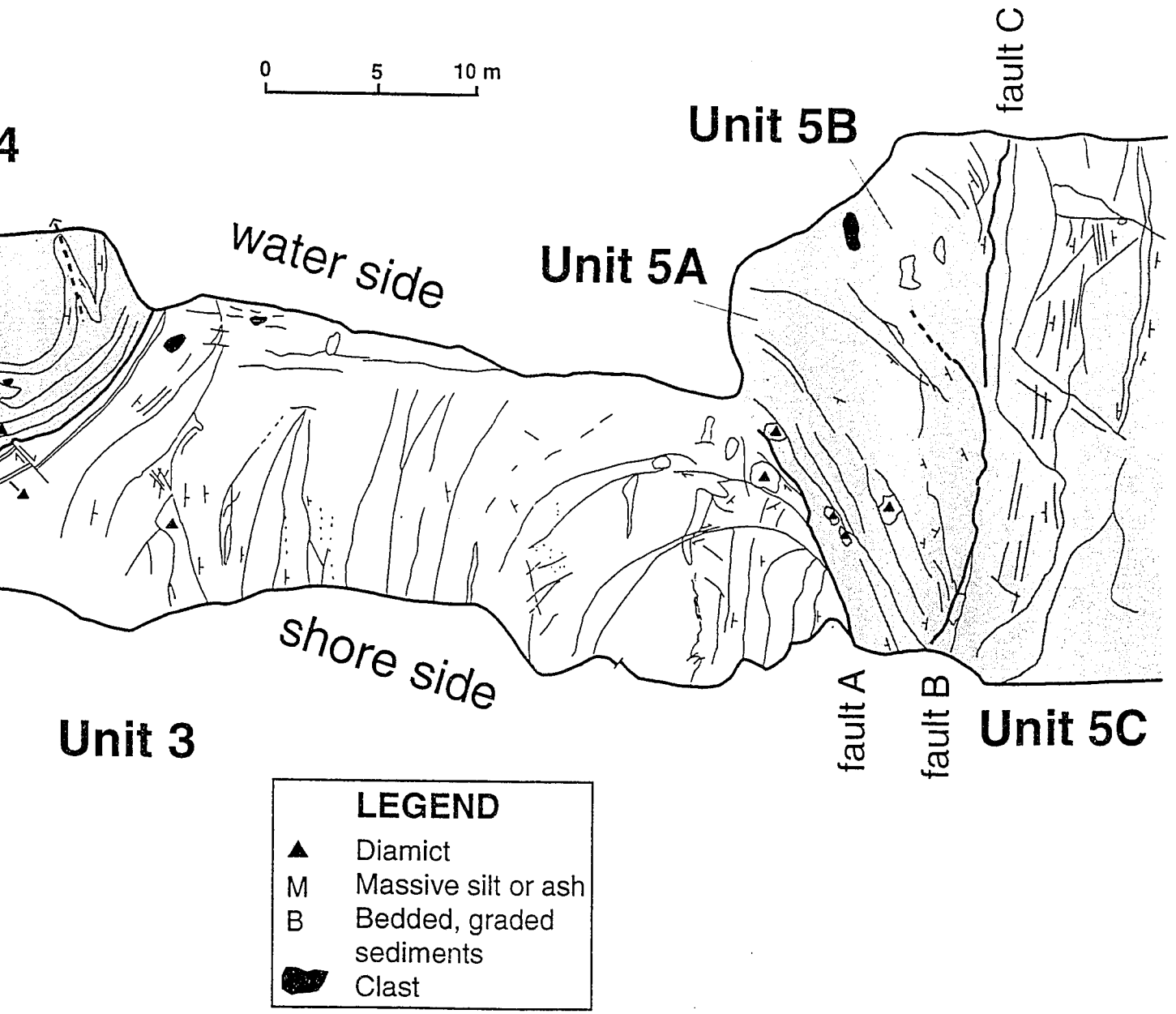

Unit 1 is a curved package of sediments at the northern end of the section, forming a set of overturned, plunging folds. A major angular unconformity separates Unit 1 from Unit 2 to the south, and may be a thrust plane.

Unit 2 contains tilted, bedded sediments. Flame structures of clay within graded-bed sequences (Figure 7) indicate that in the present SE-dipping orientation of the beds, stratigraphic up is to the southeast.

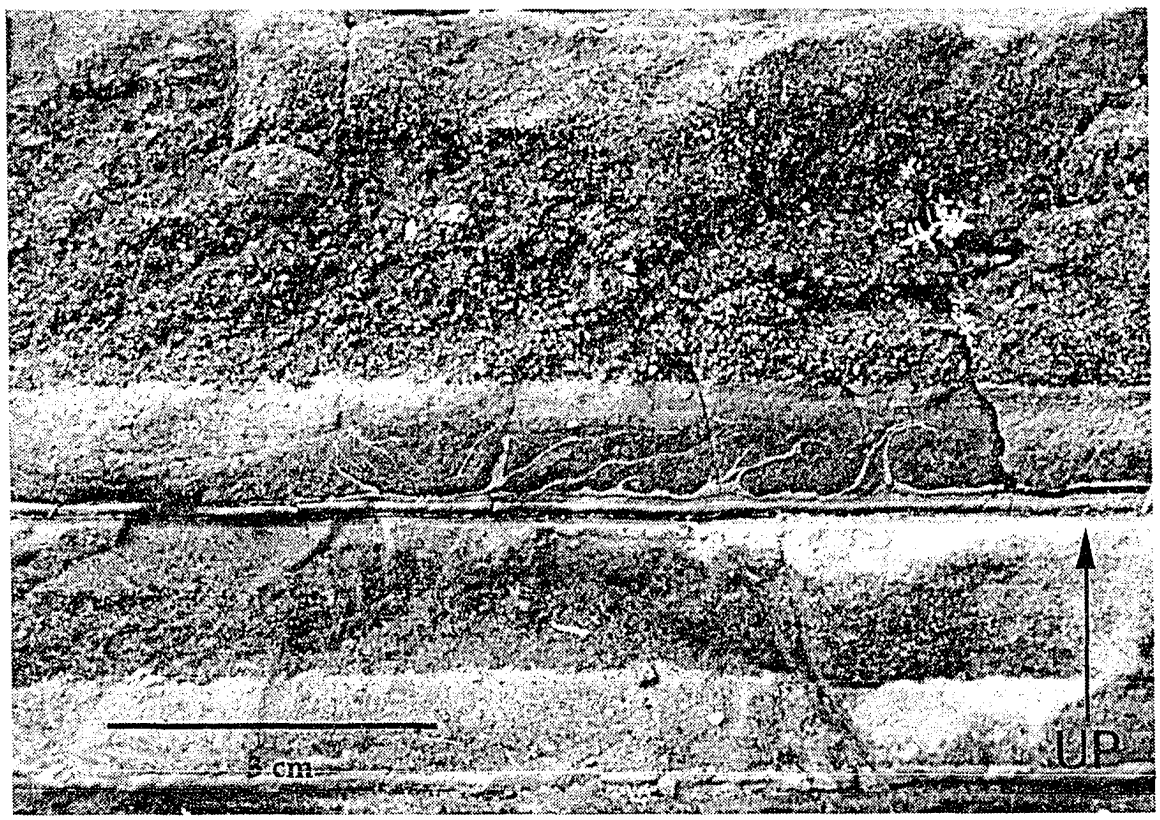

Figure 7. Photograph of a fining-upward bed sequence within Unit 2 of the Puerto Varas Beach section, showing flame structures of clay into the coarser material above. These flame structures formed as glacial debris flows moved over the depositional surface.

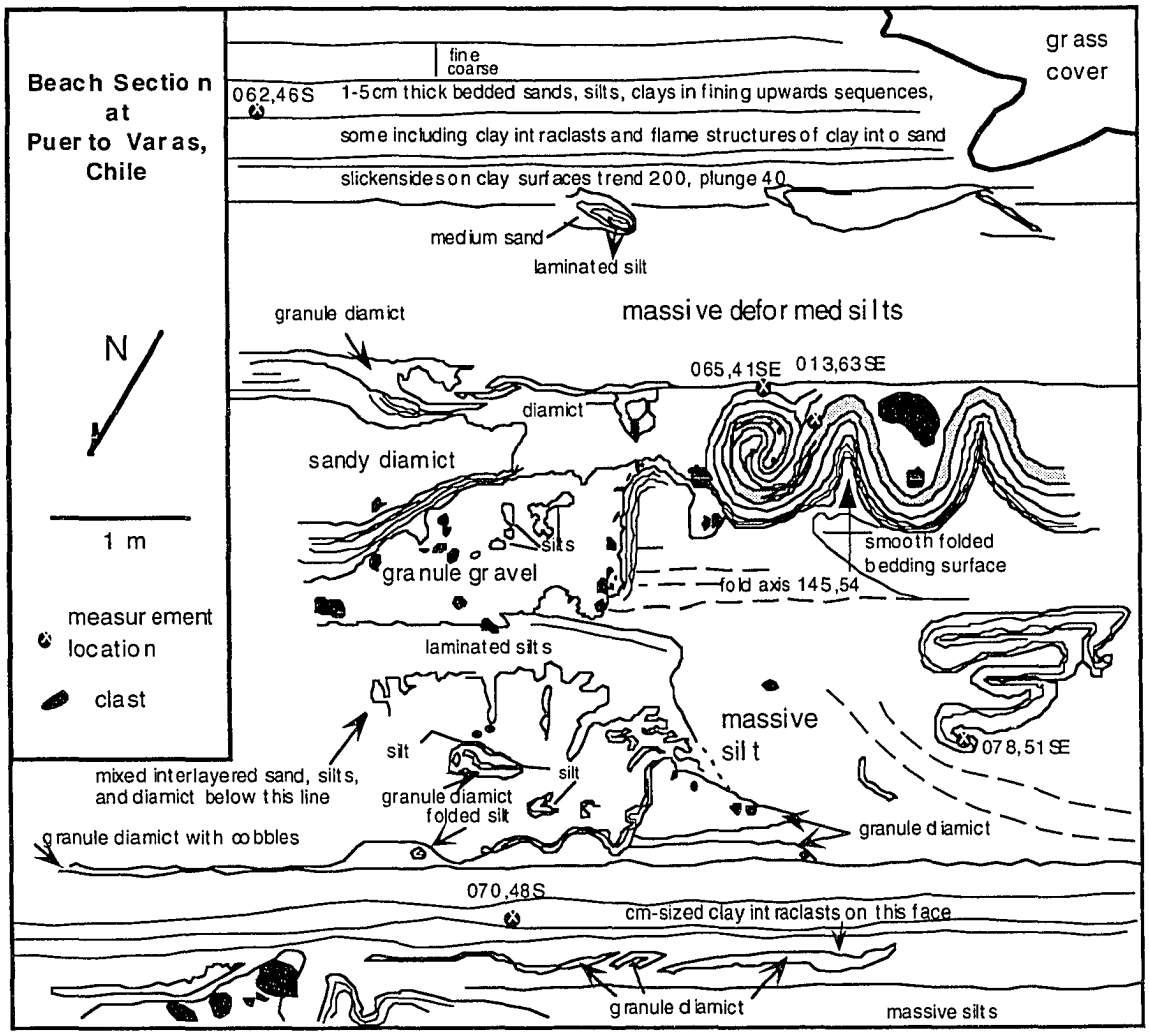

Figure 8. Map of one massive silt layer, bedded between thin graded-bed sequences, which contains truncated, deformed sediment layers and the sediment roll, in Unit 2 of the Puerto Varas Beach section. The close association of deformed layered sediments with irregular gravel or diamicton pods suggests that deposition of the coarser diamicton units caused the syndepositional deformation.

One especially interesting zone (Figure 8), near the base of Unit 2, contains irregularly-shaped diamictons, folded sections of layered sediments, and one rolled section of fining-upward beds (Figure 9). This roll structure traces westward into a sequence of two anticlines and two synclines before

Figure 9. Photograph of the roll structure in Unit 2 of the Puerto Varas Beach section. The formation of this sediment roll occurred as the adjacent sediments were depositing.

disappearing under modern soil cover. Discontinuous diamictons, some with large cobbles, occur in the troughs of these folds. An irregular granule-rich diamicton contacts the base of the roll to the east. The bedding orientation in the axes of the folds is similar to the orientation of graded-bed sequences above and below the roll zone. This indicates that rolling of the sediment layers occurred as the adjacent diamicton was being deposited, and that tilting occured after deposition of Unit 2.

Within Unit 3, more tilted, bedded sediments are folded into a syncline. At the northern end of Unit 3, bedded layers were kink-faulted in a zone about a meter wide, reorienting the strike of bedding from ~ E to ~ SSE

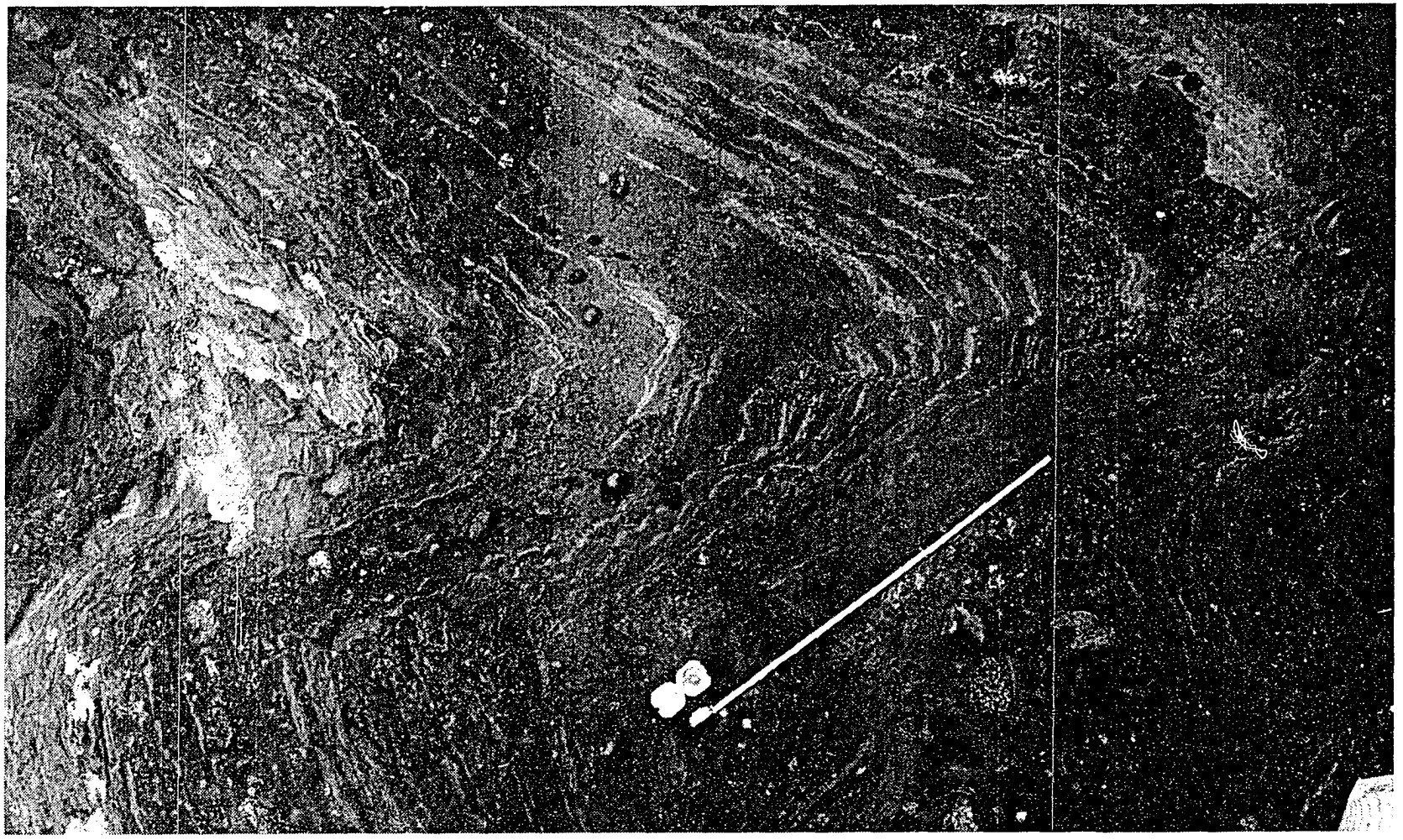

Figure 10. Photograph of the kink-faulted sediments in Unit 3 of the Puerto Varas Beach section. Movement of Unit 4 fault block from the northeast by the glacier resulted in this kink-faulting. One meter is shown for scale. The Brunton compass is oriented north-south, with black arm pointing south.

(Figure 10). Unit 4 consists of massively-bedded sediments that have been pushed westwards over part of Units 2 and 3, a few meters east of the kink-faulted zone. Unit 5A and Unit 5B are blocks of sediments faulted from the syncline. The curvilinear traces of these W- to NW-dipping beds indicate that they were once part of the syncline. Differential movement has occurred along a north-trending fault (fault B) between these two packages. The beds of Unit 5B are truncated by a massive silt unit that marks the beginning of Unit 5C. Unit 5C contains SE-dipping layered sediments (similar to Unit 2) that have been thrust against Units 5A and 5B.

The association of diamictons with pieces of deformed, bedded sediments suggests a cause-and-effect relationship. Large boulders or cobbles at the base of these diamictons sometimes formed folds or wedges to their "western" side as they ploughed through the underlying sediments. At another place, bedded sediments were folded "westward" over the top of a cobble. Orientations are relative to their current position, which may not be their original depositional position. However, these directions uniformly imply that during deposition, compression or movement was from one direction, probably the ice margin in the northeast.

The push directions of the faulted blocks are estimated based on the orientation of folded and faulted bedding. Unit 1 was pushed approximately toward azimuth 150°. Unit 4 was pushed approximately toward azimuth 130-200°. The syncline at the southern end of Unit 3 implies compression either

from or toward azimuth 330°. Unit 5C may have been pushed toward azimuth 330°. These directions are up to 50° off from the ice direction.

Significance of Puerto Varas Beach Section

Flame structures in graded beds form because of movement of flowing sediment and water over the previously-deposited sediment surface (Brodzikowski and Haluszczak, 1987). The truncated and deformed silt and clay layers require an abrupt force to tear them up in intact sections; a gradual force would probably neither pick up sections nor preserve their internal layering. The fact that these deformed layers are contained within massive sediment beds, deposited in a regular sequence, requires a force that is generated during deposition. This type of abrupt force would be generated if the glacial sediments traveled as turbidity currents. Graded bedding within the layers is indicative of turbidites as well.

The bedded sediments in this section, then, indicate a glaciolacustrine environment in which sediments shed from the glacier accumulated as turbidites. With glacier advance, the input of coarser sediment flows, granite gravel, and cobbles caused fine-grained, cohesive sediment layers to be ripped up, folded, and rolled. These deformed, fine-grained layers were then deposited within the coarser-grained beds.

Later, parts of the sequence were folded into a syncline and tilted to the SSE. Faulting created and translocated multiple blocks of these glaciolacustrine sediments. One hypothesis to explain this folding and

faulting involves regional tectonic activity, perhaps associated with the formation of Volcán Calbuco. However, this hypothesis is not favored because these fault blocks are not found everywhere along the southern shore of Lago Llanquihue, where Volcán Calbuco formed.

A second hypothesis involves glacial activity. This section forms a minor topographic point out into the basin, which may indicate that it was formed in a minor indentation or interlobate region at the ice margin. Within an interlobate region, thrusting from the advancing ice margin converges from either side onto a triangular wedge of sediments not confined by glacier ice. Sediments are thrust into this wedge-shaped space within the ice margin. The fact that the estimated push directions of the faulted sediment blocks vary up to 50° to either side of the ice flow direction offers support for this hypothesis. Although subsequent ice advances and modern shoreline erosion have planed off the top of the wedge, its map expression remains.

At this lower slope position, all deposition was glaciolacustrine. Subsequent ice contact probably produced the folding and movement of massive fault blocks. No lodgement tills or deformation tills were deposited.

Frutillar Beach Section

The Frutillar Beach section also occupies a lower slope position at present lake level (Figure 11), but no evidence of direct glaciogenic activity remains. Protruding ridges of sediments are exposed above the modern

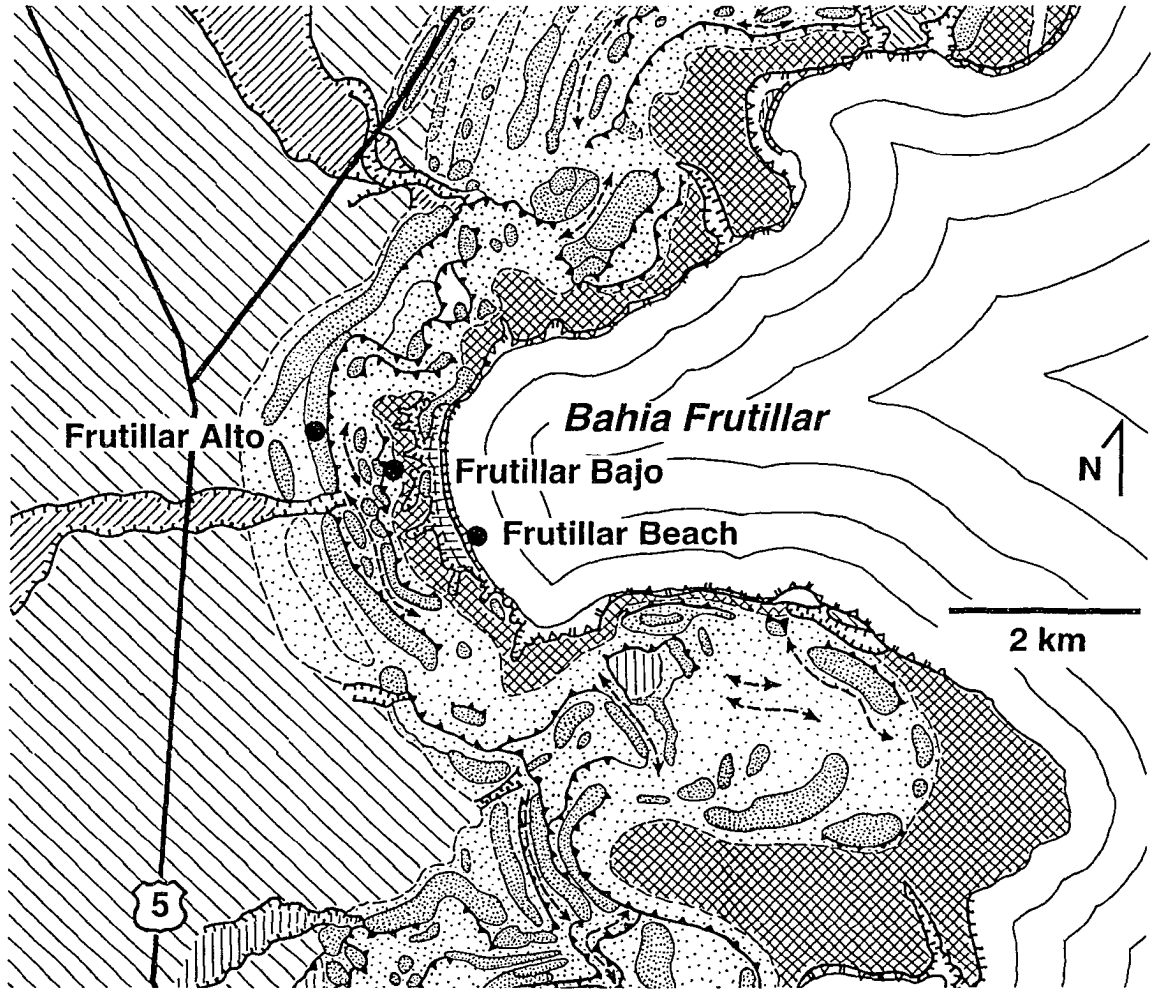

Figure 11. Map of the geomorphic landforms surrounding the Frutillar basin (from Andersen, in press). The Frutillar Alto, Bajo and Beach sections lie within two kilometers of the maximum ice extent. The Frutillar Alto section is a cross-section of a terminal moraine.The Frutillar Bajo section lies between moraine and the youngest kame terrace (formed by the last Llanquihue glacier advance). The Frutillar Beach section lies within the present lake basin. See Figure 5 for legend.

sandy lake bottom. These ridges are made up of randomly-oriented, steeply-tilted blocks, up to a few meters on a side, and consisting of graded beds of fine sands to silts. Clastic dikes fill the spaces between the sediment blocks. These dikes are amalgamations of sand and laminated sediment clasts up to a few centimeters in size. None of the sediment blocks is in its original depositional orientation.

Significance of Frutillar Beach Section

These bedded sediments are also glaciolacustrine in origin, like those at the Puerto Varas Beach site. However, no diamicton units or syndepositional deformations are observed within the sediment blocks at this location, suggesting a more distal position relative to the ice front. Formation of the clastic dikes is probably glaciogenic in origin. The advancing ice margin drove groundwater to break through less-permeable, overlying layers. Clastic dikes formed between these chaotic blocks of sediment when water of decreasing energy deposited sand and rip-up clasts.

All deposition is glaciolacustrine at this lower slope position. Groundwater flow, driven by the weight of the advancing glacier margin, fractured sediments into chaotic blocks and injected clastic dikes upwards between the blocks. No lodgement tills or deformation tills were deposited.

Discussion of the Lower Slope Position

Both of these lower slope sections tell a similar story of glaciolacustrine deposition. When the glacier advanced across the lake, it dammed up numerous sub-basins along the opposite shore. Within these isolated sub-basins, sediment flows shed from the glacier moved as turbidity currents down a slope from the ice margin and were deposited in fining-upward, laminated sediment sequences. At any one location, sediments coarsen upward because of glacier advance. Coarser sediment flows had sufficient energy to pick up and deform short lengths of underlying sediment layers. Much coarser diamicton units and cobbles were deposited as well, shed from the glacier margin and probably also from icebergs calving off the glacier front. Hydrofractures and clastic dikes were formed. Eventually, blocks of these glaciolacustrine sediments were folded and thrust, possibly within interlobate regions of the ice margin.

Ice/sediment interactions were subaqueous until the glacier had advanced above the elevation of the dammed lake surface; above this elevation, subglacial ice/sediment interactions were terrestrial in nature. The last glacier advance in Lago Llanquihue terminated within the lake basin and formed a kame terrace (Figures 4 and 11) around the southern and western sides of the lake (Porter, 1981) before retreating. This terrace has a surface elevation of 90 meters in the Frutillar sub-basin. Although this terrace was not overrun by the glacier, other older terraces, formed by the processes

described above, provided material for subsequent glacier advances which reached the middle slope and upper slope positions.

Middle Slope Position

The middle slope position (Figure 3) ranges from approximately 70 to 110 meters elevation in the Frutillar basin, occupying approximately the middle third of the exposed topography. Deposits found here consist of thin, low-angle thrust slices of lacustrine sediments with diamictons at their base, formed in sub-thrust shear zones. Lodgement till caps the sequence.

Frutillar Bajo Section

The Frutillar Bajo section extends eighty meters along the slope, from the basin in the east towards the inner moraine crest in the west (Figure 11). The formation of this outcrop occurred through a sequence of nine events, shown schematically and numbered in order of occurrence (Figure 12). The sediments are depicted and characterized in Figures 13 and 14, Appendix 2-Table 2, Appendix 3-Table 1, and Plate I.

Five of these units offer clues to the subglacial processes occurring at this topographic position. Unit 4 is an amalgamation of outwash gravel, sand, and boulders with diamicton (Figure 13 and Plate I). This unit is deposited into a channel cross-cutting the older Units 2 and 3. Deposition here is ice-marginal, as indicated by the deposition of flow till diamict.

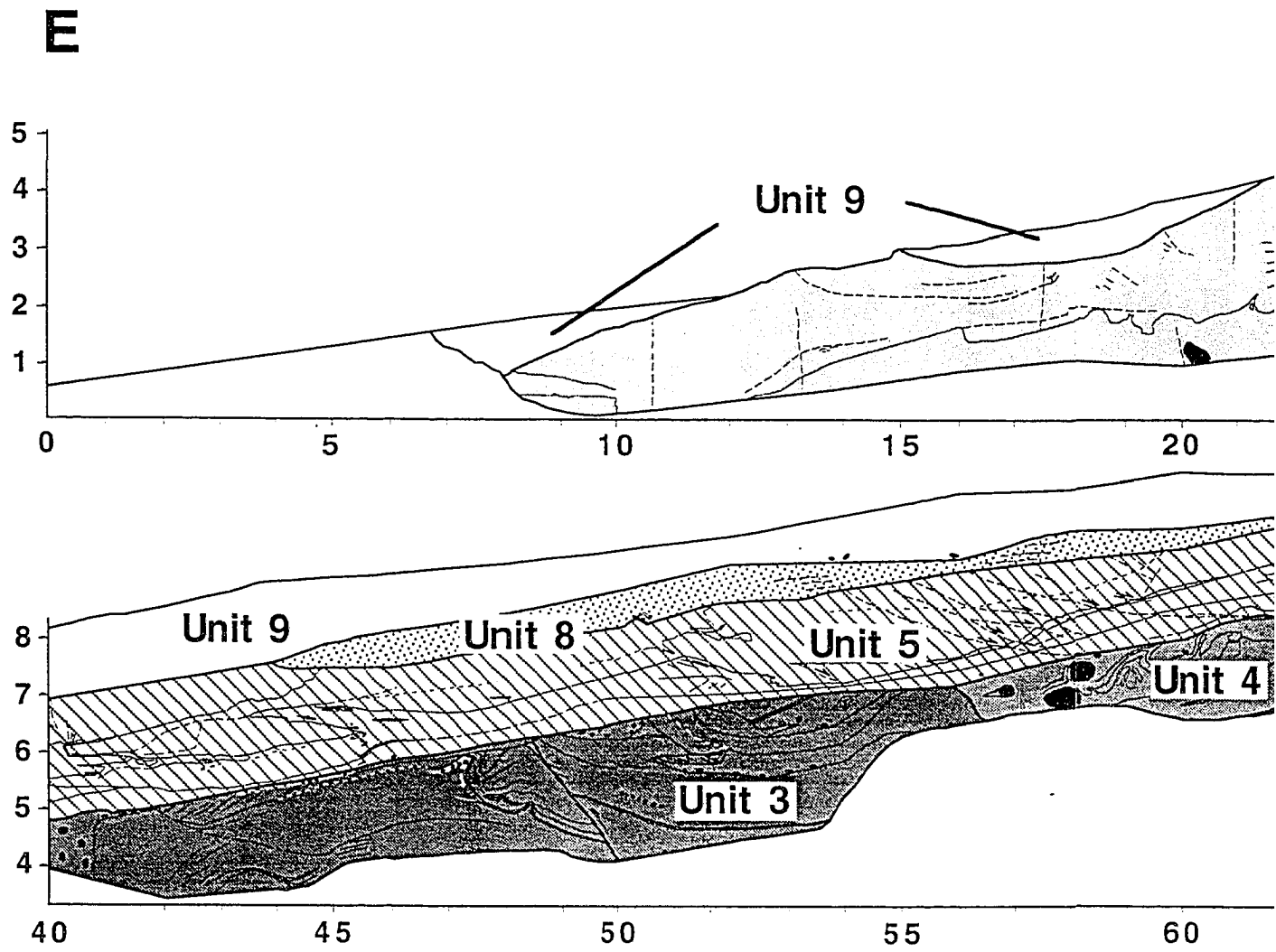

Figure 12. Schematic diagram of Frutillar Bajo section, showing the nine sediment units. Unit 3 resulted from ice-marginal sedimentation as the glacier was advancing up the slope. Units 5 and 7 are lake terrace sediments which were thrust as thin slices underneath the glacier. Unit 6 is a block of lake terrace sediment which was probably pushed at the ice margin after glacier retreat and readvance. Unit 8 is a subglacial till, possibly of lodgement origin.

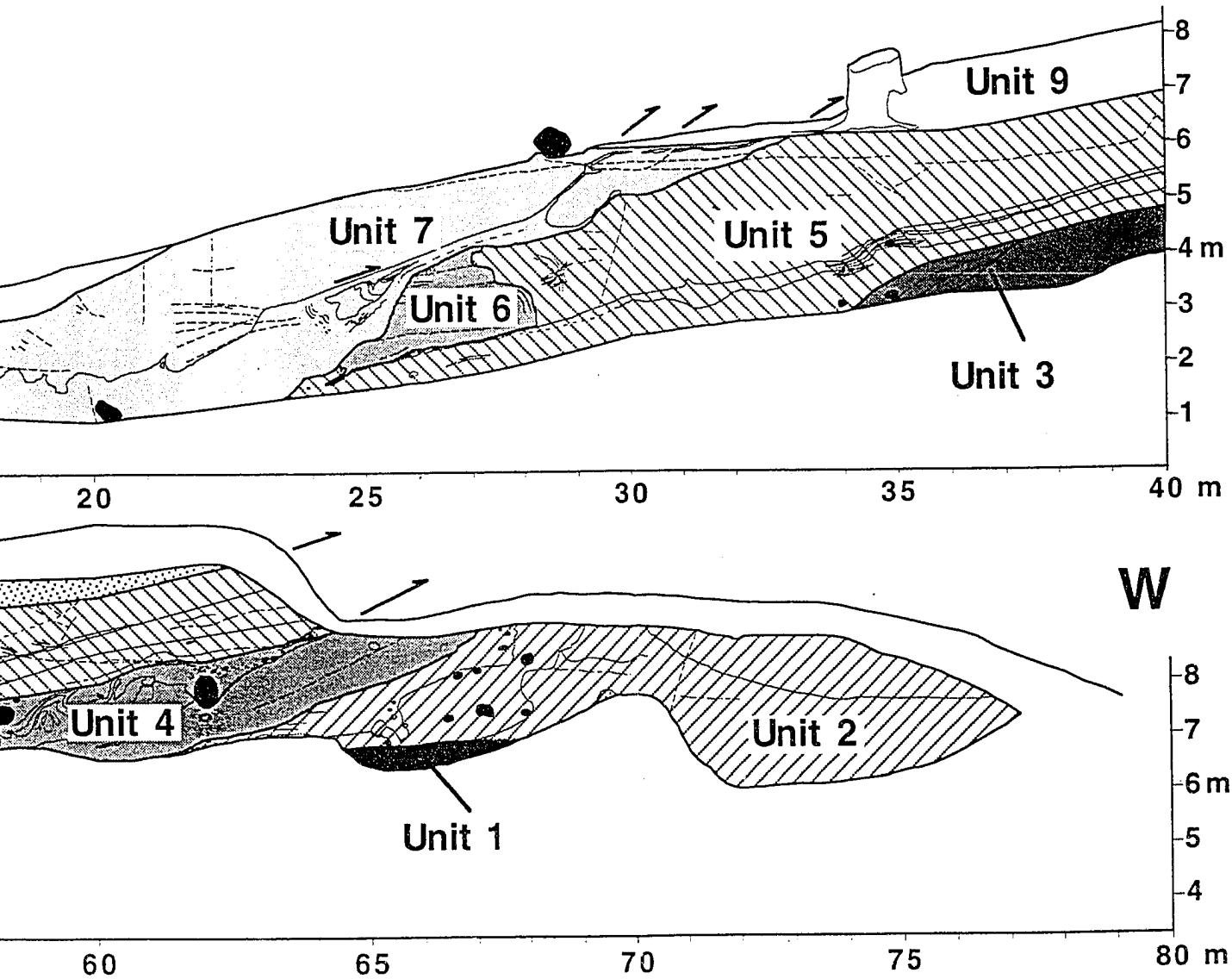

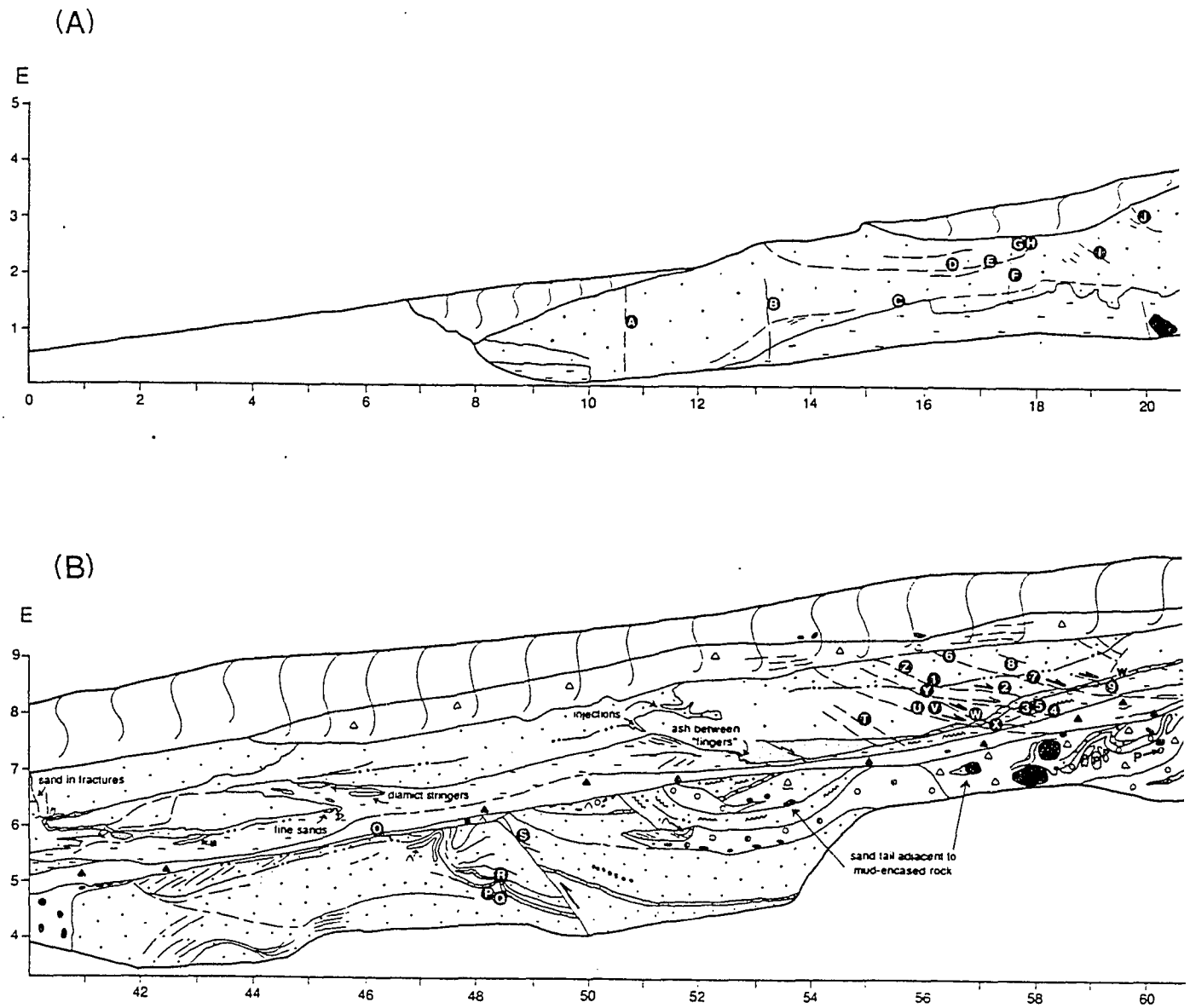

Figure 13. Detailed map of the sediments and structures of the Frutillar Bajo section. See also Plate I, which shows this outcrop in a larger form. See Figure 14 for the legend.

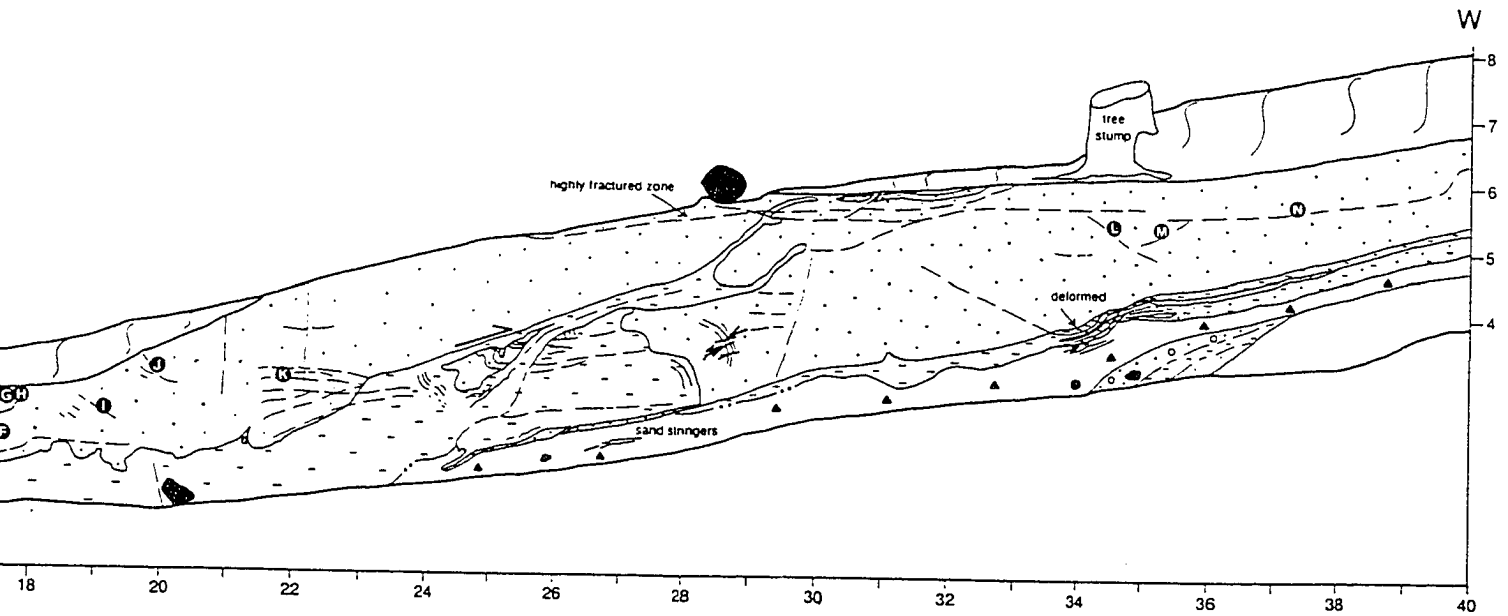

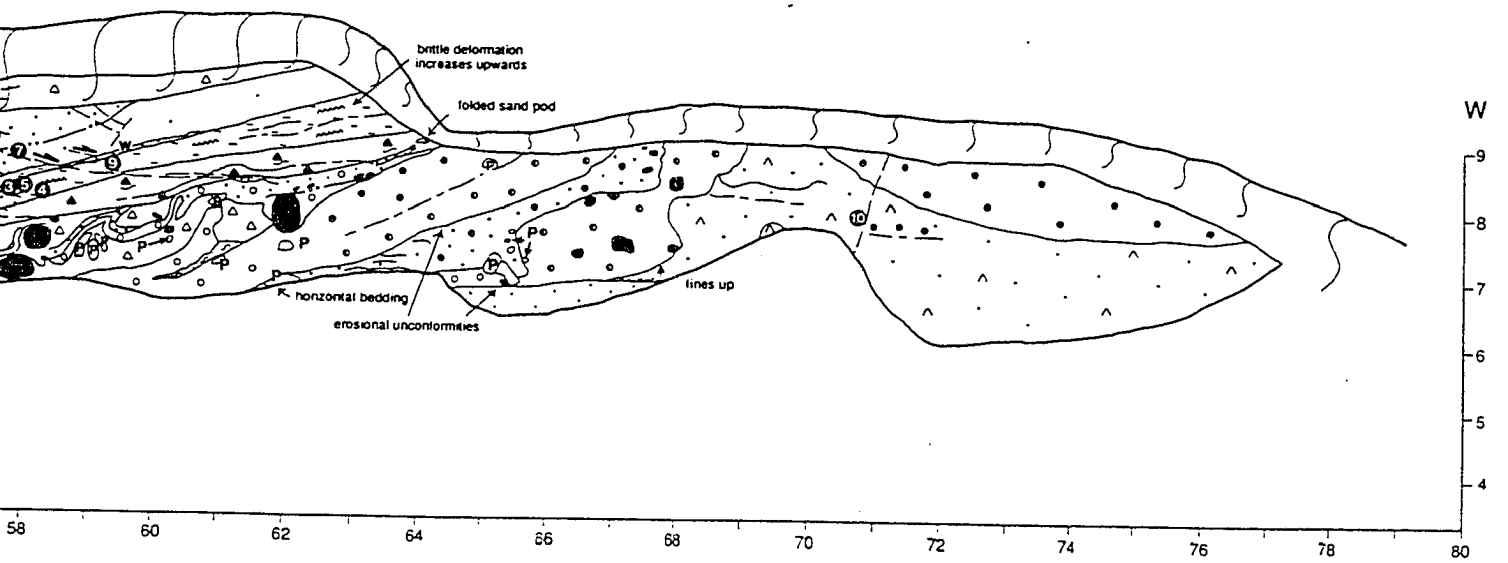

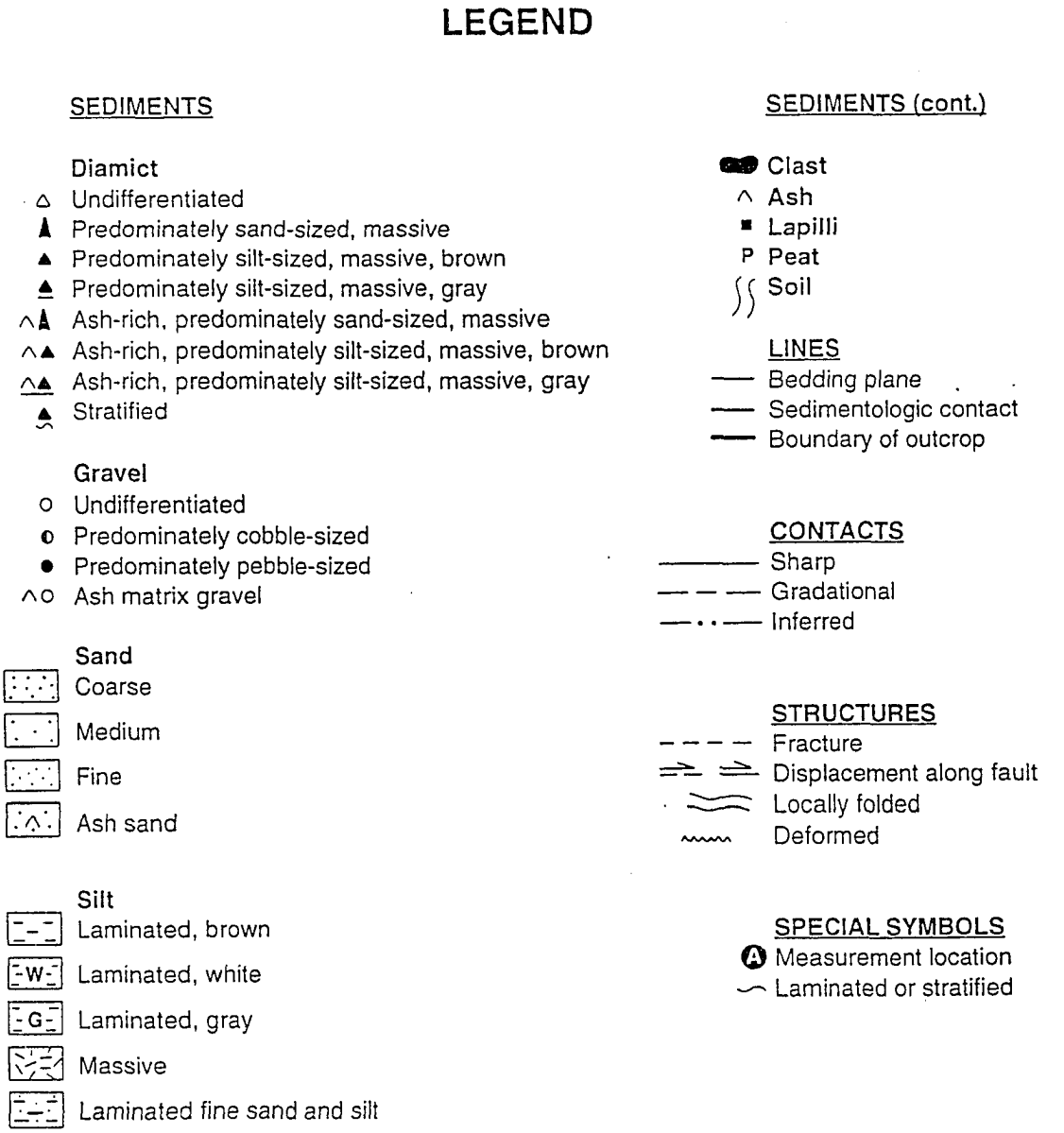

Figure 14. Legend for the Frutillar Bajo and Frutillar Alto outcrop maps (Figure 13 and 25).

Unit 5 is a 40 meter-long sequence of lake terrace silt and overlying sand, not in its original depositional orientation. Diamict formed at the base of the sequence as it was thrust subglacially. Thin stratification planes within the diamict indicate localized water flow and therefore an unfrozen condition for the thrust slice. A sand wedge in the silt (meter 45) suggests rethrusting along the sand/silt contact. Injection of coarser sand into underlying finer-grained sediments (meter 51) occurred, probably through hydrofracturing (Boulton and Caban, 1995), also suggesting a subglacial position for the thrusting.

Unit 6 is a three-meter block of brown silt, probably removed from a lake terrace. Laminae at the top of this block are folded upwards and slightly overturned at the eastern end of the block where it contacts Unit 7. The ice margin probably thrust Unit 6 against the sand of Unit 5, and later subglacial thrusting of Unit 7 resulted in further deformation.

Unit 7 is another silt/sand sequence that has been sheared off a kame terrace and thrust subglacially. At meter 25 (Figure 13 and Plate I), tan laminae within the basal silt reveal details of the shear zone developed at the base of the thrust sheet. A meter-long sand pod (Figure 15), presumably displaced from the terrace sand above, is engulfed by laminated brown silt at this location. The bedding within this sand pod is folded, with fold noses pointing uphill. Beneath the sand pod, silt laminae are faulted and rotated clockwise (Figure 16). To the eastern side of the sand pod, silt laminae are dragged upwards around the sand, forming boudins. Brown silt dragged

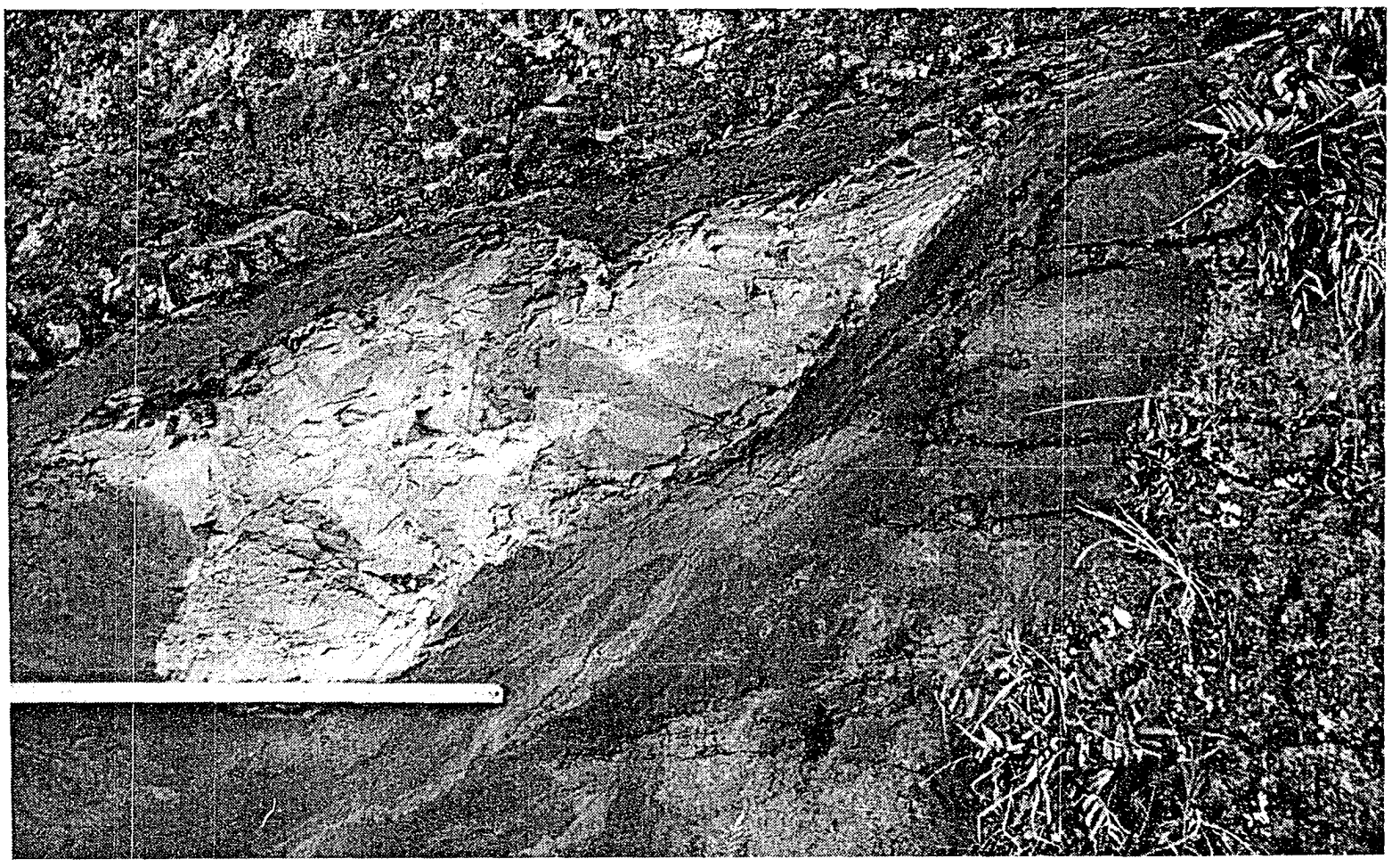

Figure 15. Detail photograph of the overthrust sand pod of Unit 7, Frutillar Bajo section. Note folding of sediment layering within the sand pod, boudinage of silt laminae around the left end of the sand pod, and reorientation of laminations (at the top of Unit 6 to the right of the sand pod) due to drag of the overlying thrust sheet. To the right is the translocated Unit 6 silt block.

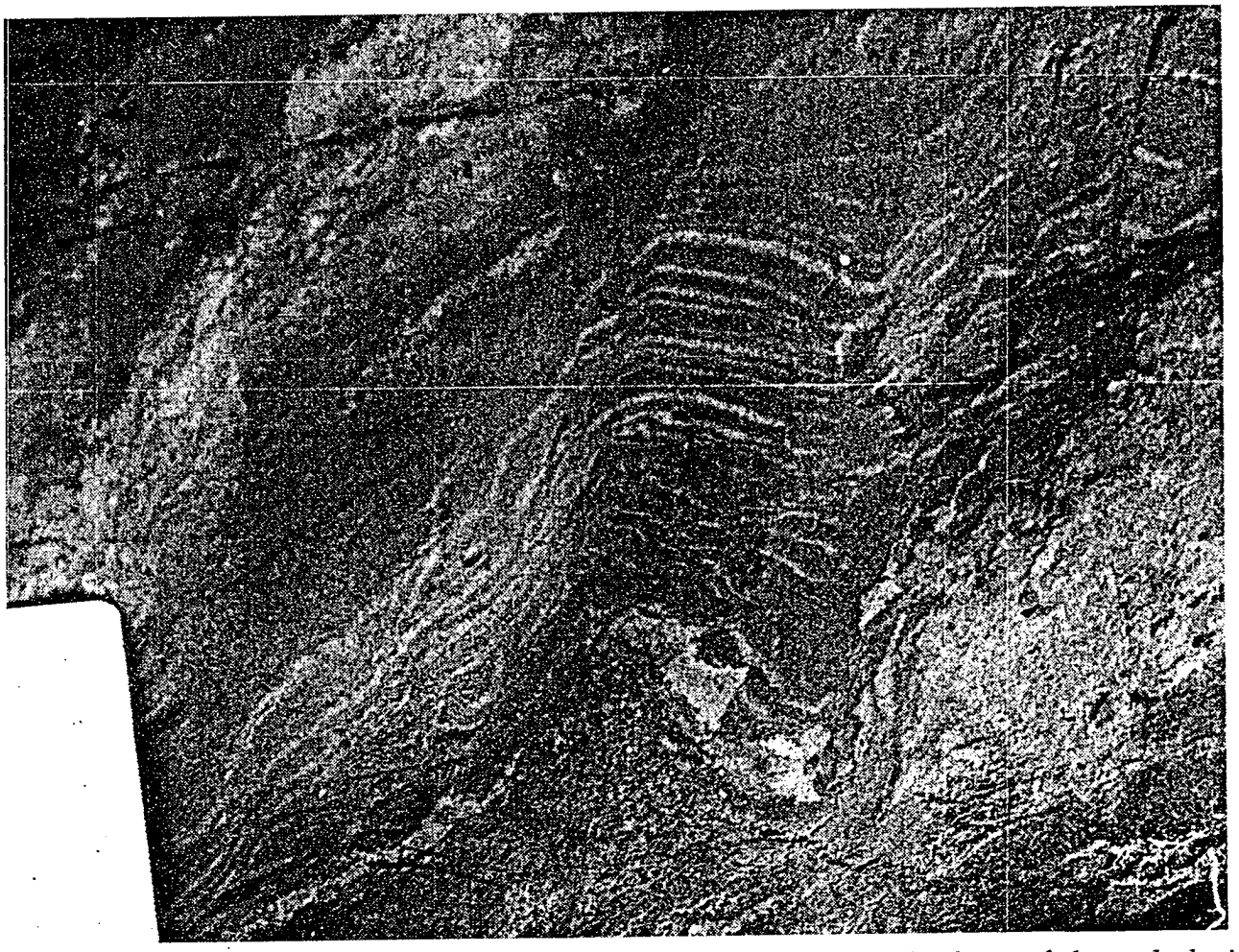

Figure 16. Detail photograph of rotational features within the shear zone at the base of the subglacial thrust sheet (Unit 7), Frutillar Bajo section. This photograph is a close-up near the end of the meter stick located in Figure 15.

along the thrust plane above the sand pod shows no laminae. A thin layer of sand was deposited along the thrust plane uphill from the sand pod.

Unit 8 is a highly-fractured, clast-rich subglacial till. Riedel shear fractures, sand-filled tension fractures, and listric normal faults developed in the underlying Unit 5 sediments indicate a shear zone (Wateren, 1995) that formed subglacially through the deposition of Unit 8. Weathering of this unit masks its origins, but lodgement till is suggested.

A contoured equal-area plot of the poles of planar fractures, faults, and contacts in this outcrop (Figure 17) shows a strong grouping of poles around pole 135°, 61°. This group is strongly influenced by the listric normal faults formed by deposition of Unit 8 subglacial till. The high-angle fractures plotted around the perimeter are Riedel fractures, formed in a subglacial brittle shear zone.

Significance of the Frutillar Bajo Section

The Frutillar Bajo section records at least three glacier advances up the slope out of the Frutillar basin. Radiocarbon dates on rip-up clasts of 30,700 ± 1300 (UW-419) and 31,700 ± 1000 (UW-430) years B.P. (Porter, 1981) at the base of the outcrop indicate that these advances occurred after approximately 30,000 years B.P. Outwash units of sand and gravel at the base of the section were deposited from meltwaters produced by the approaching glacier, these units culminating in the minor formation of localized flow till diamicts as the ice margin passed over this location. As the glacier advanced to its

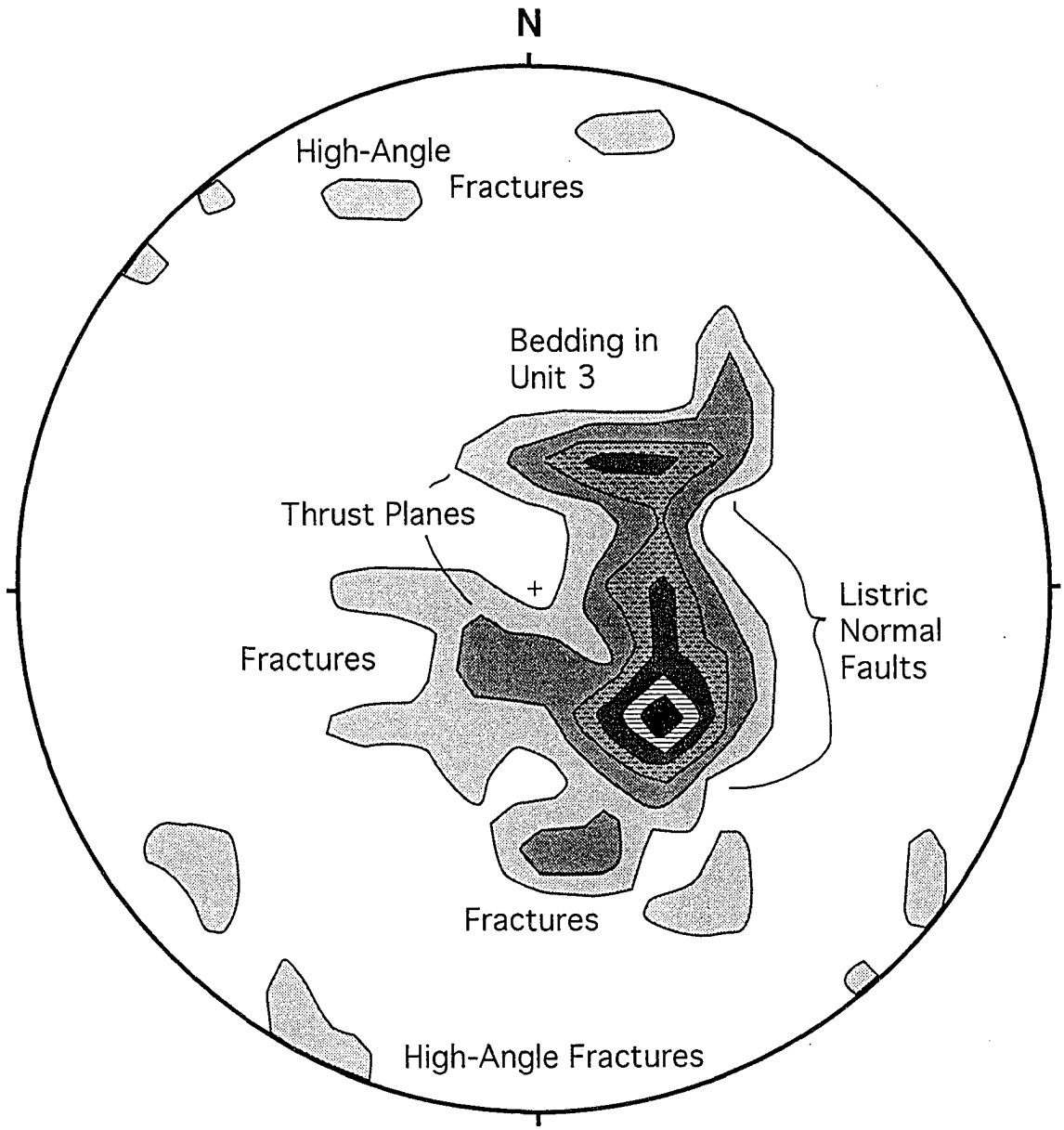

Figure 17. A contoured equal-area plot of the poles to planar features (fractures, faults, and contacts) of the Frutillar Bajo section, using the 1% area method. Contours are drawn at 2% intervals. The major grouping of poles is strongly influenced by the listric normal faults that formed with the deposition of Unit 8 subglacial till. This figure is modified from one produced using the Stereonet program, version 4.9.5, copyright 1988-1995 by Richard W. Allmendinger.

maximum position and ice thickness increased, a long thin sheet of lake terrace sediments (Unit 5) was thrust subglacially over the gravel and flow till. Diamict that formed along the base of the thrust contains thin layering, similar to that proposed by Hart and Boulton (1991) to represent subglacial ductile deformation. However, the Hart and Boulton (1991) model predicts that massive diamict will overlie laminated diamict, opposite to what we find at this section. We propose that sub-thrust water flow winnowed out the fines from localized zones within the diamict, leaving behind sandy stratifications.

An ice marginal retreat past this location, followed by readvance, emplaced a three-meter silt block (Unit 6), causing a slight differential movement of the sand with the underlying silt. After the ice margin advanced again to the upper slope, another subglacial thrust sheet (Unit 7) was transported. Later ice advance formed a new diamict capping the outcrop (Unit 8) and formed the listric normal faults and fractures (Riedel shears) through the underlying thrust slice. Some sand infilling of tensional fractures occurred as well. These tension fractures and Riedel shears indicate that brittle shear (Wateren, 1995) was the primary deformation mechanism underneath the glacier.

At the middle slope position, ice-marginal glacier activity deposited flow till. Later subglacial activity under thicker glacier ice produced thrusting and injection of saturated sediments. The cohesion of the thrusted sediments did not result from their being frozen; this is shown by localized water flow

beneath the thrust sheet and hydrofracturing within the thrust sheet. Angularity of sediment grains may promote cohesion within these sediments. Thrusting produced a brittle shear zone in underlying sediments. Later, subglacial till was deposited, capping the sequence.

Punta Penas Section

About 3 km east of Puerto Montt, resistant sediments form a small point, Punta Penas, into the Seno Reloncaví basin (Figures 1 and 18); the top of this point has been modified by the local people to look like a grounded ship (Figure 19). Datum for this site is the high tide mark along the rip-rap banked against the west side of the site. The site consists of two exposures: a sea cliff with associated sediments in the tidal zone, and a roadcut northwest of the sea cliff (Figure 19). There is evidence for five major events at Punta Penas. The relationships between sediment units are shown in Figure 20, numbered in order of occurrence. Details are listed in Appendix 2-Table 3.

Two units give clues to subglacial processes at this middle slope position. The sediments in Unit 3 result from subglacial thrusting and till deposition. Unit 3 is made up of four subunits and forms the core of the sea cliff (Figure 21 and 22). Unit 3A, the lowest part of Unit 3 (Figure 22), consists of transported gravels. At the base is a sheared zone containing numerous angular clasts. Unit 3B is a laminated silt, not in its original depositional orientation, that is highly faulted at steep angles, with displacements up to a

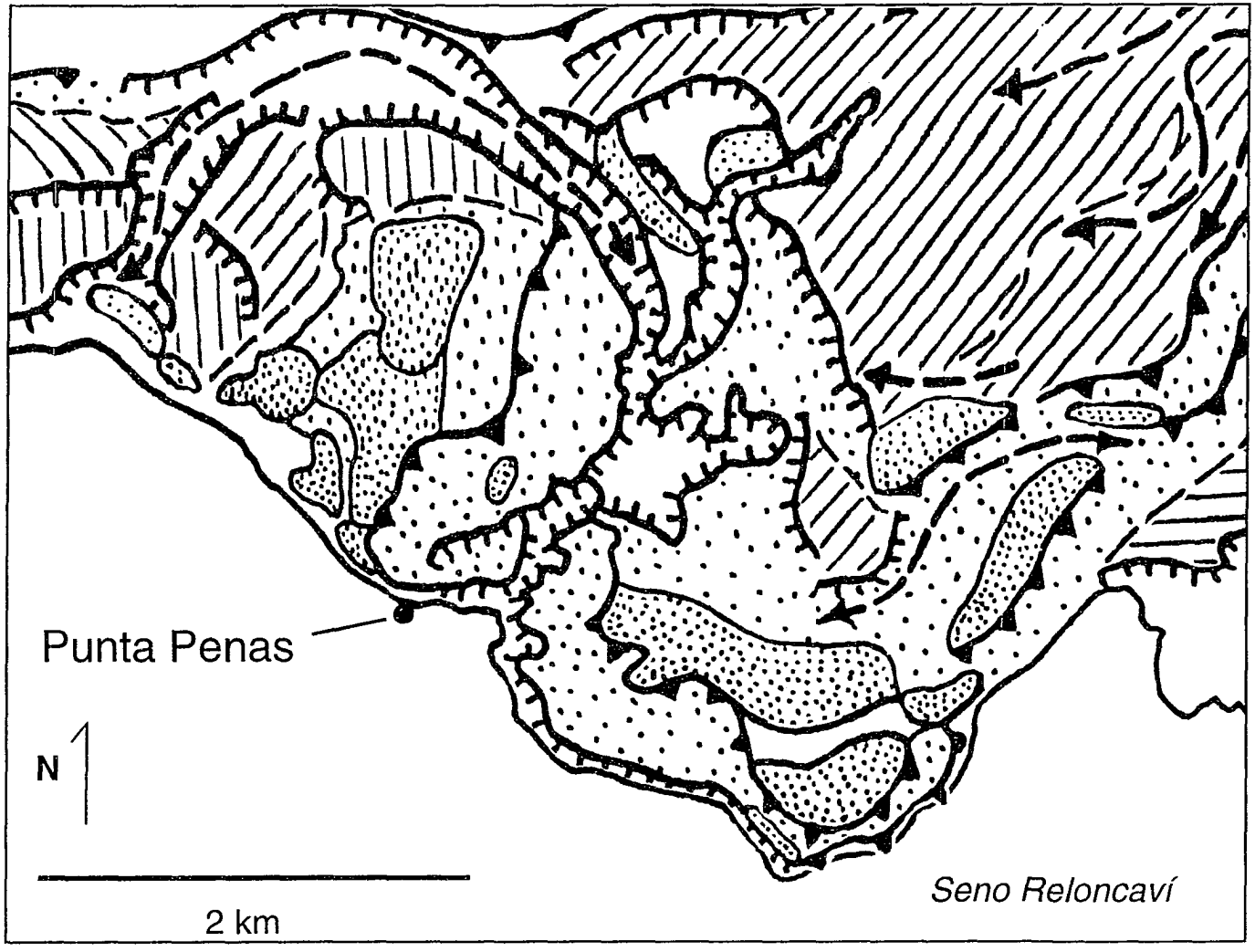

Figure 18. Map of the geomorphic landforms surrounding the Punta Penas section. This section lies at the base of an erosional scarp cut into moraine hills (from Andersen, in press). Ice flow here terminated at moraines less than ten kilometers to the northwest. See Figure 5 for legend.

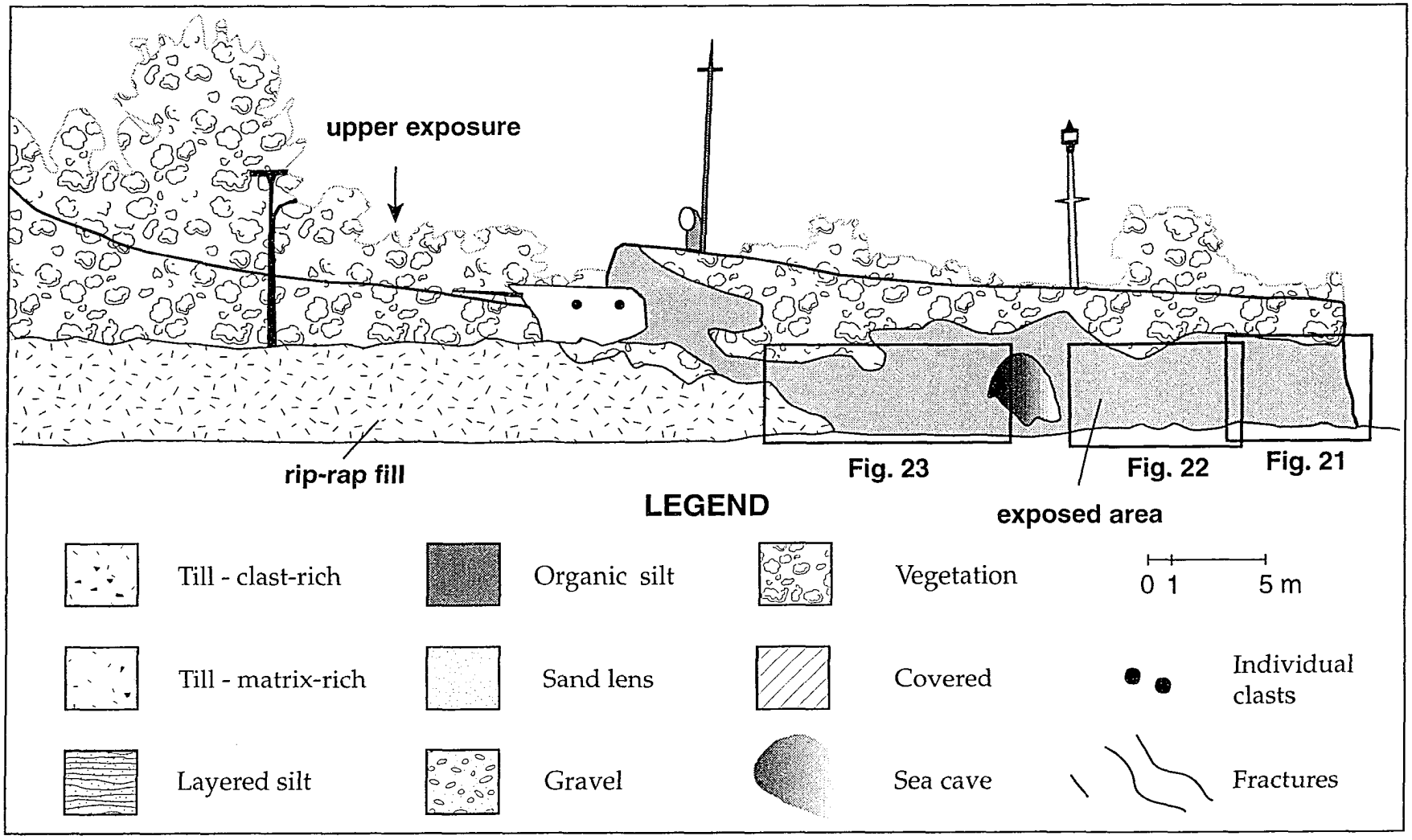

Figure 19. Overview and legend for the Punta Penas section. View is toward the east from the intertidal zone. In addition to the sediments exposed in the sea cliff (Figures 21-23), other exposures lie in roadcuts on the north side of the road and within the intertidal zone. The legend is for Figures 20-23 (locations shown by boxes).

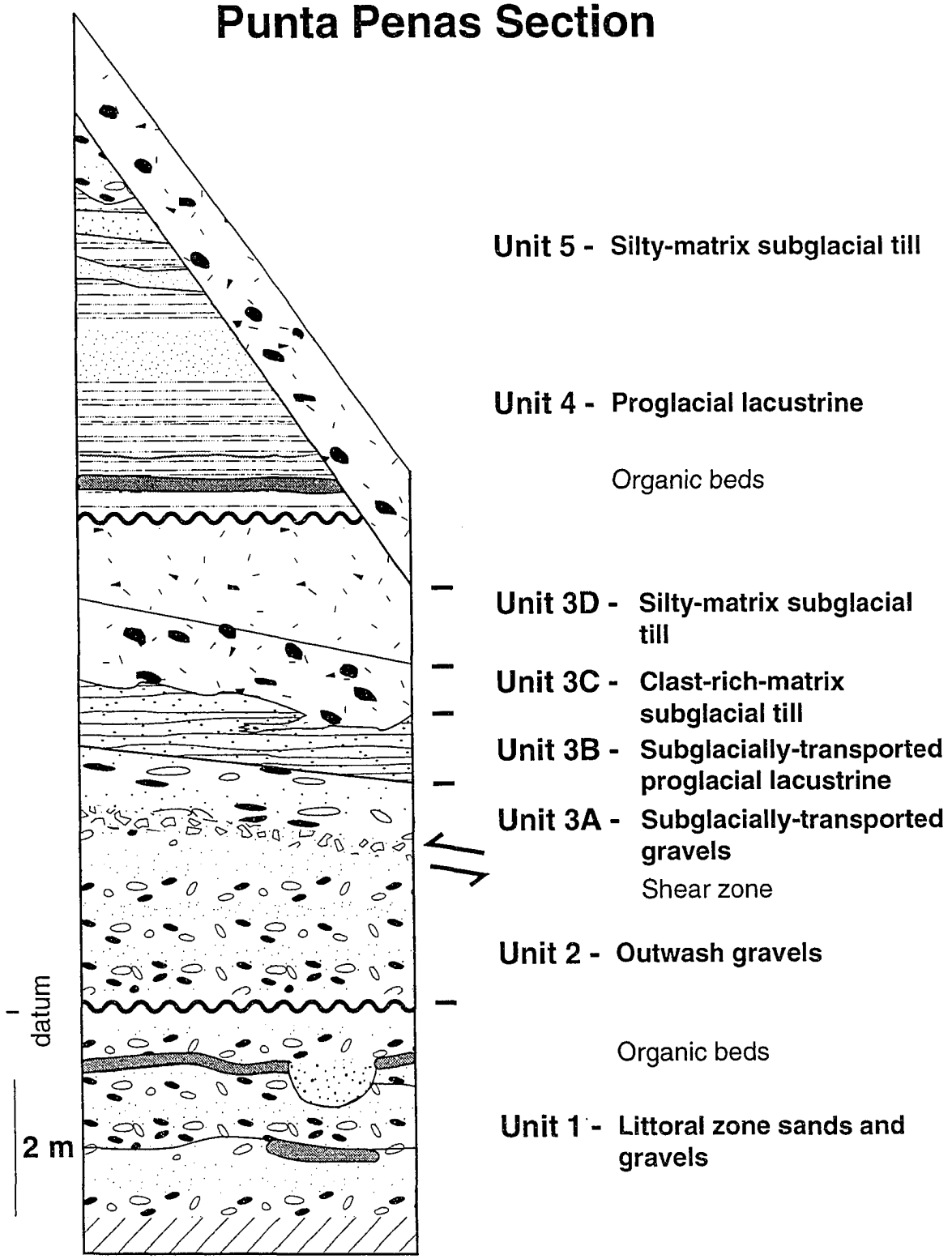

Figure 20. Composite stratigraphy of the Punta Penas section. Units 3 and 5 formed during different glacial advances. Both units provide clues to the subglacial processes of thrusting and lodgement till deposition.

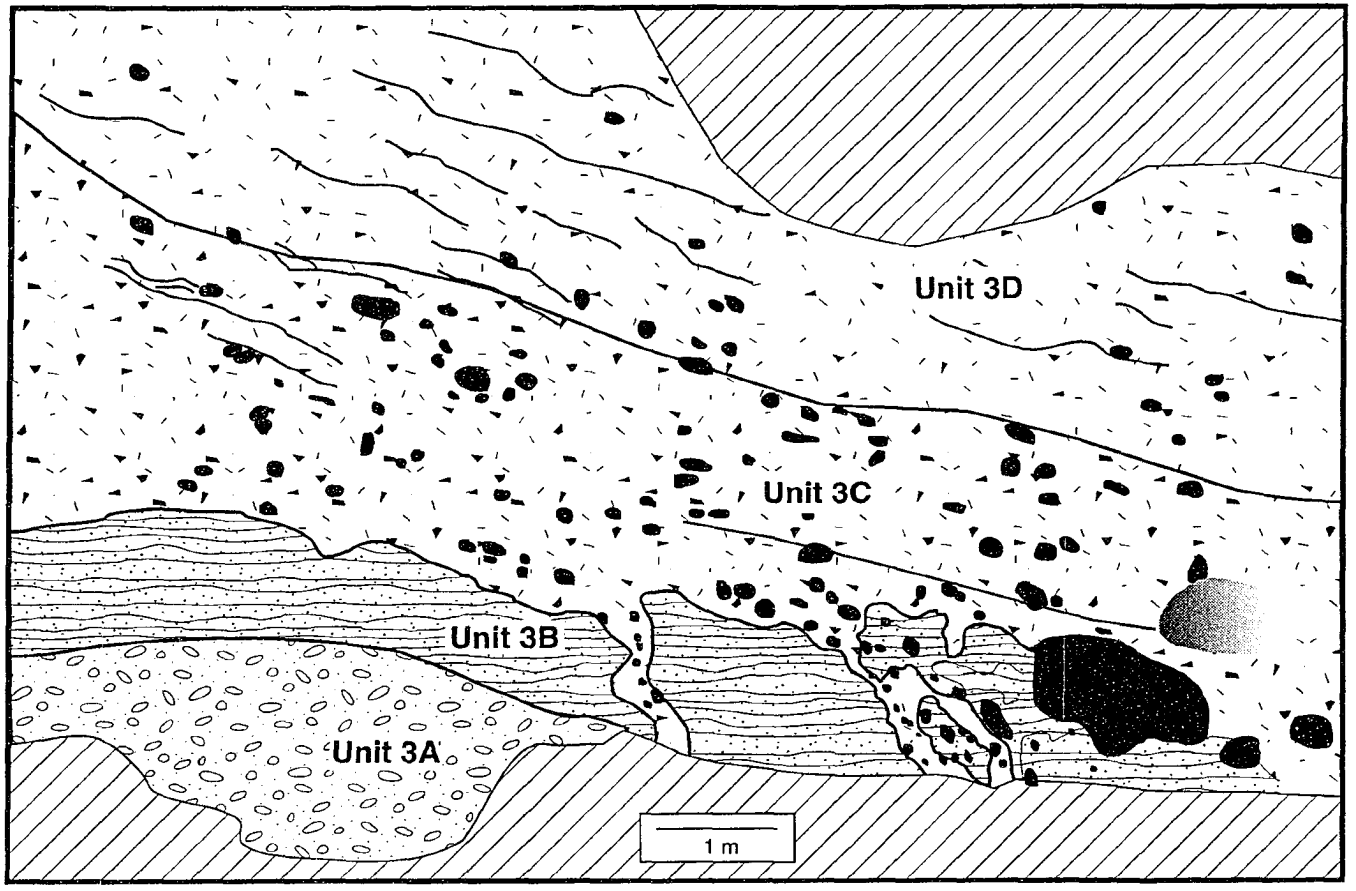

Figure 21. A) Complete section of the Unit 3 components in the Punta Penas section. Note the irregular contact between Units 3B and 3C that is broken by injections of Unit 3C diamicton into Unit 3B; these injections occurred subglacially. Overall, the lower parts of Unit 3 have nearly original composition and structure, whereas Units 3C and 3D are subglacial tills that appear to have been reworked. See Figure 19 for legend.

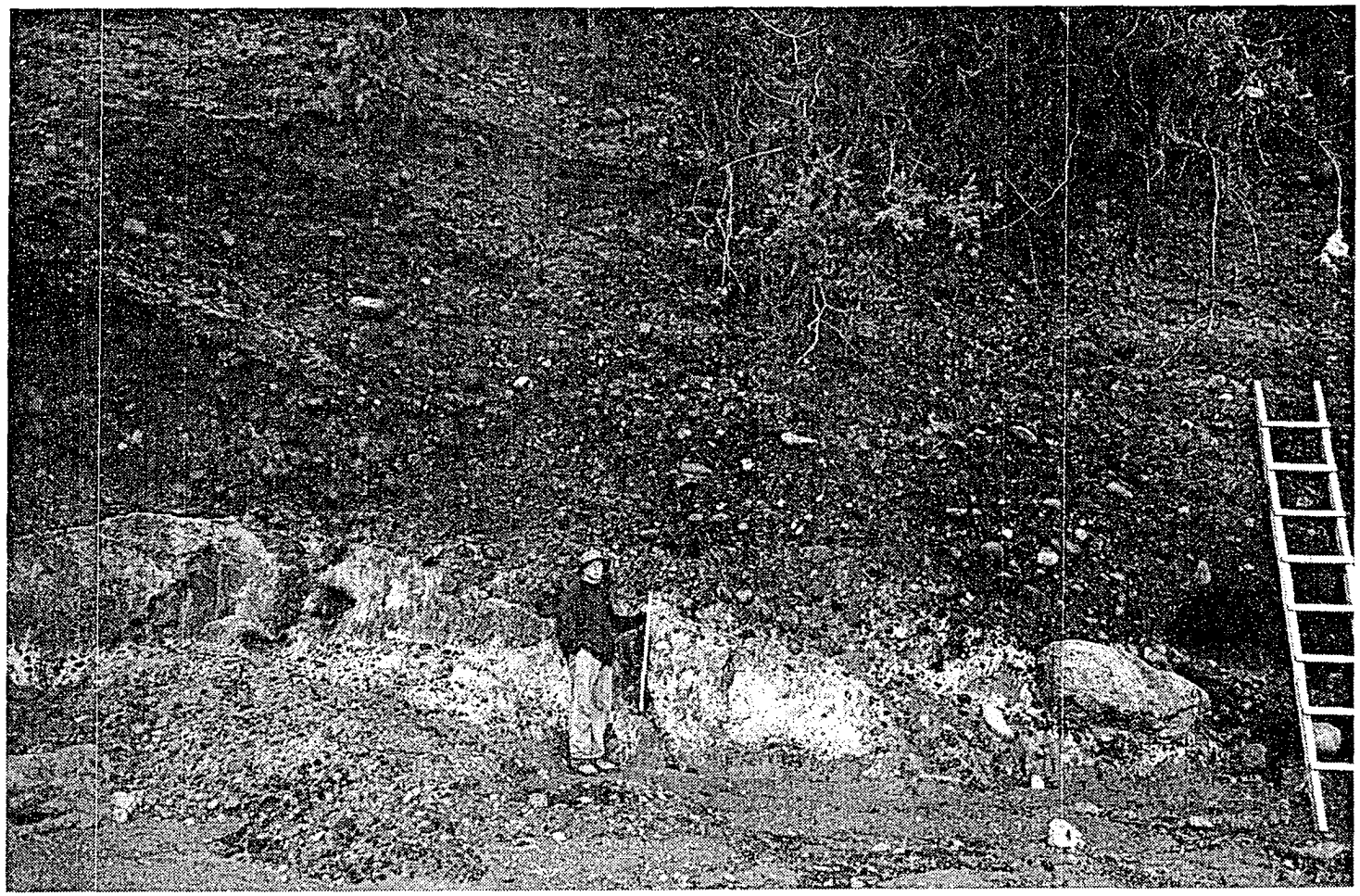

Figure 21. B) Photograph of the Punta Penas section showing the middle section of the sea cliff. I am standing next to one injection of Unit 3C downwards into Unit 3B silt; others can be seen halfway between the ladder and myself. The division of units is shown in part A of this figure.

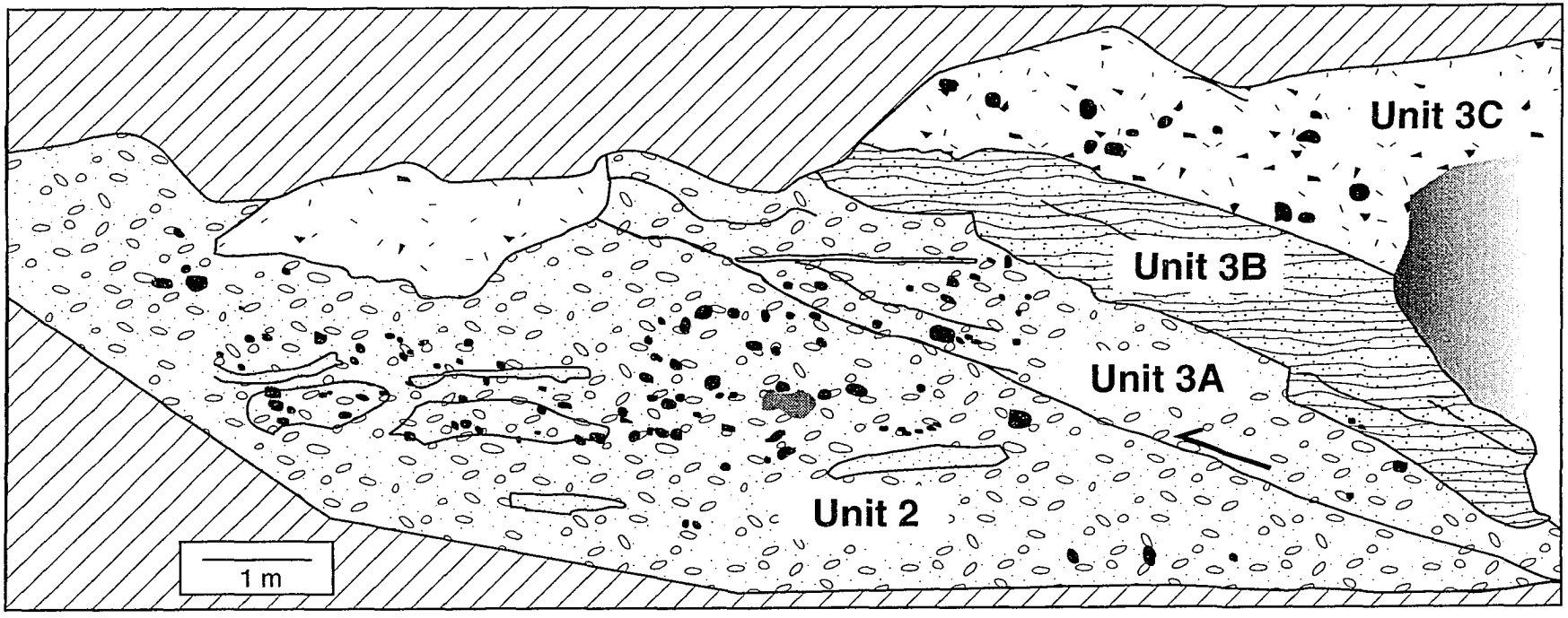

Figure 22. A) The contact between Units 2 and 3 in the Punta Penas section. Unit 2 is horizontally-bedded outwash gravel. The shear zone at the base of Unit 3A marks the beginning of the subglacial sequence. The outwash gravel of Unit 3A was thrust subglacially along with Unit 3B silt. See Figure 19 for legend.

Figure 22. B) Photograph of the Punta Penas section showing the landward portion of the sea cliff. The white box marks the approximate area represented in part A of this figure.

few centimeters. The discontinuous nature of the silt, its irregular contacts, and the extensive internal fracturing indicate that this unit was transported in the subglacial position. Small injections of Unit 3C diamicton can be traced in fractures downward into this silt. At the seaward side of the exposure, diamicton was injected upward through this silt. At the landward side of the exposure, much smaller injections penetrate downward into the silt package (Figure 21) from Unit 3C, a subglacial till. The uppermost subunit, Unit 3D, is a subglacial till of lower clast concentration than Unit 3C.

The entire Unit 3 package is interpreted as (1) subglacial thrust slices of marine terrace sediments (Units 3A and 3B), overlain by (2) these same sediments reworked and deposited as subglacial till at the top (Units 3C and 3D).

Unit 5 is a subglacial till, deposited by a subsequent glacial advance, that crosscuts Unit 3 sediments at the tip of the point (Figure 23) and Unit 4 sediments on the terrace. Fracture planes parallel the angular unconformity with Unit 3.

Significance of the Punta Penas Section

The overall stratigraphy (Figure 20) indicates that at least two glacial advances overran this site. Ives *et al.* (1964), Porter (1981), and Lowell *et al.* (1995) have reported radiocarbon dates from this site of two different ages. The sediments from the older advance (Unit 3) are complex but informative. The base of Unit 3 is a zone of broken clasts, indicating that differential

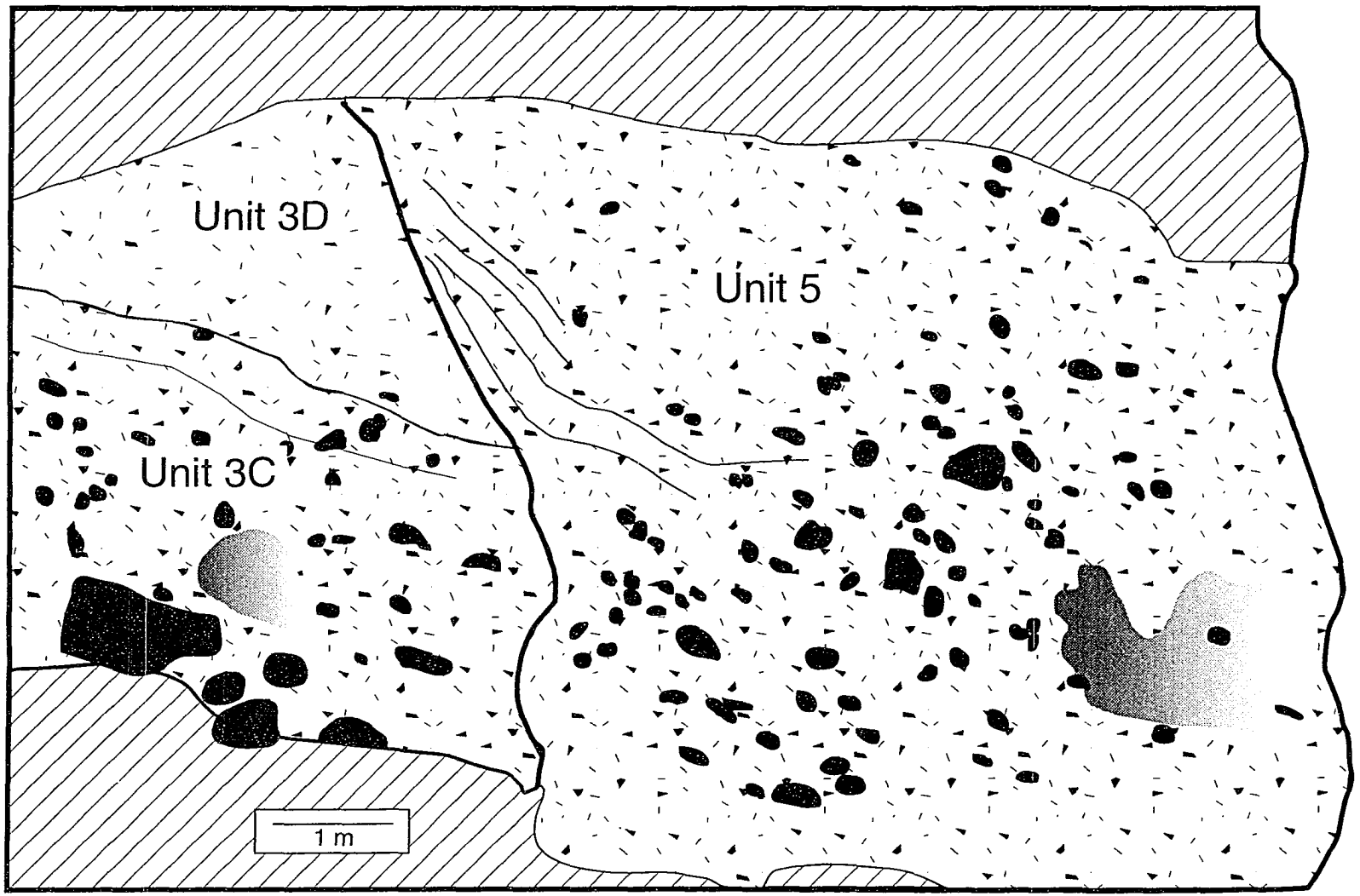

Figure 23. A) Unit 5 cross-cutting the older sediments of Unit 3 in the Punta Penas section. Because Unit 5 subglacial till is resistant to erosion, it forms a cap that protects the point. The fractures that parallel the base of Unit 5 are evidence of the subglacial deposition of this till. See Figure 19 for legend.

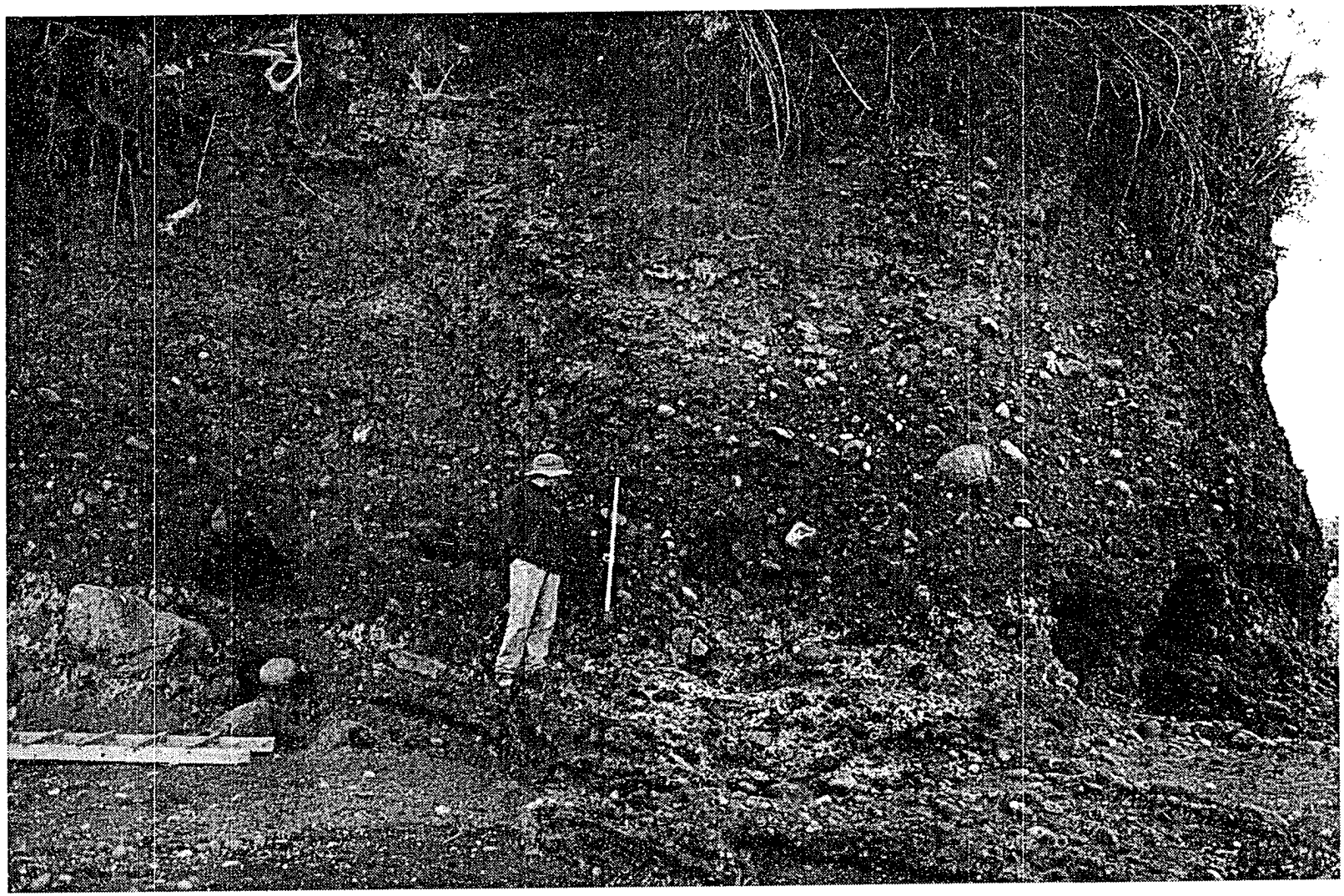

Figure 23. B) Photograph of the Punta Penas section (corresponding to part A of this figure) showing the seaward section of the sea cliff. I am standing at the contact where Unit 5 subglacial till overrides Unit 3 subglacial till.

movement occurred. Hydrofractures into the silt suggest that water was present during the faulting; therefore, the thrust slice was not frozen. That the silt was transported intact requires some cohesive force during its transport. Hydrofracturing and clastic dike formation (Boulton and Caban, 1995) downward into the silt reveal the subglacial position of the thrust slice. Upward hydrofractures formed during a later glacial advance, with the silt acting as a low-permeability layer near the ice margin.

The general upward-fining of the diamicton matrix in the upper two subunits of Unit 3, combined with the corresponding drop in clast concentration, may imply that the subglacial lodgement process is able to rework the underlying sediments.

The younger advance also deposited a subglacial till (Unit 5), but had a basal sole inclined at an angle slightly higher than that of the older advance (Unit 3). The shear planes at the base indicate that the sole alternately slipped over the bed, moving and depositing till as a result of friction on basal sediments, or coupled with underlying till, shearing through it. The fine matrix containing rounded clasts indicates reworking of sediments. The degree of reworking can not be quantified, however, because the unit overlies another subglacial till.

At this middle slope position, initial glacial activity produced low-angle subglacial thrusting of marine terrace sediments, indicating that the glacier was coupled to its bed. Later, the glacier began slipping over its bed, resulting in the deposition of lodgement tills. Deposition of lodgement till

(upper slope facies) capping the middle-slope sequence indicates that the subglacial conditions found at each slope position can change over time. Fluctuations between the conditions causing coupling of the glacier with its bed and those causing sliding of the glacier over its bed resulted in shearing through the till. Reworking within the tills is indicative of a subglacial shear zone throughout the till sequence.

Discussion of the Middle Slope Position

Two different sets of processes are seen at the middle slope position. Ice-marginal processes resulted in the deposition of flow till and movement of large sediment blocks, as at the Frutillar Bajo section. A second set of processes occurred subglacially when the glacier was standing at its maximum position. This second set of processes includes large-scale subglacial thrusting of unconsolidated sediments, fluid injection, and lodgement till deposition.

Permafrost is commonly suggested to influence the distribution of subglacial processes (Piotrowski, 1993; Boulton and Caban, 1995) and promote cohesiveness of unconsolidated sediments (Wateren, 1995). However, Heusser *et al.* (1996) estimate a mean annual temperature of 6-8 °C for this area at maximum glaciation, based on pollen data. These conditions are too warm to allow permafrost to develop; this implies that permafrost is not necessary to cause cohesiveness of unconsolidated sediments, as seen here.

However, some winter freezing of sediments certainly occurred, allowing the possibility that short-term freezing events promoted

cohesiveness of thrusted sediments. In a modern analog, Krüger (1993) described thrust slices moved by the glacier margin after winter freeze-on. These thrust slices were 0.3 to 0.9 meters thick and developed under thin ice less than 20 meters from the margin. Freeze-on during winter cycles, then, is a viable method for thrusting thin layers of unconsolidated sediments at the glacier margin, where the ice is thin and allows penetration of winter cold to the glacier base. However, the middle slope thrust sheets we have studied are from 1 to 4 meters thick and 25-40 meters long, and were transported under thicker ice (probably at least fifty meters thick, based on the elevation difference to the moraine crest). We suggest that the ice thickness at the middle slope position prevented propagation of the 0 °C isotherm to the glacier base, ruling out winter freeze-on.

By what mechanism, then, are these unconsolidated sediments thrusted? We propose that two factors may be involved in promoting unconsolidated thrusting: subglacial bed angle and porewater pressure.

We propose that there is an optimal angle (10-15°) that allows thrusting to occur, because that angle minimizes the overburden while at the same time maximizing basal shear stress to produce thrusting. All middle slope thrust slices, characteristic along the inside of these basins, had this 'optimal angle' orientation.

The second mechanism relates to the porewater pressure in the subglacial regime. Piotrowski (1993) reported that ice overburden caused high pore-water pressure in undrained outwash sediments, which in turn induced

thrusting. Boulton and Caban (1995) also propose that a high porewater pressure gradient plays a major role in promoting thrusting. Porewater pressure builds up beneath an aquiclude, causing the effective pressure to decrease towards zero; a natural slip plane is formed along the base of the aquiclude layer where the effective pressure is small.

Upper Slope Position

The upper slope position (Figure 3) ranges from 110 to 160 m elevation in the Frutillar basin, and encompasses approximately the upper third of the exposed topography. The sediments found here are lodgement till, flow till, and high-angle thrust slices of previously-deposited sediments.

Frutillar Alto Section

The Frutillar Alto section is located in the distal moraine crest on the road from Frutillar Bajo to Frutillar Alto (Figure 11). An ice marginal channel with a basal age of 19,760 +250/-240 years B.P. (A-8534R- Denton *et al.*, 1997) separates this moraine from the Frutillar Bajo section (Figure 11), allowing the possibility that the advances forming this moraine may be older than those recorded in the Frutillar Bajo section. Nine units form this outcrop; these are shown schematically in Figure 24 in order of occurrence, with details given in Figures 25 and 14, Appendix 2-Table 4, Appendix 3-Table 2, and Plate II.

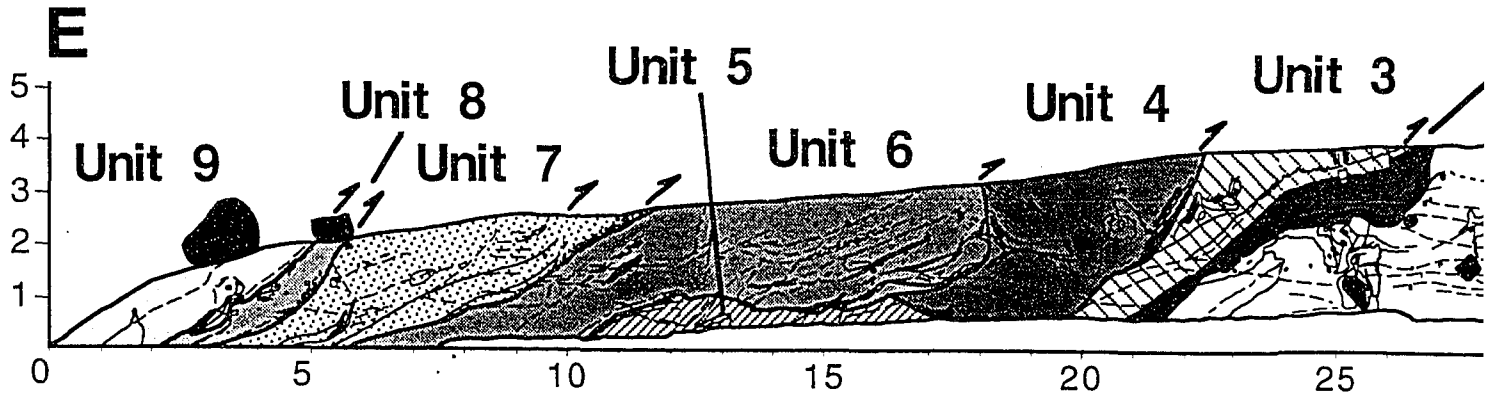

Figure 24. Schematic diagram of the Frutillar Alto section, showing the nine sediment units. Units 3, 4, 6, 7, 8, and 9 are ice-marginal thrust slices of flow till diamict or brown silt, probably transported by the winter freeze-on method observed by Krüger (1993).

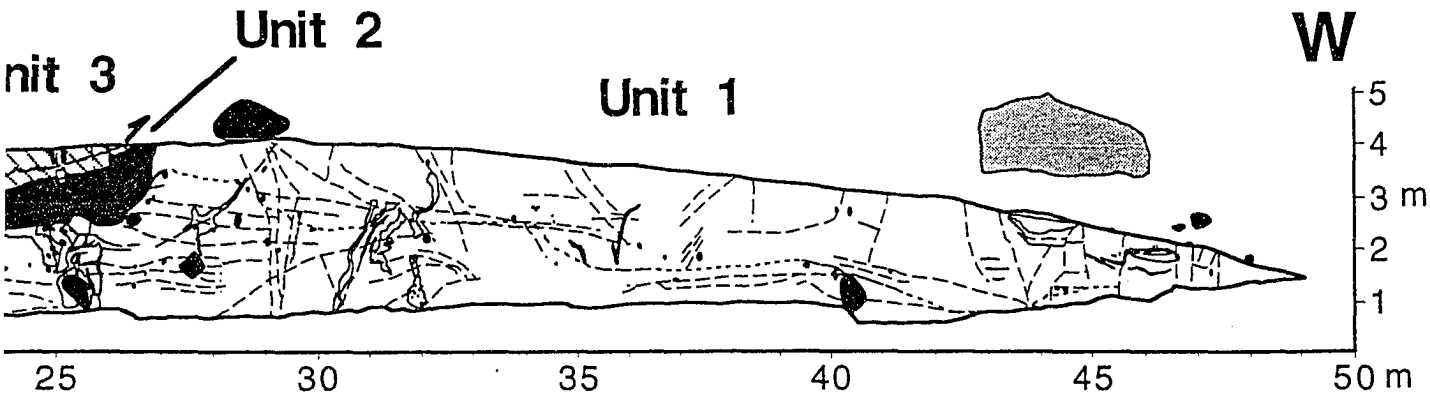

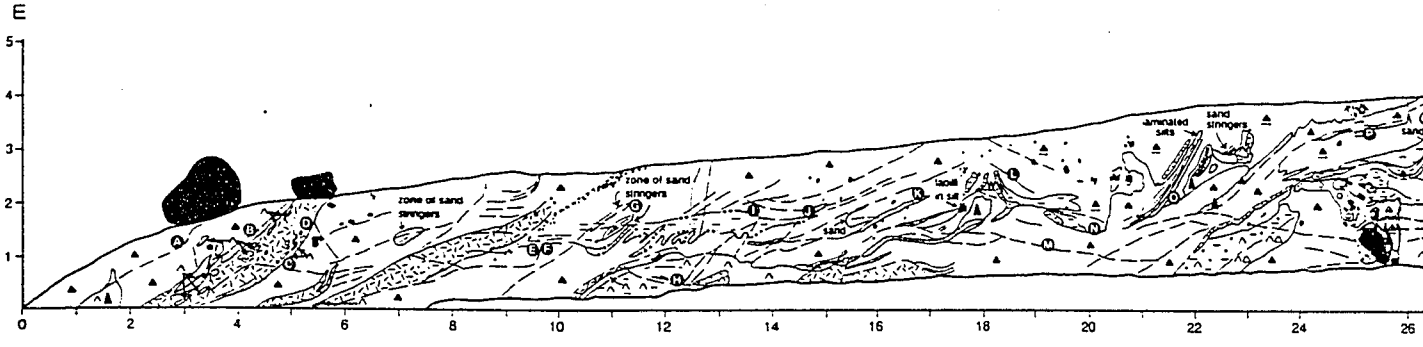

Figure 25. Detailed map of the Frutillar Alto section, which occupies an upper slope position. See Figure 14 for the legend.

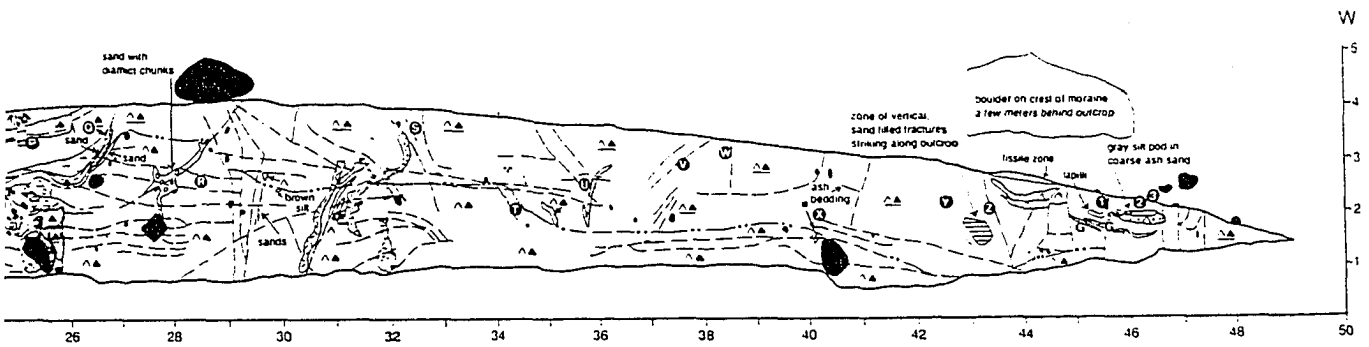

In general, the outcrop is composed of two diamicton units- one brown overlain by one gray. However, only brown diamicton is present east of the 18 meter mark (Figure 25 and Plate II), suggesting that color indicates a difference in composition between the diamictons, rather than a difference in weathering between the top and bottom of the outcrop. These diamicts are interpreted as debris flow tills from the glacier margin. Sediment pods contained in the diamicts formed as lithologically-different flows or as a result of localized ponding and deposition therein. Sand-filled fractures suggest minor episodes of fluidization and injection. This injection occurred after rapid deposition sealed off saturated sediments in locally-ponded waters; the imposition of overburden gave trapped water enough pressure to break through in fractures.

The sediments in Units 1, 2, and 5 were probably deposited in place. The remainder of the units (Units 3, 4, 6, 7, 8, and 9) have been affected by thrusting. These units record at least six fluctuations of the glacier margin. Units 3, 4, 6, and 9 are slices of previously-deposited flow till diamict, thrust at steep angles. Unit 7 is a slice of brown silt overlain by diamict, thrust over a stone layer previously-developed along the glacier sole. Unit 8 is a thrust slice of brown silt.

A contoured equal-area plot of the poles to the fractures, faults, and contacts in this outcrop shows several groupings (Figure 26). These orientations form part of a NW-SE great-circle girdle, indicating that these

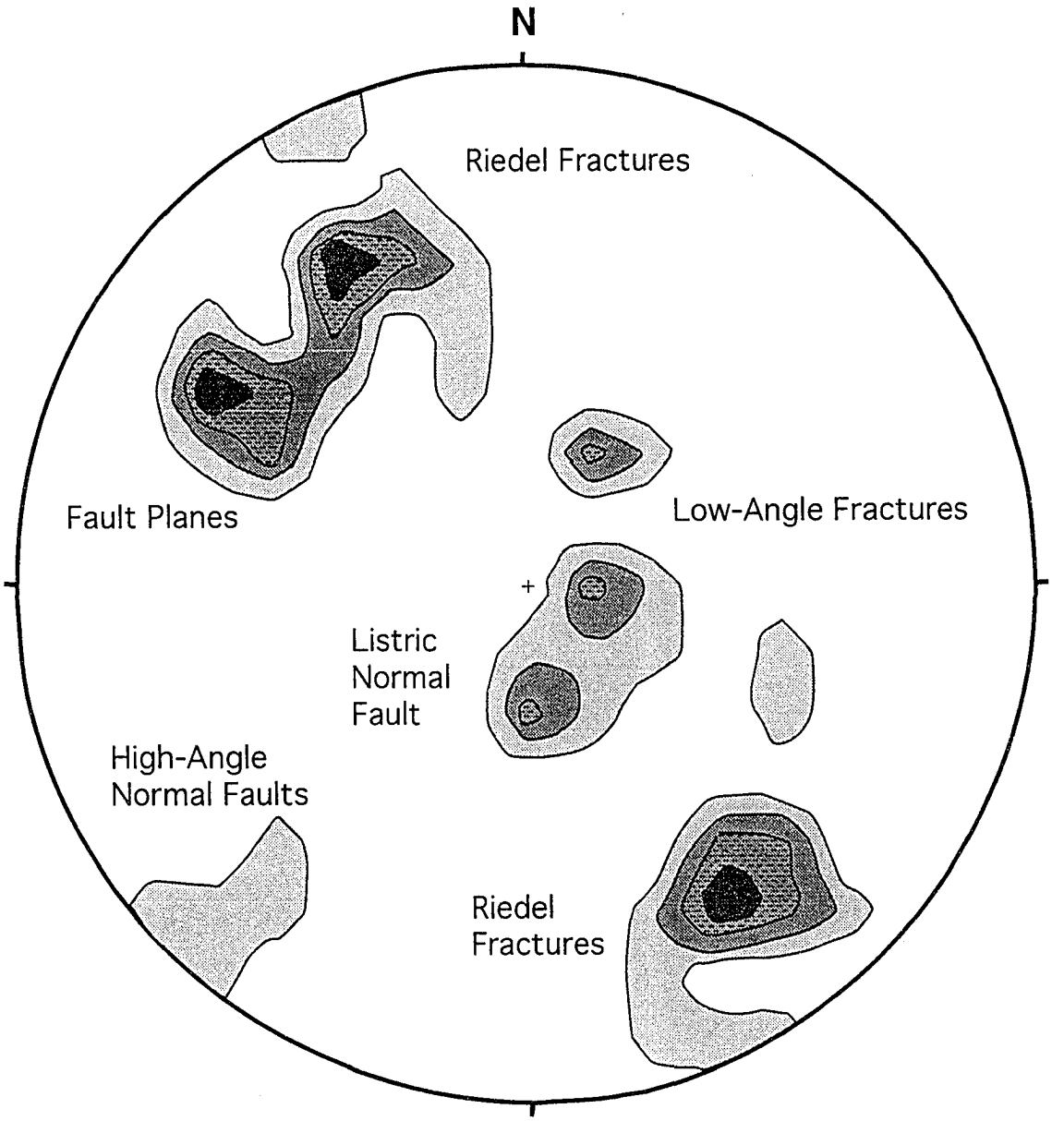

Figure 26. A contoured equal-area plot of the poles to the planar features (fractures, faults, and contacts) of the Frutillar Alto section, using the 1% area method. Contours are drawn at 2% intervals. The groupings of poles form a NW-SE great-circle girdle, indicating that all features were oriented perpendicular to one stress direction, in this case the ice flow direction to the northwest. This figure is modified from one produced using the Stereonet program, version 4.9.5, copyright 1988-1995 by Richard W. Allmendinger.

planar features were all oriented so that they were dipping directly toward or away from one major stress direction. This stress direction is the ice flow direction, to the northwest at this upper slope position. The shallowly-dipping poles at either end of the girdle correspond to the steeply-dipping Riedel fractures; the high-angle thrust planes dip slightly more westward than the NW-dipping Riedel fractures. The middle group of poles corresponds to the listric normal fault and low-angle fractures found in this outcrop.

Significance of the Frutillar Alto Section

The lack of internal deformations within these thrust slices suggests that these thrusts are subglacial features, not resulting from proglacial ice push. The stone layer developed along the thrust plane beneath Unit 7 suggests a short period of lodgement during which the glacier sole slipped over its bed, before Unit 7 sediments were thrust into their present position. Except for this minor episode of slip, the glacier margin was coupled to its bed. Krüger (1993) described a process of ridge formation in Iceland by which this Chilean ridge probably formed. The stable, thin ice margin of Myrdalsjökul glacier allowed winter freeze-on of subglacial sediments. Minor, yearly fluctuations of the margin then thrust these frozen sediment slices to the maximum ice position and stacked them at high angles. The ice-marginal position of this section encouraged deposition of debris flows along with the thrust slices.

At this upper slope position, glacier activity resulted in the deposition of flow tills in conjunction with multiple thrusting events as the glacier margin fluctuated. Only minor lodgement of clasts occurred. Localized ponding developed between thrust slices; fluid injections occurred after deposition of flow till sealed off these saturated sediments and overburden of ice and sediment was imposed.

Trapén Section

This north-facing section is located along a gravel road near Trapén, north of Ruta 5 (Figure 1). This section is part of the moraine crest for the Seno Reloncaví lobe (Figure 27). Where this road cuts through the moraine the road has a downhill projection towards azimuth 120° with slope of 10°. The sediment units at this site are described in detail in Appendix 2-Table 5.

In this section, basal lodgement till (Unit 2) overlies proglacial outwash gravel (Unit 1). At the base of this till, stratified sediments (Unit 3) were deposited. Drag-folds formed as this unit was thrust subglacially (Figure 28). Diapirs of silt rise upward through the overlying till from the tips of the thrust planes. These silt diapirs resulted either from liquefaction during faulting or from groundwater flow carrying silt into fractures originating at the fault plane. Another sequence of stratified sediments (Unit 4) was deposited above till, half a meter from the basal gravel/till contact. Open matrix, grain-to-grain contacts within sands of this unit indicate water flow during deposition.

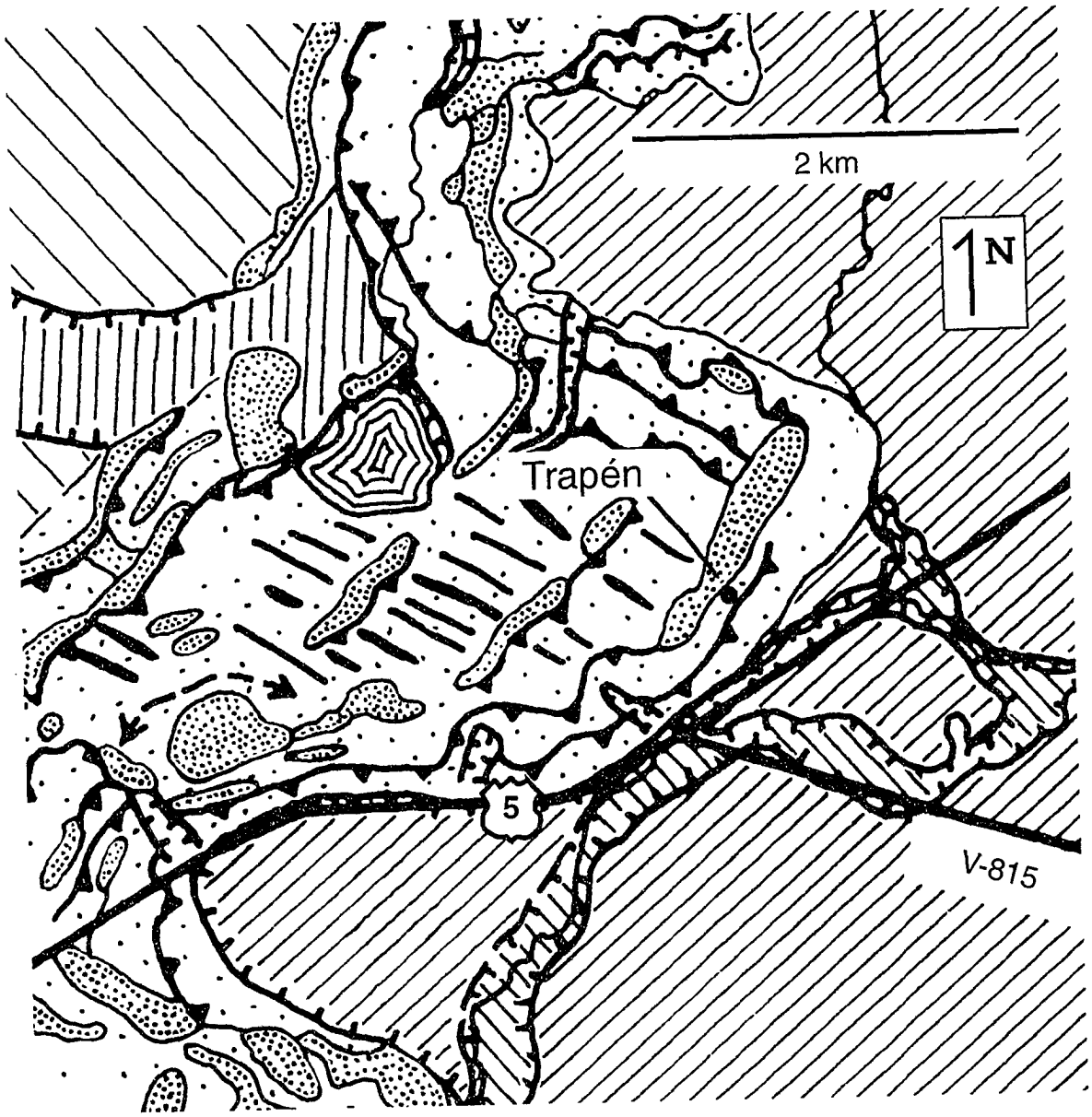

Figure 27. Map of the geomorphic landforms surrounding the Trapén section (from Andersen, in press). This section lies within a moraine crest formed at a terminal position of the Seno Reloncaví lobe. Ice flow was to the northwest. See Figure 5 for legend.

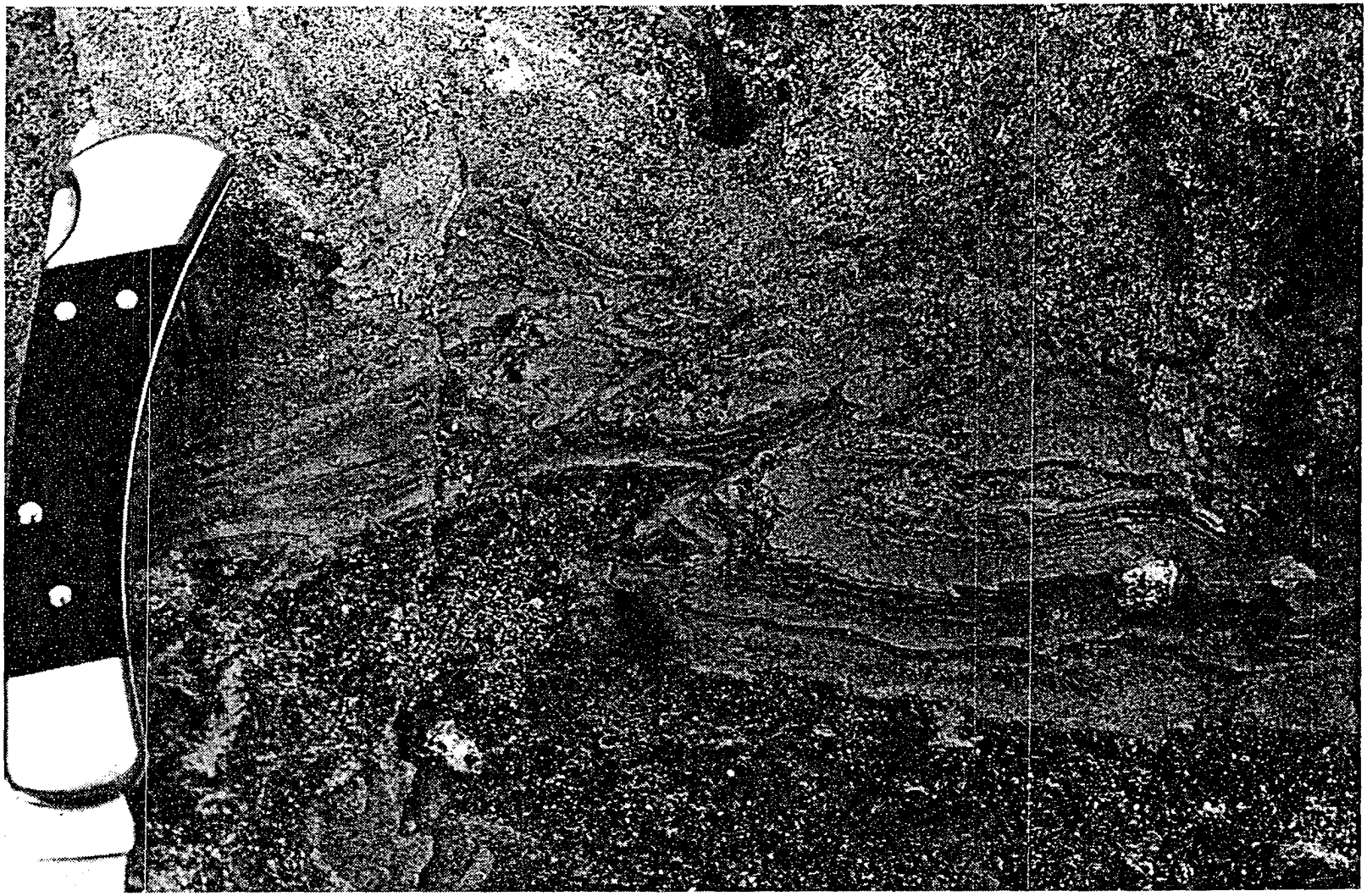

Figure 28. Detail photograph in the Trapén section, showing the thrusts through Unit 3 silt and sand beds and their associated silt injections upward into Unit 2 lodgement till. The handle of the knife is approximately 4.5 inches long.

Significance of the Trapén Section

Lodgement till was deposited at this upper slope position. Sediments resulting from localized ponding and ice-marginal water flow (Units 3 and 4 respectively) were deposited within the till as the ice margin fluctuated.

Shear planes in the till and Unit 3 silt indicate episodes during which the glacier was coupled to sediment at its base. Except for some localized areas of stratified sediment deposition within till, all sediment found here is lodgement till or proglacial outwash gravel. The preservation of stratified sediments within the lodgement till rules out deposition of the till by the deformational process as proposed by Hart and Boulton (1991), unless this process was only initiated at the top of the sequence.

Discussion of the Upper Slope Position

Glacial processes at the upper slope position resulted in small-scale thrusting of thin sediment slices at high angles, and lodgement till deposition. In all sites studied, lodgement till was only deposited higher up in the topography- on the upper slope or capping the slope stratigraphy, as at Punta Penas.

Freeze-on during winter cycles is a viable method for thrusting thin layers of unconsolidated sediments at the upper slope position (as at Frutillar Alto), where the ice margin is thin and allows penetration of winter cold to the glacier base. Krüger (1993) describes this process as it occurred in Iceland.

Thrusting events on the upper slope have a different style than those seen on the middle slope. In the upper slope, thrust planes are steeper and cut through glacial diamicton units, because previously-deposited glacial sediments were frozen-on to the glacier sole. In the middle slope, subglacial thrusting formed lower-angle, continuous slices of older lake terrace or marine terrace sediments, with diamicton formed at the base. The boundaries of a middle slope thrust sheet were controlled by lithology of the subglacial sediments, not by depth of freezing.

Discussion and Conclusions

Dreimanis' model of the temporal relationships between till types (1988) shows the vertical sequence of the four end-member sediments (melt-out till, deformation till, lodgement till, and gravity flowtill) that develops at one location over time. This study looks instead at the spatial distribution of glacially-derived sediments that develops at one time. Ultimately, this study proposes a model in which topography controls the spatial distribution of subglacial sediments and processes during one time slice (Figure 29D).

In summary, the glacially-derived sediments in the Lago Llanquihue region of Chile resulted from two different sets of glacial processes. One set occurred over time as the glacier advanced and retreated. These processes include glaciolacustrine sedimentation and clastic dike formation at the lower slope position (Figure 29A and B) and outwash and flow till deposition at the

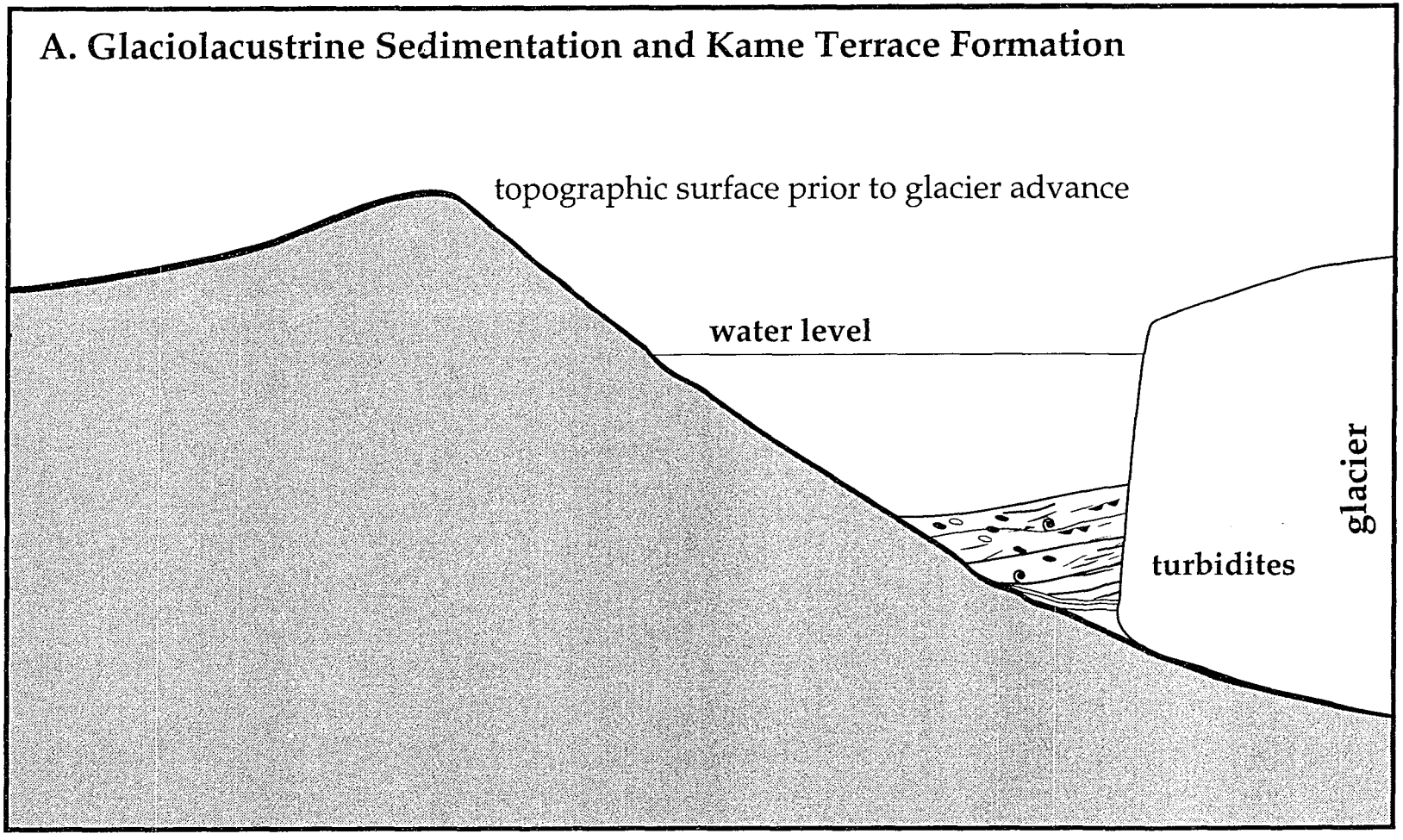

Figure 29. Topography-Dependent Facies Model of Glacial Deposition, Lake District, Chile.
A) Ice-marginal sedimentation over time into a glacially-dammed sub-basin builds a kame terrace of turbidite layers. The force of the turbidity currents deforms underlying layers.

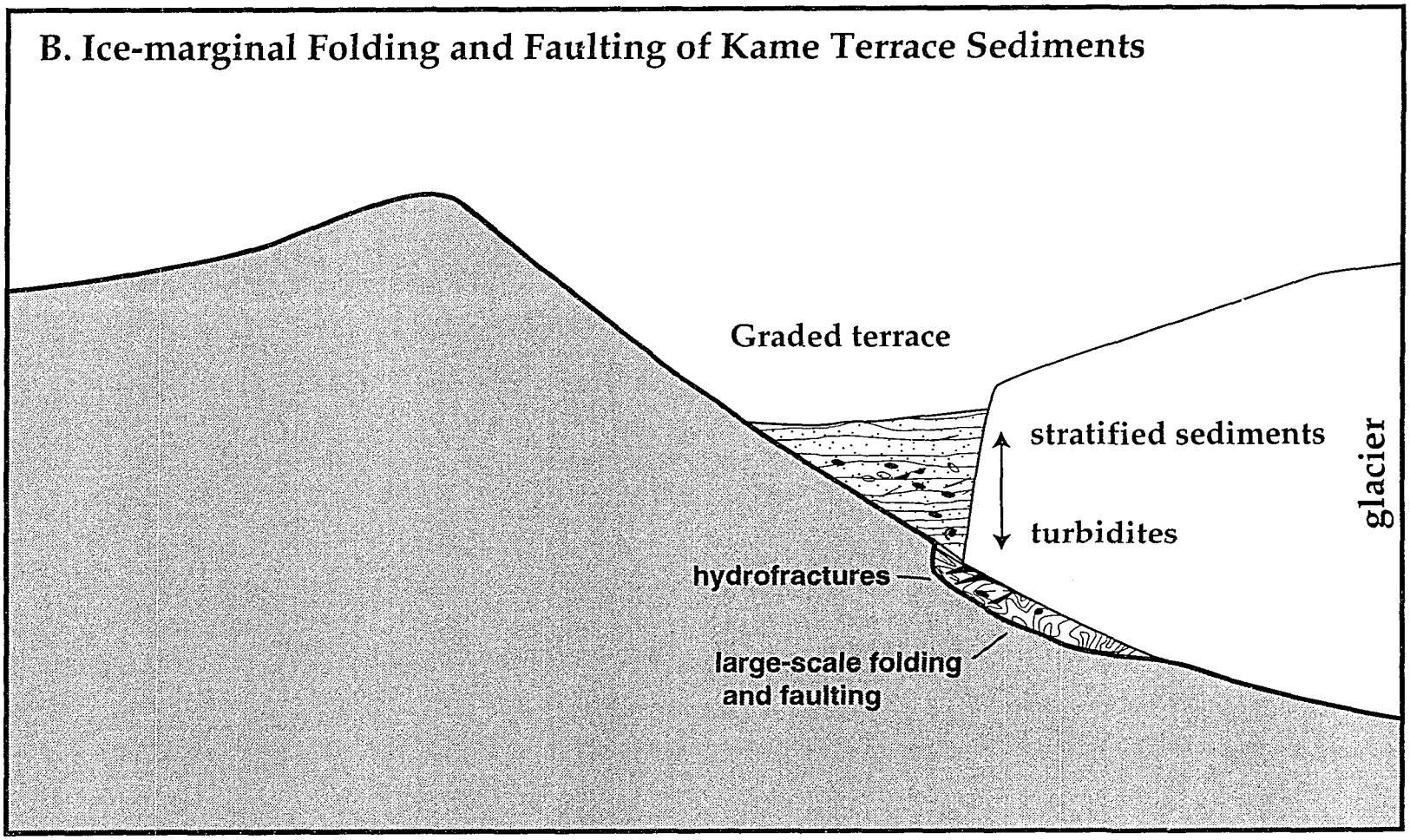

Figure 29. B) Ice advance causes hydrofracturing and large-scale thrusting of sediment blocks, especially in interlobate regions of the ice margin where stresses converge. Ice advance could occur at any time after kame terrace formation; the ice advance that formed the terrace is not necessarily the same advance which later deforms it.

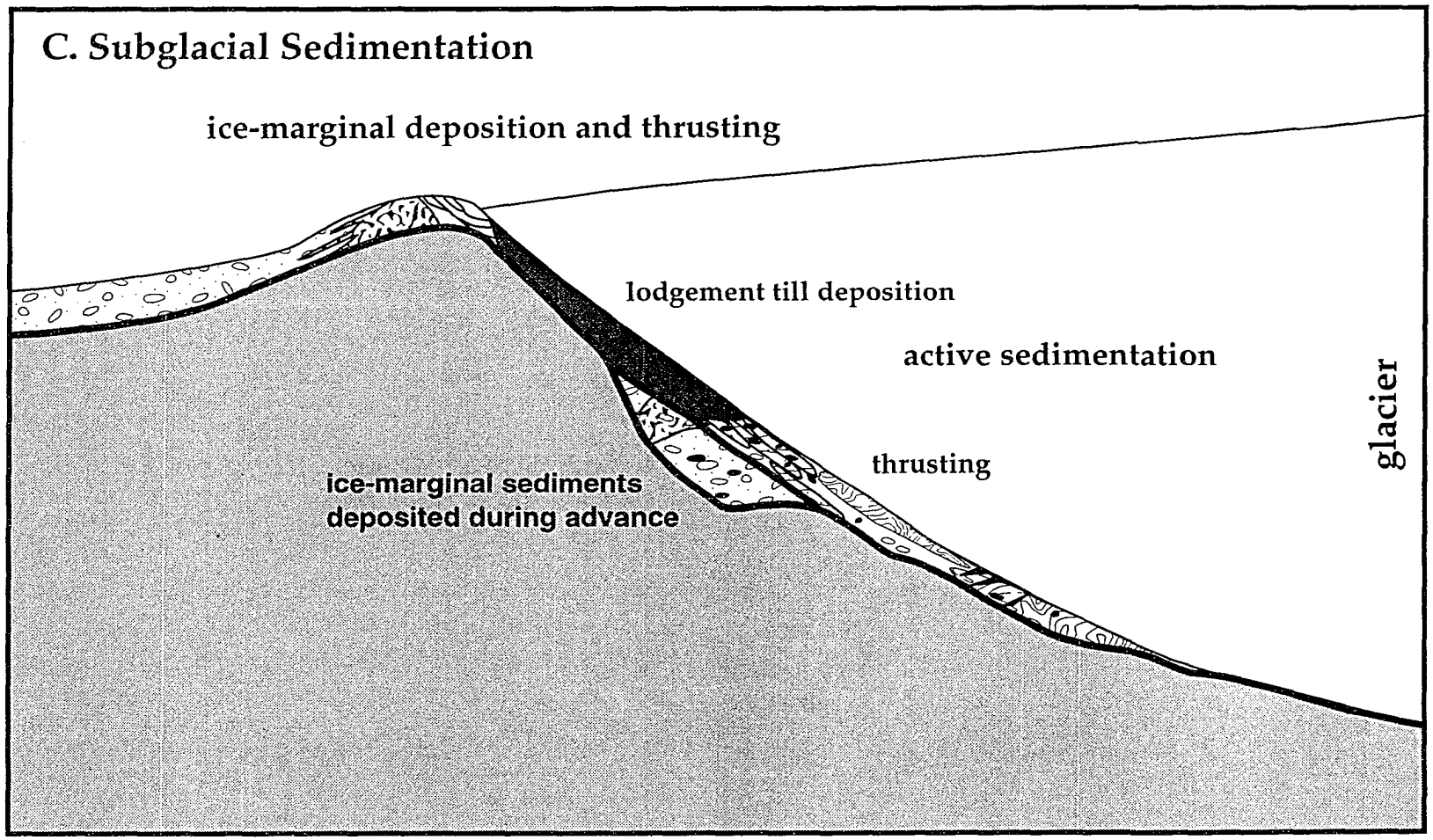

Figure 29. C) The processes that are occurring subglacially at the same time are dependent on topographic position. Large-scale, low-angle thrusting of unfrozen sediment sheets occurs on the middle slope; these sediment slices are carved off subglacially from the kame terrace. Small-scale, high-angle thrusting occurs on the upper slope because of winter freezing of sediments to the glacier sole. Lodgement till is deposited subglacially while flow tills are deposited at the ice margin.

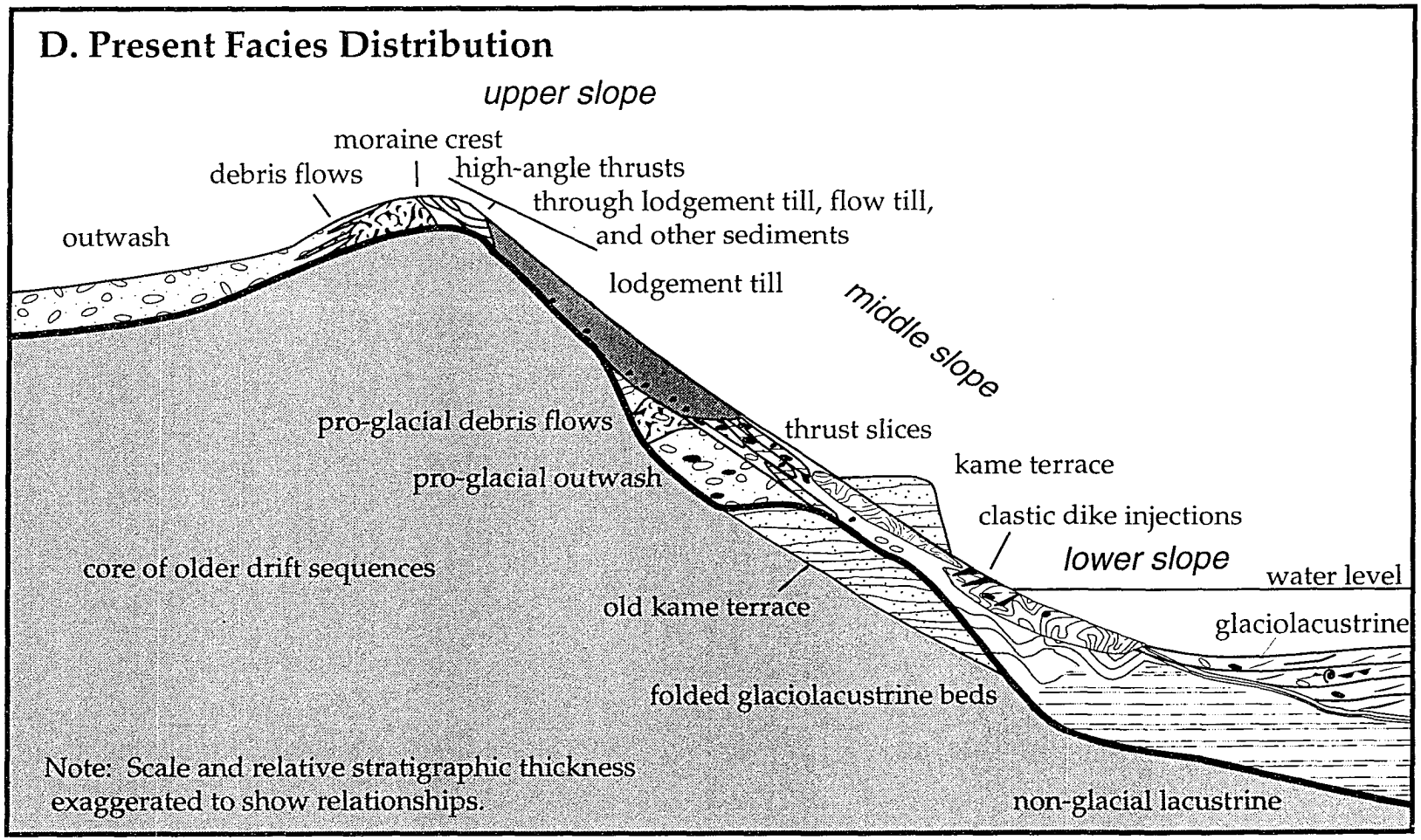

Figure 29. D) This figure represents the facies distribution of glacially-derived sediments as it is seen today. Similar sequences of processes presumably formed the core of older drift sequences, over which the last glacier cycles advanced. The kame terrace which is present on the slope today was built by the last glacial advance, which terminated inside the lake basin; this terrace has never been overrun by a glacier.

middle slope position (indicated by a relict deposit beneath active subglacial sedimentation in Figure 29C).

The processes of the second set, however, are more interesting and informative, because they occurred subglacially *at the same time in different topographic positions*, as the glacier stood at the moraine crest (Figure 29C). These processes must be a function of topography, since no lodgement till is found at the base of the advancing glaciogenic sequence, except at the upper slope position (Figure 29D). In a subglacial facies model that is *not* dependent on topography, lodgement till would be deposited along the entire slope, unless a subglacial erosional zone destroys all deposited lodgement till, except within a narrow band near the ice margin.

The subglacial facies and their respective topographic positions are depicted in Figure 29C. On the middle slope, long, thin sediment slices were thrust subglacially along low-angle thrust planes, as at the Frutillar Bajo and Punta Penas sections. Drag along the thrust plane formed thin diamicton units (Frutillar Bajo), broke rocks in clast clusters (Punta Penas), and smeared soft sediments along the thrust plane (both Frutillar Bajo and Punta Penas sections). At the same time on the upper slope, however, either (1) lodgement till or flow till was depositing, as at the Trapén section and the Frutillar Alto section, respectively, or (2) thin, frozen sediment slices were being thrust along high-angle shear planes, as at Frutillar Alto. The lower slope processes occurring at this time are unknown; all sediments and

deformations found at this position can be explained by ice-marginal processes occurring prior to the time of maximum ice extent.

Why is sedimentation a function of topography? One possibility is that topography causes different hydrostatic pressures to develop at different slope positions; it is the hydrostatic pressures, then, that control subglacial processes. Menzies (1989) acknowledges that subglacial hydrology plays an important role in subglacial sedimentation, to an unknown extent. He proposes a close relationship between spatial and temporal changes in porewater and meltwater conditions, subglacial bed formation, and subglacial sedimentary and deformational facies. Also, as discussed previously, both Piotrowski (1993) and Boulton and Caban (1995) invoke porewater pressure as a major factor in promoting thrusting.

We propose that topography controls hydrologic conditions for this temperate piedmont glacier system, at maximum ice extent, as follows. Lower and middle slope positions have a thicker ice cover and therefore experience greater hydrostatic pressures. Within this zone, subglacial thrusting of large, thin sediment slices occurs. Upper slope positions experience smaller hydrostatic pressures, as the ice overburden thins toward the margin. Lodgement till is deposited high in the topography, where hydrostatic pressures are low and effective pressures are correspondingly high. Low hydrostatic pressures favor lodgement by friction at the sliding base of the glacier (Dreimanis, 1988).

In conclusion, we suggest that our topography-dependent facies model, developed for these temperate, piedmont glaciers, be tested in other glacier systems. If validated for glacier systems in general, the integration of this model into a generalized till genesis model will increase our understanding of the basal dynamics of glacier systems.

Bibliography

Andersen, B.G., in press: Quaternary geologic maps of the Southern Lake District, Chile. *Geografiska Annaler* .

Boulton, G.S. and Caban, P., 1995: Groundwater flow beneath ice sheets: Part II- Its impact of glacier tectonic structures and moraine formation. *Quaternary Science Reviews* 14: 563-587.

Boulton, G.S. and Dobbie, K.E., 1993: Consolidation of sediments by glaciers: relations between sediment geotechnics, soft-bed glacier dynamics and subglacial ground-water flow. *Journal of Glaciology* 39 (131): 26-44.

Boulton, G.S., Caban, P.E., and van Gijssel, K., 1995: Groundwater flow beneath ice sheets: Part I- Large scale patterns. *Quaternary Science Reviews* 14: 545-562.

Brodzikowski, K. and Haluszczak, A., 1987: Flame structures and associated deformations in Quaternary glaciolacustrine and glaciodeltaic deposits: examples from central Poland. *In*: Jones, M.E. and Preston, R.M.F. (eds), Deformation of Sediments and Sedimentary Rocks: Geological Society Special Publication No. 29: 279-286.

Dreimanis, A., 1988: Tills: Their genetic terminology and classification, *In*: Goldthwait, R.P. and Matsch, C.L. (eds), Genetic Classification of Glacigenic Deposits: Balkema, Rotterdam: 17-84.

Hart, J.K. and Boulton, G.S., 1991: The interrelation of glaciotectonic and glaciodepositional processes within the glacial environment. *Quaternary Science Reviews* 10: 335-350.

Heusser, C.J., Lowell, T.V., Heusser, L.E., Hauser, A., Andersen, B.G., and Denton, G.H., 1996: Full-glacial-late-glacial palaeoclimate of the Southern Andes: evidence from pollen, beetle and glacial records. *Journal of Quaternary Science* 11 (3): 173-184.

Heusser, C.J., Heusser, L.E., and Lowell, T.V., in press: Paleoecology of the Southern Chilean Lake District and Isla Grande de Chiloe during Middle-Late Llanquihue glaciation and deglaciation. *Geografisca Annaler* .

Ives, P.C., Levin, B., and Rubin, M., 1964: U.S. Geological Survey radiocarbon dates VIII. *Radiocarbon* 6: 37-76.

Krüger, J., 1993: Moraine-ridge formation along a stationary ice front in Iceland. *Boreas* 22: 101-109.

Lowell, T.V., Heusser, C.J., Andersen, B.G., Moreno, P.I., Hauser, A., Heusser, L.E., Schlüchter, C., Marchant, D.R., and Denton, G.H., 1995: Interhemispheric correlation of Late Pleistocene glacial events. *Science* 269: 1,541-1,549.

Menzies, J., 1989: Subglacial hydraulic conditions and their possible impact upon subglacial bed formation. *Sedimentary Geology* 62: 125-150.

Piotrowski, J.A., 1993: Salt diapirs, pore-water traps and permafrost as key controls for glaciotectonism in the Kiel area, Northwestern Germany. *In*: Aber, J.S., (ed), Glaciotectonics and Mapping Glacial Deposits: Hignell Printing Limited, Winnipeg, Canada: 86-98.

Porter, S.C., 1981: Pleistocene Glaciation in the Southern Lake District of Chile. *Quaternary Research* 16: 263-292.

Wateren, F.M. van der, 1995: Processes of Glaciotectonism, *In*: Menzies, J., (ed), Modern Glacial Environments: Processes, dynamics and sediments, Glacial Environments: Volume 1: Butterworth-Heineman, Oxford, England: 309-335.

Appendix 1 - Methods

Mapping

Detailed mapping was done at each site, either by measuring and hand drawing features onto a grid, or by drawing onto a photographic composite. Strike and dip measurements were located and recorded on the maps. The Frutillar Beach section was mapped in plan view and consists of a composite of measured-grid maps and detailed, oriented sketches. From the Frutillar Beach section, Unit 5 and part of Unit 3 were taken from measured grid maps produced by Tom Lowell and Rebecca Hinnefeld.

The other sections were mapped in cross-section. The Frutillar Alto and Bajo sections were measured and drawn in cross-section on a grid. The Punta Penas section was mapped in cross-section on a photographic composite.

Sections were divided into units to simplify description and interpretation. Unit divisions are based on cross-cutting relationships (unconformities) and similarity of age, depositional history, and structural features of the sediments.

A elevation survey was done to produce a topographic map for the Frutillar basin. The locations of measurement positions were recorded on aerial photographs. This survey was accomplished using an altimeter which was accurate to two meters. This altimeter calculates elevation by sensing changes in barometric pressure with elevation above some calibrated base level. Base level was set for this survey at the lake level. Periodically

throughout the survey, an altimeter reading was taken at lake level. The time of measurement was recorded along with the elevation value. Changes in elevation of the base level, caused by fluctuations in barometric pressure over time, were used to calculate correction factors for each altimeter reading. These were subtracted from each altimeter reading to get an elevation value resulting only from pressure differences caused by changing elevation. The corrected elevation values were then plotted on the aerial photographs.

The resulting aerial photographs were used as a base for photogrammetry, to allow contouring of areas where the altimeter survey data was sparse. Metric photogrammetry uses the stereoscopic parallax of an point to calculate its elevation. Stereoscopic parallax is "the apparent displacement of an object, with respect to a frame of reference, caused by a shift in the position of observation" (Wolf, 1974). The amount of parallax is greater for higher elevation points than for lower elevation points. Thus, when the elevations of two points are known, the parallax difference between them on aerial stereophotograph pairs can be measured using a parallax bar, then divided by the elevation difference, to give a constant value for change in parallax with elevation. By setting the parallax bar to a particular elevation value, then contours can be drawn directly onto the aerial photographs. This procedure was used to produce the Figure 2. As a result, the topographic setting of the geologic sections can be mapped.

Topographic Survey Results Table

STATION	TIME	READING	CORRECTION	ELEVATION	NOTES
lake	3:00	51		51	
2	3:04	85	-0.07	85	intersection at curb- Frutillar profile base
pole 16	3:05	95	-0.09	95	
pole 18	3:07	103	-0.13	103	
pole 24	3:11	127	-0.20	127	
pole 30	3:13	136	-0.23	136	
pole 33	3:15	143	-0.27	143	
crest after 35	3:17	151	-0.30	151	
pole 36	3:20	151	-0.36	151	
pole 38	3:21	156	-0.38	156	
1	3:25	160	-0.45	160	
3	3:27	161	-0.48	161	furthest moraine crest
4	3:29	152	-0.52	151	moraine/ outwash contact
5	3:32	146	-0.57	145	outwash at road intersection edge of town
6	3:37	140	-0.66	139	road intersection
7	3:40	141	-0.71	140	road intersection
8	3:42	164	-0.75	163	moraine crest
9	3:45	175	-0.80	174	** maximum moraine crest
10	3:48	157	-0.86	156	outwash beyond crest
11	3:56	125	-1.00	124	base of gully head
12	4:01	148	-1.09	147	edge of ice contact slope
13	4:06	169	-1.18	168	inner moraine crest
14	4:07	152	-1.20	151	barn
15	4:11	144	-1.27	143	
16	4:17	157	-1.38	156	channel floor
17	4:20	170	-1.43	169	outer moraine crest (max prob >10m higher)
18	4:22	164	-1.46	163	upper outwash surface
19	4:25	155	-1.52	153	water table- lowest channel terrace
20	4:33	163	-1.66	161	crest of inner moraine
21	4:39	142	-1.77	140	Hotel Volcan Puntiagudo surface
22	4:42	125	-1.82	123	"antiformal" outcrop
23	4:44	123	-1.86	121	crest above Puntiagudo site
24	4:45	117	-1.88	115	Hotel Puntiagudo site
25	4:47	93	-1.91	91	moraine slope to terrace contact
26	4:49	86	-1.95	84	cemetery
lake	4:52	53	-2.00	51	
27	5:04	92	-2.17	90	sublobe terrace
28	5:10	95	-2.26	93	terrace
29	5:17	95	-2.35	93	terrace - new sublobe
30	5:52	147	-2.85	144	moraine crest
31	5:56	142	-2.91	139	terrace beyond crest

32	6:00	136	-2.96	133	channel bottom
33	6:10	149	-3.11	146	delta outcrop
STATION	TIME	READING	CORRECTION	ELEVATION	NOTES
34	6:15	155	-3.18	152	crest of delta/moraine
35	6:18	168	-3.22	165	top of delta?
36	6:26	168	-3.33	165	road junction
37	6:30	182	-3.39	179	bouldery moraine crest- max ~10 m higher
38	6:39	182	-3.52	178	bouldery moraine crest (surface is ~2 m higher)
39	6:43	164	-3.57	160	moraine/outwash contact next to outwash rumple
40	6:47	157	-3.63	153	channel crossing road to Puerto Octay
41	6:53	204	-3.72	200	outer max moraine crest
pole 30	7:09	141	-3.94	137	back to recheck altimeter
lake	7:13	55	-4.00	51	
42	7:30	92	-3.30	89	terrace
43	7:34	135	-3.13	132	bog channel- coring site 535
44	7:38	168	-2.97	165	moraine crest beyond bog
45	7:41	166	-2.84	163	another crest
46	7:48	148	-2.55	145	bend in road- approx elev of inner moraine crest
47	8:00	93	-2.06	91	terrace at base of Driveway site
48	8:05	139	-1.85	137	Driveway section base
49	8:09	156	-1.69	154	crest above Driveway section
50	8:25	115	-1.02	114	crest in moraine complex- not highest
51	8:40	101	-0.40	101	edge of moraine above small lake
52	8:52	90	0.09	90	terrace on road to Tepual(V- 155)
53	8:56	105	0.26	105	intermediate level terrace
54	8:58	143	0.34	143	inner moraine
55	9:01	187	0.46	187	~3 m below moraine crest
56	9:02	179	0.50	180	small channel
57	9:04	170	0.59	171	big channel
58	9:05	182	0.63	183	outer moraine crest- surface is ~2m higher
lake	9:14	50	1.00	51	

Analysis

Stereographic projections were made on equal-area stereonets using the *Stereonet* program, (version 4.9.5, © 1988-1995 by Richard W. Allmendinger). For the Frutillar Bajo and Frutillar Alto sections, the poles to the orientations of planar features in the outcrop were plotted. These poles were contoured using the 1% area method. This method uses a counting circle constrained to be 1% of the area of the stereonet, and calculates the point density of each 1% area in the stereogram. A uniform distribution of points would give a point density of 1%. Contours were drawn at 2% intervals (2-4, 4-6%, 6-8%, 8-10%, 10-12%) per 1% area of the stereonet.

The highest point density areas (black zones) indicate preferred orientations of poles to the features in the outcrop. A great-circle girdle is a concentration of points approximating a great-circle. When the points plotted are poles to planar features, a great-circle girdle indicates that all the planes could intersect along the same line (Marshak and Mitra, 1988).

References

Marshak, Stephen and Mitra, Gautam, 1988: Basic Methods of Structural Geology: Part 1- Elementary Techniques: Prentice Hall, Englewood Cliffs: 148-156.

Wolf, Paul R., 1974: Elements of Photogrammetry: McGraw Hill, Inc., New York, 562 p.

APPENDIX 2

Lithology, Structures, and Interpretations for Units

Table 1. Puerto Varas Beach Section.

UNIT	LITHOLOGY	STRUCTURES	INTERPRETATION
1	Folded sequence of alternating beds, coarser- and finer-grained layers of coarse sand to silt, slightly graded, containing some granite-rich diamictons. Finer-grained beds often are amalgamations of laminated silt intraclasts, chaotically-oriented. Overlain by horizontal or gently-dipping laminated gray silts.	Overturned anticline, plunging westwards. Curvilinear angular unconformity with Unit 2.	Glaciodeltaic sediments folded by ice contact or tectonic activity, overlain by younger sedimentation, and re-exposed by glacier advances and wave action.
2	Alternating sequences of **1)** graded-bedded zones (1-2 m thick containing many smaller 1-7 cm thick, fining-upward beds of medium sand to silt to clay. Clay drawn up in flame structures into sand (Fig. 6). Sand often contains rounded clay intraclasts up to 10 mm.), **2)** massive silt or ash beds (1-5 m thick, often containing pieces of folded silt and clay layers, and granite granules), and **3)** granite gravel-rich diamictons (often with boulders at the base having folds or sediment wedges verging westwards from ploughing). Entire sequence is dipping ~50° SE, with beds striking 065°.	Syndepositional folding of layers. Sediment roll of graded-bed sequence, 85 by 85cm (Fig. 8 and 9), overturned ~1 1/8 turns, containing two centers (one a pebble gravel and one a fine silt) rolled 'yin/yang' style into it, beds of variable thickness (2-4 cm) graded silty-sands, separated by thin clay slip planes (exhibiting parallel step-like lineations). Slickensides on clay planes of graded beds (trend 200°, plunge 40° on beds oriented 062°, 46°S). Entire sequence is tilted to SE. Left-lateral faulting, some normal component, trending ~340°.	Glaciodeltaic sedimentation. Syndepositional deformation (folding, rolling, and truncation of graded beds) caused by turbidity currents and input of coarser material (diamicton and boulders). Tilting due to glacier contact or tectonic activity. Faulting postdates tilting.

Table 1. Puerto Varas Beach Section, continued.

UNIT	LITHOLOGY	STRUCTURES	INTERPRETATION
3	Alternating sequences of thin graded-beds, massive silts, and granite-rich diamictons, similarly oriented to Unit 2. Incidence of diamictons and massive silt/ash beds is greater than Unit 2, and increases to south.	Kink-faulting (Fig. 10) at northern end of unit reorients bedding from ~E to ~SSE. Synclinal folding, gently SW-dipping, at southern end of unit (Fig. 6). Curvilinear fractures and faulting in syncline. North-trending left-lateral faulting.	Glaciodeltaic sedimentation. Syndepositional deformation. Tilting and syncline formation due to glacier contact or tectonic activity. Faulting occurs with and after tilting and folding. Kink faulting at the time of thrusting of Unit 4.
4	Massive curvilinear beds dipping NE.	Overturned anticline/syncline pair, plunging NE. Fold axis of anticline strikes 039°. Angular unconformity with Units 2 and 3.	Block of glaciodeltaic sediments thrust and folded by ice margin.
5A	Beds as in Unit 3.	Major faults to north and south of unit (faults A and B, Fig. 6). Fractures common.	Curving orientation of beds indicates that this unit is part of southern limb of syncline. Glacial stresses faulted syncline into a few blocks and rearranged them.
5B	Beds as in Unit 3.	Major faults to west and south of unit (faults B and C, Fig. 6). Beds truncate against Fault C. Fractures common.	Curving orientation of beds indicates that this unit is part of southern limb of syncline. Glacial stresses faulted syncline into a few blocks and rearranged them.
5C	Alternating graded beds, diamictons, and massive silt or ash beds. Beds strike NW-SE and are laterally continuous well east of syncline structure of Unit 3. Adjacent to fault C, there is a massive silt bed, with adfacent beds dipping NE. Beds to south dip SE and continue several hundred meters southwards along shoreline.	Major fault to north of unit (Fault C, Fig. 6), postdates syncline formation. Fractures common. Possible anticline folding adjacent to northern boundary of unit (fault C).	Faulting and thrusting of glaciodeltaic sediments by ice marginal stresses concentrated within interlobate regions of the ice margin.

Table 2. Frutillar Bajo Section.

UNIT	LITHOLOGY	STRUCTURES	INTERPRETATION
1	Coarse sand.	Erosional unconformity at top.	Older glacial outwash.
2	Ashy sand, fines up at base. Overlain by pebble gravel pod. Irregular cobble gravel inset on eastern side. Coarse sand and pebble gravel pod inset to east of cobble gravel, horizontally-bedded, containing rip-up peat pods and fine sand pods.	Bedding in upper half of ashy sand is gently- folded. Unconformity at eastern side of unit.	Older glacial outwash.
3	Major unit of coarse sand containing some thin, fine sand, ash, and granule bedding. Overlain by gravel and cobble bed with cross-bedded coarse sand pod. Overlain by deformed sand beds and gravels. Large cross-bedded sand, overlain by an unconformable ash and lapilli sand, caps this sequence. Unconformable to the east of the major sand are a large gravel and cobble unit, and layers of sand, silt, and gravel.	Bounded on top and sides by erosional unconformities. Channel deposits. Folding due to settling and/or thrusting of overlying sediments. Reverse faulting due to settling. Injections depositing fine sand within Unit 3 (meter 60).	Older glacial outwash.
4	Inclined pebble gravel grades to cobbles over unconformity (with Unit 2) and contains rip-up peat pods. Overlain by fine sand containing rip-up peats and granite boulders up to 80 cm long, thin gravel and sand layers, diamict, and sandy gravel.	Bounded by erosional unconformities, to east with Unit 3, west with Unit 2, and above with Unit 5. Injections depositing fine sand from Unit 4 into Unit 5 (meter 63).	Glacial outwash and ice marginal debris flows deposited in an ice-marginal channel as the glacier advanced up the slope.
5	Basal brown silty diamict with thin sand stratifications, grades up into brown silt up to 70 cm thick, in places highly laminated with thin sand beds at the base, overlain by thin white silt bed in one place, overlain by thick gray sand (generally finer at the bottom and coarser on top). Thin white beds in sand at eastern end of unit.	Subglacial thrusting and fluid injections. Riedel shear formation represented by fractures and listric normal faulting (induced by Unit 8 subglacial zone). Tension fractures filled with fine sand. Minor faulting at eastern end along gentle east-dipping fault planes.	Kame terrace deposition of sediments. Subglacial thrusting of lake terrace sediments, with a shear zone underneath the thrust slice forming diamict. Localized sub-thrust water flow.
6	Massive brown silts, laminated in places. Mainly horizontal laminations, but folded to near vertical at the top (Fig. 15).	Bounded by unconformities because of subglacial thrusting.	Proglacial pushing followed by subglacial thrusting.

Table 2. Frutillar Bajo Section, continued.

UNIT	LITHOLOGY	STRUCTURES	INTERPRETATION
7	Brown silt overlain by gray sand. Silt contains a gray sand pod sheared off from above sand (Fig. 15), and many thin, tan laminations which are rotated upwards and clockwise (Figures 15 and 16).	Shear zone formed at base from subglacial thrusting. Clockwise rotation within shear zone.	Kame terrace deposition of sediments. Subglacial thrusting of lake terrace sediments, with the sub-thrust shear zone producing rotation of sediments.
8	Weathered brown silty diamict, contains many granite clasts.	Fractures.	Subglacial lodgement till or sub-thrust diamict.
9	Soil.		Modern land surface.

Table 3. Punta Penas Section.

UNIT	LITHOLOGY	STRUCTURES	INTERPRETATION
1	Interbedded horizontal sands, ash beds, and gravels, some containing rip-up clasts. Organic-rich silt beds, tree remains, and trees rooted in place [42,400±500 years old (QL-1337)-Porter (1981)]. Channel fills of partly-consolidated pebble gravels.	Infilled channels.	Littoral zone.
2	Horizontally-bedded gravels, matrix- supported, subtle bedding, well-rounded clasts, containing some sand layers, a few boulders (up to 30 cm), and an organic-rich silt rip-up clast. Maximum thickness 2.7 m.		Glacial outwash.
3A	Horizontally-bedded gravel, ~1 m thick. Base is a 20 cm thick shear zone rising 13° toward the northwest and containing numerous angular pieces of broken clasts. In some places fragments of clast are separated by less than 2 cm, indicating little transport after breakage. Some sand layers surrounding clasts. Minimum vertical displacement is 1 m with beds of Unit 2.	Subglacial thrust slice.	Subglacial thrusting.
3B	Laminated silt, maximum 1 m thick, inclined, 3-8 mm laminations, disturbed, highly faulted at steep angles.	Subglacial thrust slice. Injections of diamict from above and gravelly-diamict from below.	Subglacial thrust slice of distal glaciolacustrine sediments.
3C	Granular matrix diamicton with clast concentrations greater than 20 percent, some striations on bullet-boulder shaped clasts, one large granite boulder and irregular contact with Unit 3B at base.	Injections of Unit 3C diamicton downwards into Unit 3B (2 m long and 0.5 to 15 cm thick). Other diamict injections upwards into silt on the seaward side of the exposure.	Subglacial till deposition. Subglacial injections along fractures due to porewater pressure buildup.

Table 3. Punta Penas Section, continued.

UNIT	LITHOLOGY	STRUCTURES	INTERPRETATION
3D	Silty-matrix diamicton with clast concentrations less than 10 percent, minimum thickness 2.8 m.	Fractures common. Pervasive shear plane at base.	Subglacial till deposition.
4	Lacustrine silts, organics, sands, gravels, at least 6.4 m thick (variable thickness due to angular unconformity with Unit 5), exposed in a roadcut across the road from the Punta Penas point (base of roadcut is 38 m NW and 3.6 m above Punta Penas section datum): 0- 2 m above base of outcrop- fine (3-5 mm) laminated silts with rare organic-rich zones, convoluted basal contacts, dipping planar surfaces, gradational contacts, lone stones; 15 cm of tan, organic-rich silt at 1.6 m with locally-disrupted bedding, overlain by individual thin (~1 cm) beds of organics which give the youngest radiocarbon samples at this site (Denton *et al.*, 1997); above 2 m- coarsely-bedded sands, coarsens upwards to small gravel at the top of the terrace.	Minor syndepositional deformation.	Proglacial lacustrine sedimentation formed a kame terrace. Coarsening upward sediments indicates approaching glacier ice.
5	Till, clast concentrations 10-20 percent, decreasing towards top.	Fracture planes parallel the base of the unit. Erosional unconformity at base.	Subglacial till.

Table 4. Frutillar Alto Section.

UNIT	LITHOLOGY	STRUCTURES	INTERPRETATION
1	Brown ash-rich diamict overlain by gray ash-rich diamict, both clast poor, containing ash sand, lapilli, or gray silt pods (slightly concave-shaped), zones of nearly-vertical sand-filled fractures, a group of nearly-vertical, sinuous silt pods, ash pods, and pebble-rich ash diamict pods, and a sand pod containing chunks of diamict. The easternmost section is a jumble of irregularly-shaped gravel, diamict, sand, and ash pods, along with a large boulder and many smaller cobbles.	Sand-filled tension fractures. Riedel fractures.	Ice-marginal flow till diamict deposition with localized ponding of water and sediment deposition.
2	Gray silt-matrix diamict overlying brown silt-matrix diamict, containing a sequence of ribbon-like sand, gray diamict, and brown silt that drapes over Unit 1 sediments (brown diamict) at western contact.	Fractures.	Ice-marginal flow till diamict deposition with localized ponding of water and sediment deposition.
3	Thin brown silt diamict, with thin sand stringer at base, overlying Unit 2 at a steep angle, overlain by gray silt diamict containing high-angle sand pods and irregularly-shaped silt and ash pods.	Minor high-angle normal and reverse faulting through thin brown silt slice.	Subglacial thrusting of flow till diamict, with flow till deposition and localized ponding deposition on top.
4	Gray silt-matrix diamict (more clast-rich) overlying brown silt-matrix diamict. Contact is a laminated brown silt pod, horizontal at its western end but steeply west-dipping at its eastern end.	Thrust plane at base oriented 210°, 63° SE (Appendix 3, Table 2, location O).	Subglacial thrusting of flow till diamict, with flow till deposition and localized ponding deposition on top.
5	Ash and silt beds at outcrop base.	Listric normal faulting with slickensides on fault plane.	Remnants of older deposits, sheared and eroded by glacier overriding.
6	Brown silt diamict, containing similarly-oriented (~45° rising to the west) sand and silt pods. One pod of sandy diamict surrounding the upslope end of a sinuous basal sand stringer. Middle zone of diamict interfingers with fine sand and silt.	Fractures. Injections.	Subglacial thrusting of flow till diamict, with flow till deposition and localized ponding deposition on top.
7	Stoney diamict layer, overlain by thick, ashy brown silt, overlain by brown silt diamict with thin sand stringers. Smaller repeat of brown silt to east within diamict.	Fractures.	Subglacial stone pavement overridden by subglacial thrust slice. Minor rethrusting within unit repeats silt pod.

Table 4. Frutillar Alto Section, continued.

UNIT	LITHOLOGY	STRUCTURES	INTERPRETATION
8	Thick brown silt containing many small ash pods. Basal contact has orientation 210°, 54° SE, steepening to 64° upwards (Appendix 3, Table 2, locations C and D).	Thrust plane at base with slickensides.	Subglacial thrusting of older sediments.
9	Brown silt diamict.	Thrust plane at base.	Subglacial thrusting of flow till diamict, partly along with Unit 8, partly rethrusting along Unit 9 base.

Table 5. Trapén Section.

UNIT	LITHOLOGY	STRUCTURES	INTERPRETATION
1	Horizontally-bedded gravels, up to cobble-size, exposed sections approximately a meter thick.	Angular unconformity at top.	Glacial outwash.
2	Compact, brown, matrix-supported, clast-rich basal till. Large boulders within till at base and in middle of section.	Many prominent shear planes (near Unit 3, oriented 166°, 47°E). Striations on clasts, 265°, 27°E.	Subglacial lodgement till deposition.
3	A 3 m long, thin sequence of silt surrounded by sand beds runs along the base of Unit 2 in one place. Uphill meter of this sequence is deformed up into Unit 2.	Multiple high angle thrusts (up to 6 cm displacements), a few mm to a few cm apart. Folding of layers. Diapirs of silt up to 17 cm long from tips of thrust planes. See Fig. 28.	Sedimentation due to localized ponding. Subglacial thrusting through till, minor folding as thrusting occurred. Diapirs of silt caused by thrusting or water flow along thrust plane.
4	Laminated clays bedded between finer- and coarser-grained bedded sands. Coarser grained sands have open matrix grain to grain contacts. Clay bedding often truncated by sand bedding. Overlain by clast-supported gravels with finer matrix. Located 10 m uphill from Unit 3.	Truncated bedding of clay by sand.	Subglacial or proglacial sedimentation in ponded water (clays and finer sands), with coarser deposition by flowing water. Outwash gravel deposited, followed by glacier readvance (till deposition).

Appendix 3 - Strike and Dip Measurements

Table 1. Frutillar Bajo Section.

LOCATION	TYPE	VALUE	WITHIN UNIT
A	FRACTURE	039, 90	7
B	FRACTURE	035, 77N	7
C	CONTACT	060, 24S	7
D	FRACTURE	067, 66SE	7
E	FRACTURE	293, 28NE	7
F	FRACTURE	050, 90	7
G	FRACTURE	000, 21E	7
H	FRACTURE	000, 31E	7
I	FRACTURE	105, 76S	7
J	FRACTURE	260, 38N	7
K	FRACTURE	295, 10NE	7
L	FRACTURE	061, 57NW	5
M	FRACTURE	324, 31NE	5
N	FRACTURE	255, 16NW	5
O	THRUST PLANE	339, 09E	5
P	BEDDING	097, 19S	3
Q	BEDDING	011, 34W	3
R	FOLD AXIS	197, 38S	3
S	BEDDING	317, 31SW	3
T	FRACTURE	320, 28S	5
U	NORMAL FAULT	181, 17W	5
V	FRACTURE	298, 84NE	5
W	NORMAL FAULT	013, 25NW	5
X	NORMAL FAULT	284, 20SW	5
X	SLICKENSIDES	207,	5
Y	NORMAL FAULT	045, 25NW	5
Z	NORMAL FAULT	258,42N	5
1	NORMAL FAULT	230, 30N	5
2	NORMAL FAULT	227, 23NW	5
3	NORMAL FAULT	309, 28W	5
3	SLICKENSIDES	225,	5
4	NORMAL FAULT	325, 09W	5
4	SLICKENSIDES	240,	5
5	NORMAL FAULT	340, 23SW	5
5	SLICKENSIDES	243,	5
6	NORMAL FAULT	223, 36N	5
7	NORMAL FAULT	218, 31W	5
8	FRACTURE	309, 45SW	5
9	NORMAL FAULT	317, 40SW	5
9	SLICKENSIDES	223,	5
10	FRACTURE	140, 75NE	2

Table 2. Frutillar Alto Section.

LOCATION	TYPE	VALUE	WITHIN UNIT
A	FRACTURE	060, 62SE	9
B	FRACTURE	230, 52SE	9
C	FAULT	210, 54SE	8
C	SLICKENSIDES	276,	8
D	FAULT	213, 64SE	8
E	FRACTURE	207, 24W	6
F	FRACTURE	009, 09W	6
G	FRACTURE	216, 46SE	6
H	FAULT	085, 16N	5
H	SLICKENSIDES	280,	5
I	FRACTURE	125, 29SW	6
J	FRACTURE	059, 54SE	6
K	CONTACT	251, 36SE	6
L	FRACTURE	202, 42W	4
M	FRACTURE	113, 22SW	4
N	CONTACT	132, 64NE	4
O	FAULT	210, 63SE	4
P	FAULT	135, 82NE	3
Q	CONTACT	072, 54SE	2
R	ROCK BOTTOM	250, 66SE	1
S	FRACTURE	053, 62NE	1
T	FRACTURE	050, 59NE	1
U	FRACTURE	058, 61NE	1
V	FRACTURE	059, 64SE	1
W	FRACTURE	242, 86SE	1
X	FRACTURE	175, 15W	1
Y	FRACTURE	048, 74N	1
Z	FRACTURE	060, 58N	1
1	FRACTURE	255, 72N	1
2	FRACTURE	249, 79N	1
3	OUTCROP TOP	068, 17N	1

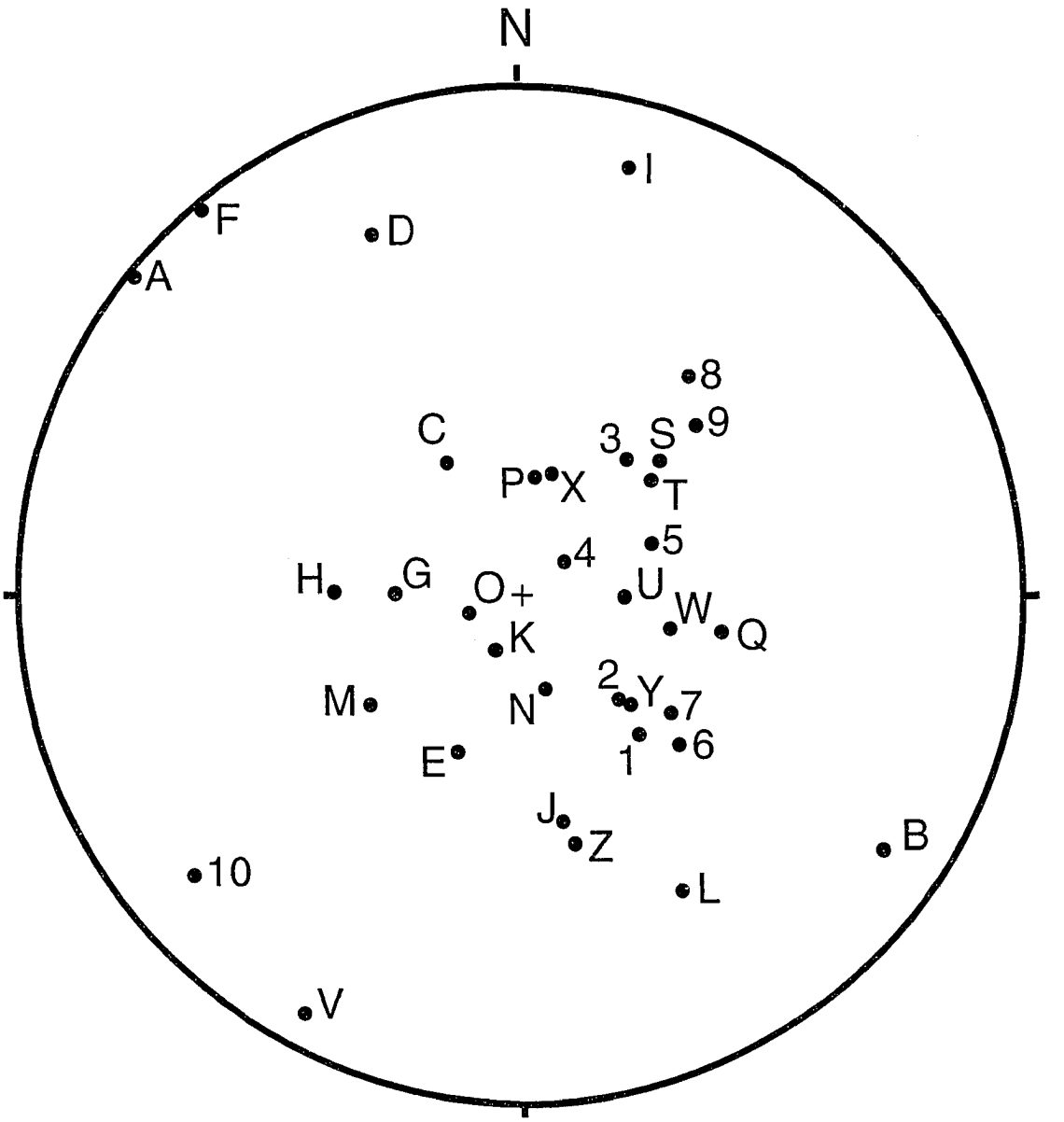

Figure 1. Equal-area stereogram of the poles to the planar features of the Frutillar Bajo section. The letters and numbers correspond to the location labels in Figure 13, in Appendix 3-Table 1, and in Plate I.

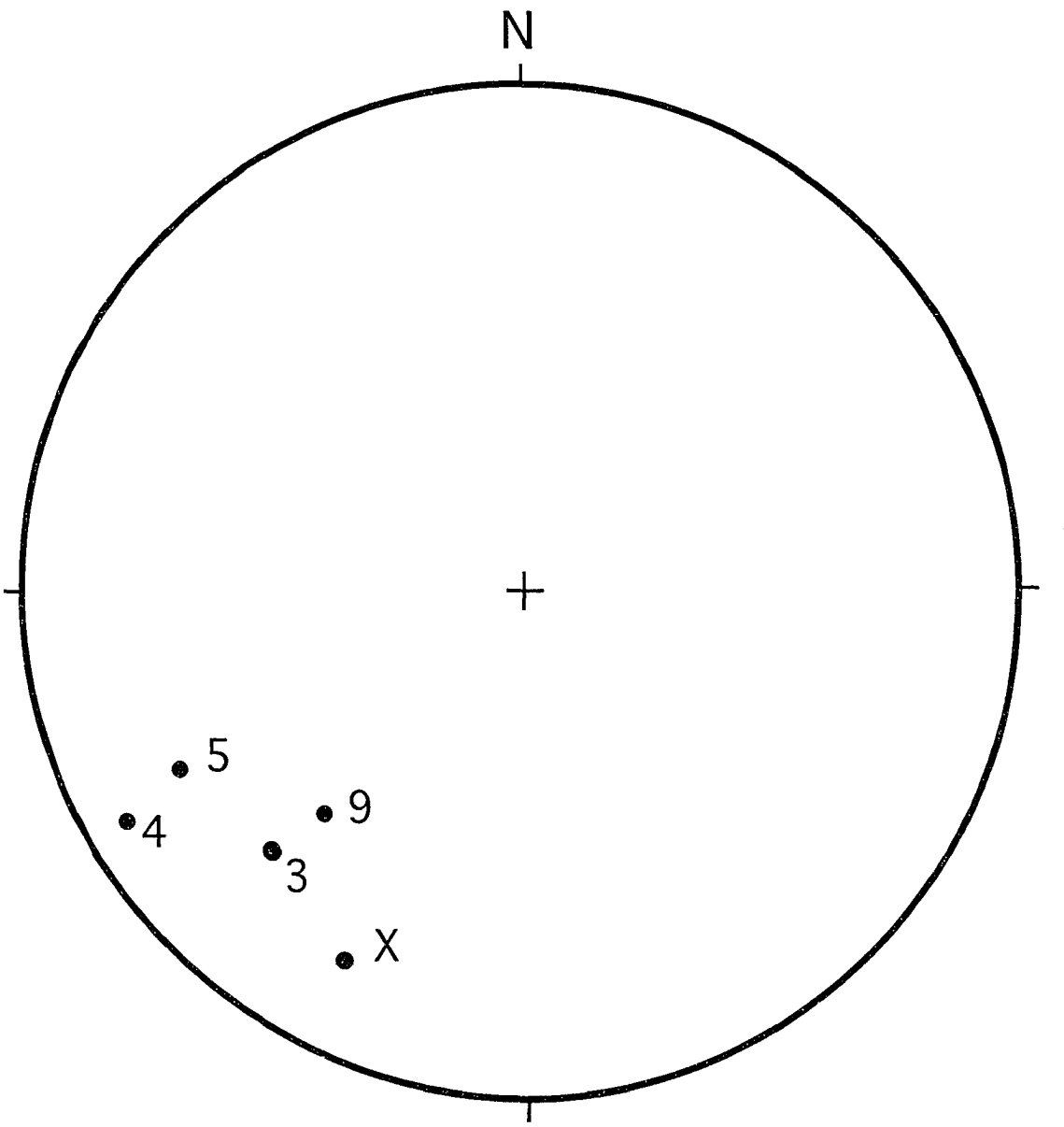

Figure 2. Equal-area stereogram of the slickensides on the normal fault planes, in Unit 5 of the Frutillar Bajo section. Letters and numbers refer to locations plotted in Figure 13 and Plate I, and listed in Appendix 3-Table 1.

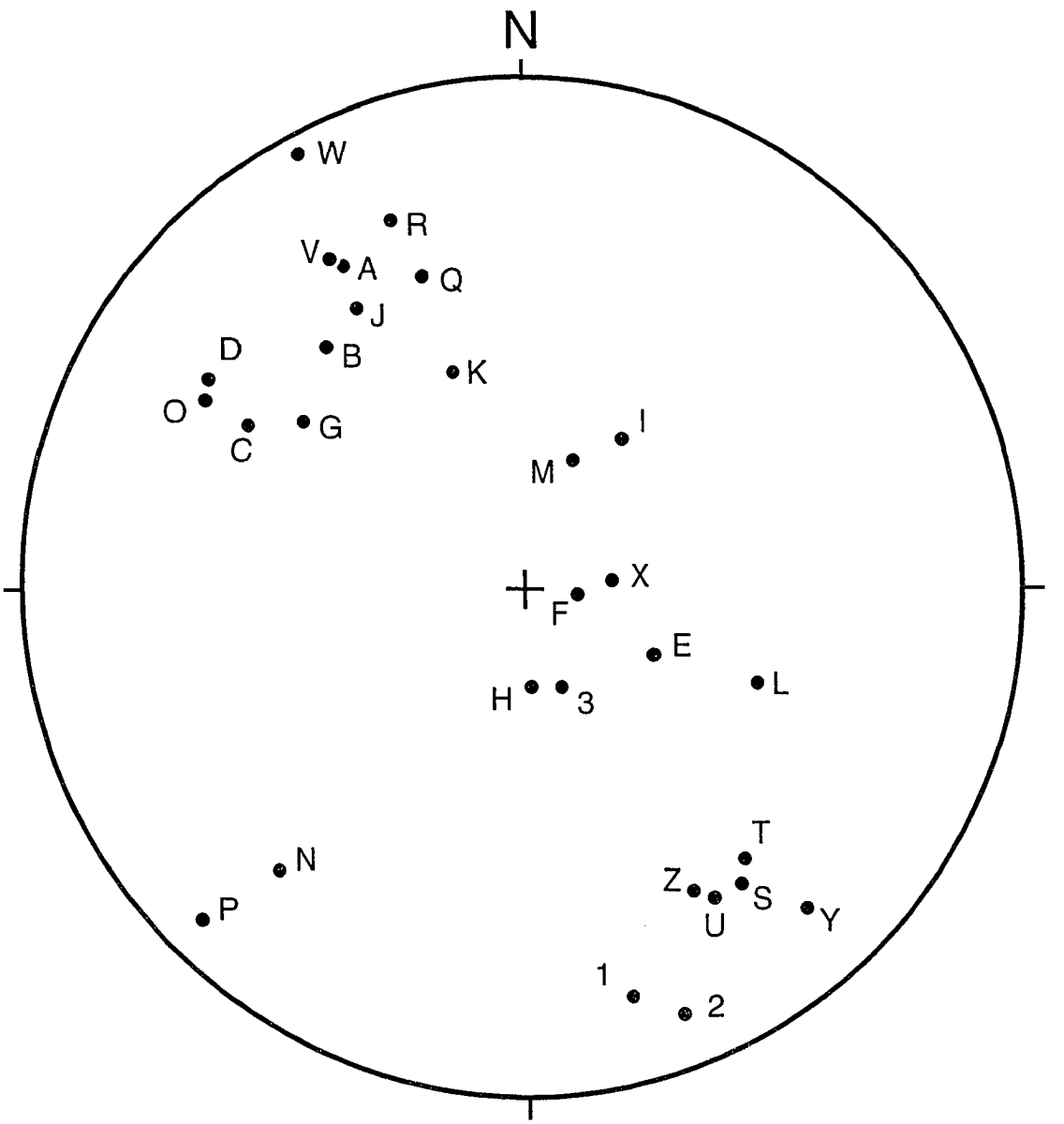

Figure 3. Equal-area stereogram of the poles to the planar features of the Frutillar Alto section. Letters and numbers refer to the locations plotted in Figure 25 and Plate II, and listed in Appendix 3-Table 2.

Appendix 4 - Other Photographs

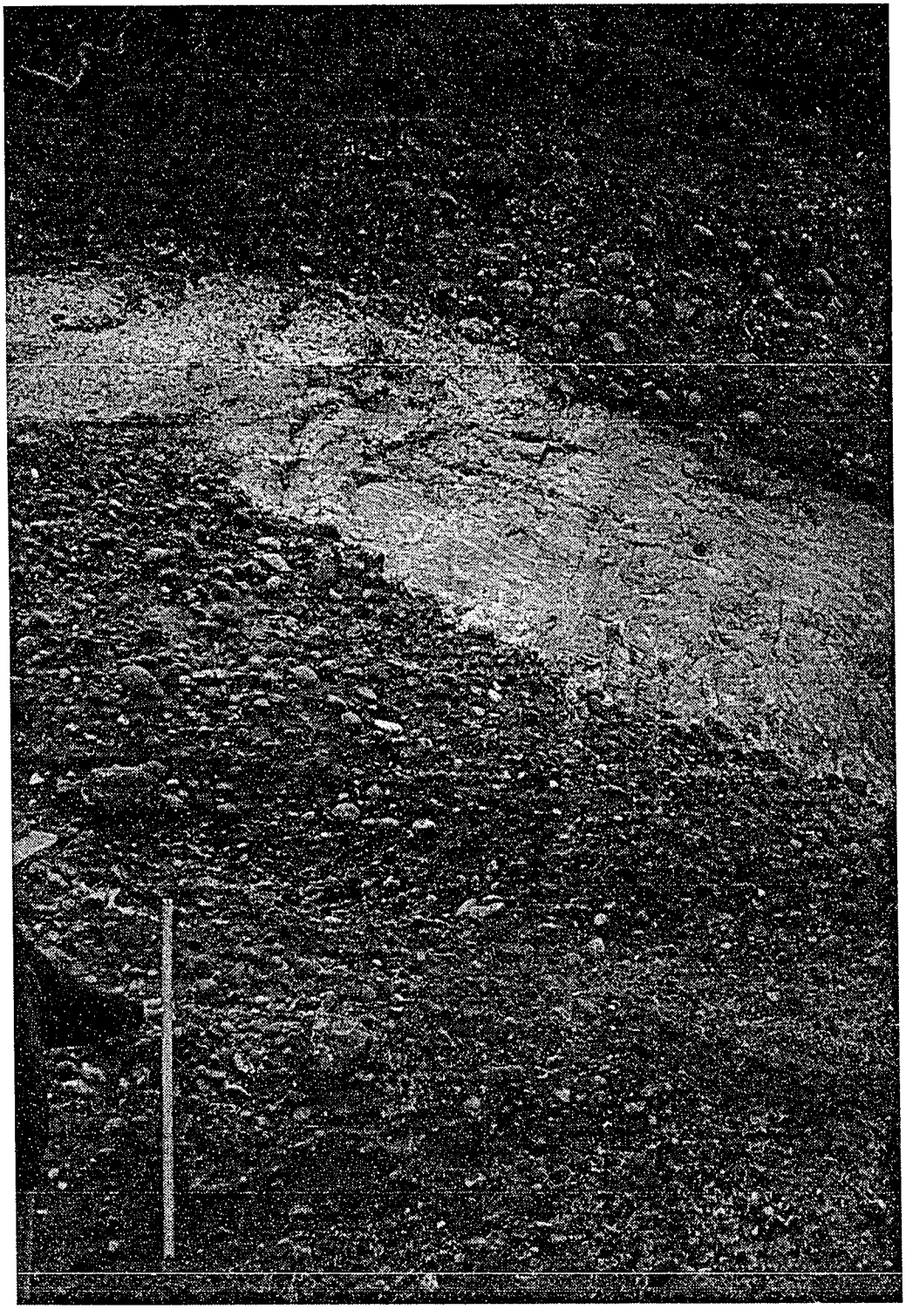

Figure 1. Photograph of the Punta Penas section, showing Unit 2 outwash gravel at the base, Unit 3A transported gravel, Unit 3B transported silt, and Unit 3C subglacial till. The upper end of the meterstick points out the shear zone at the base of Unit 3A, which contains broken clasts.

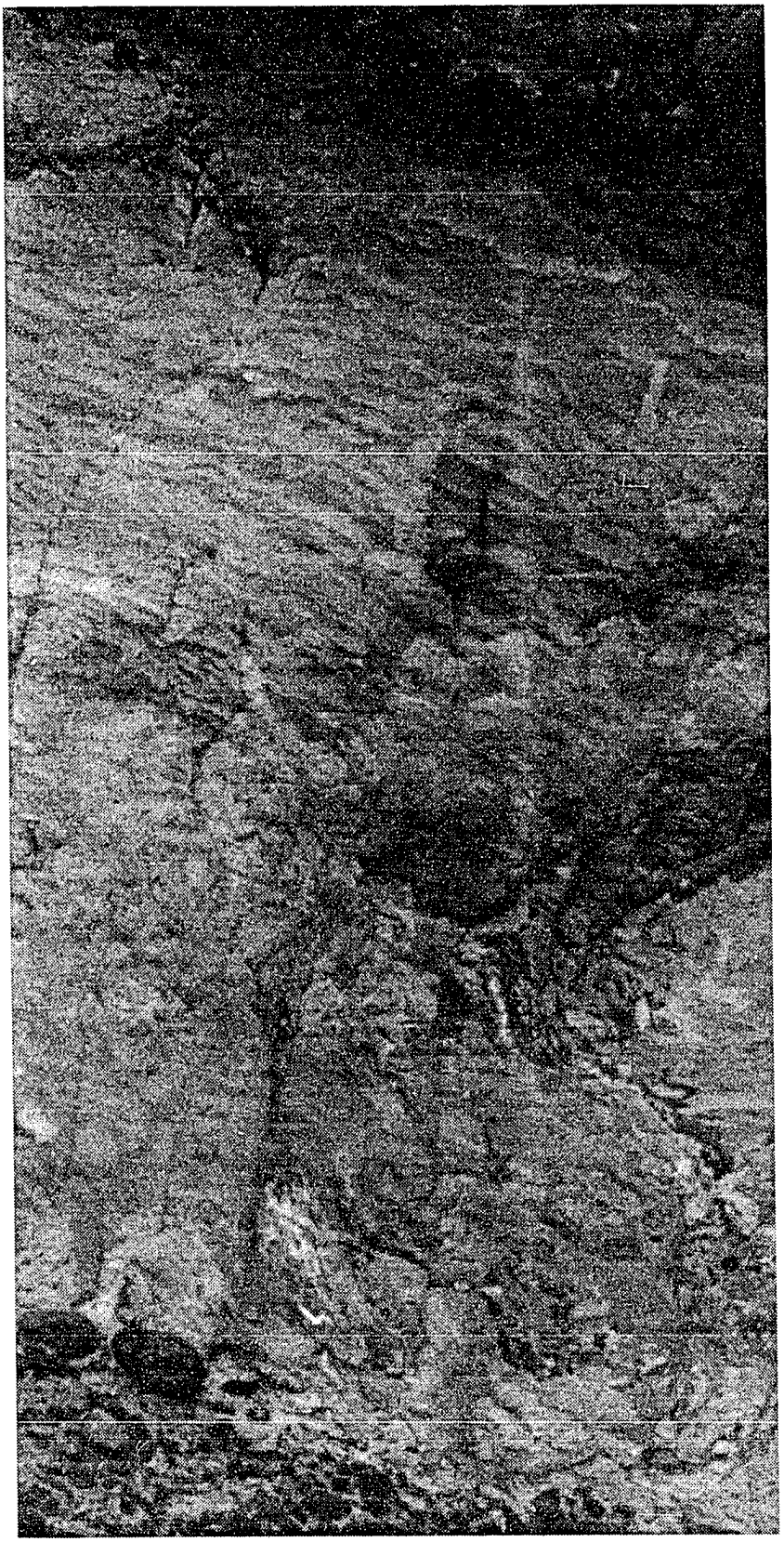

Figure 3. Closeup of the highly-fractured, laminated silt of Unit 3B, Punta Penas section.

PLATE I
The Frutillar Bajo Section

(A)

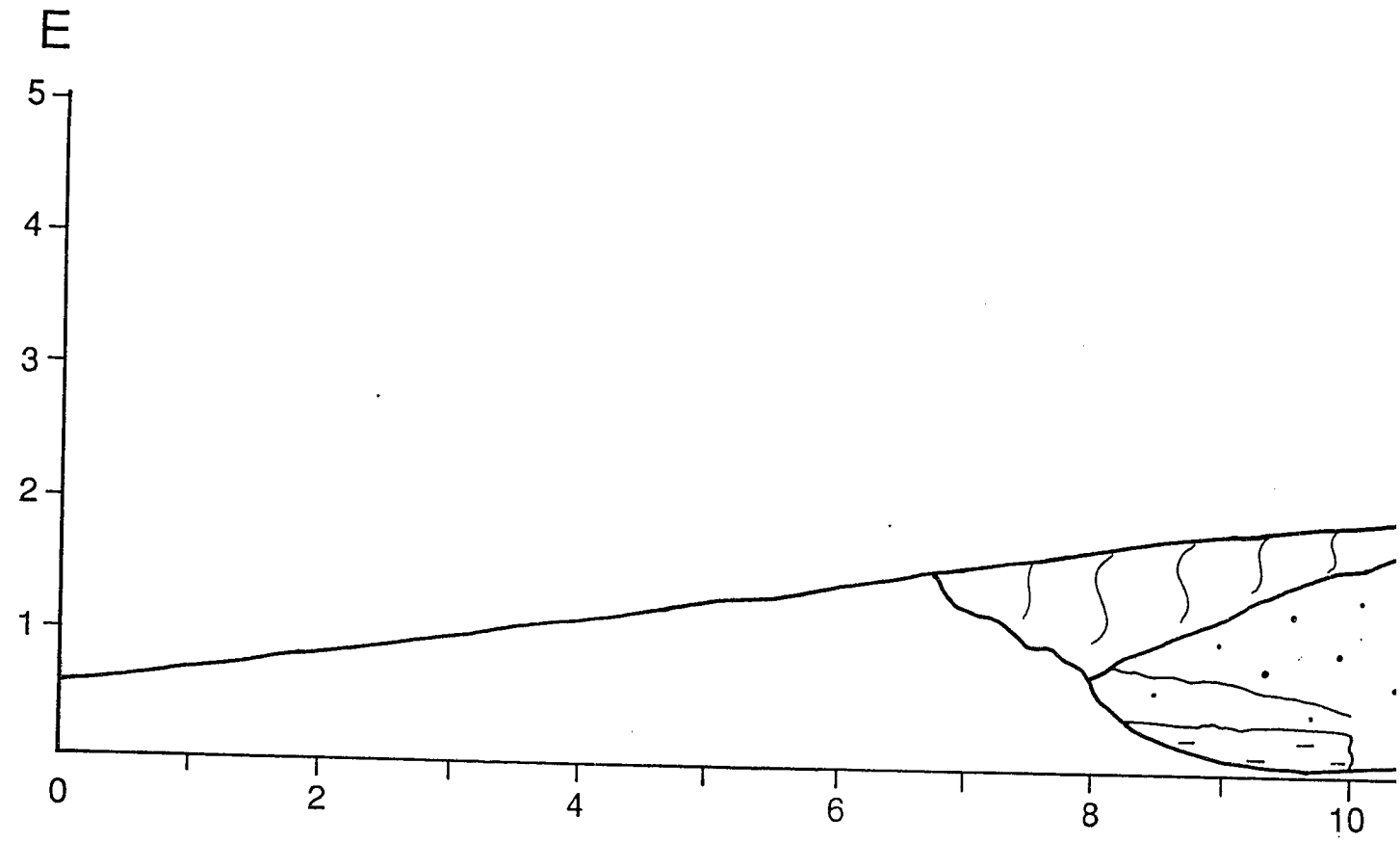

(B)

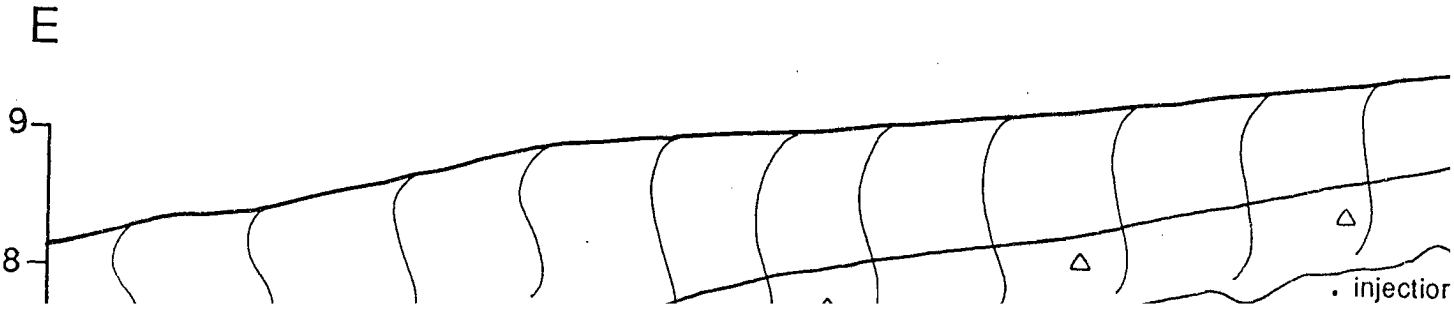

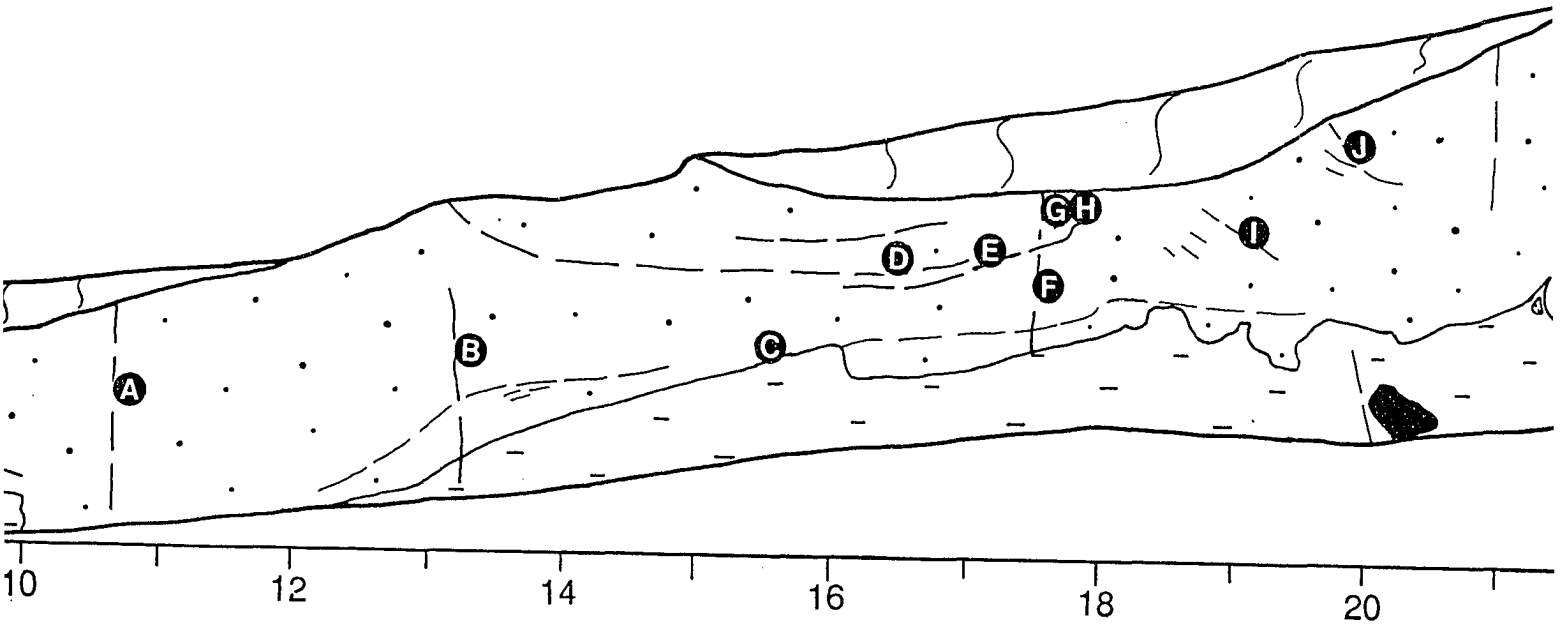

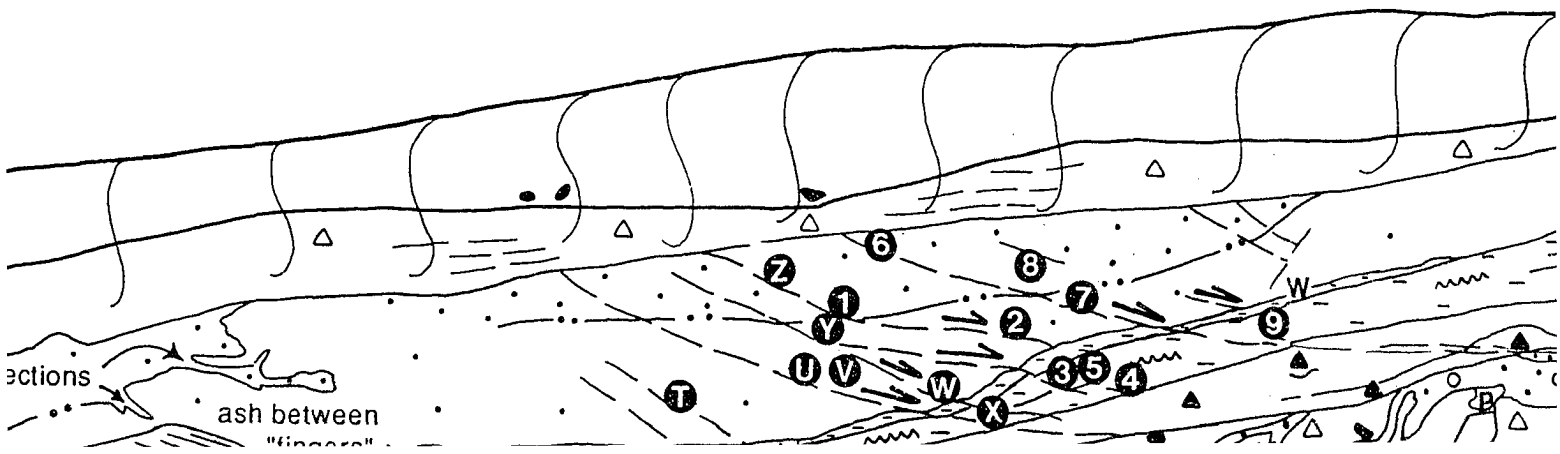

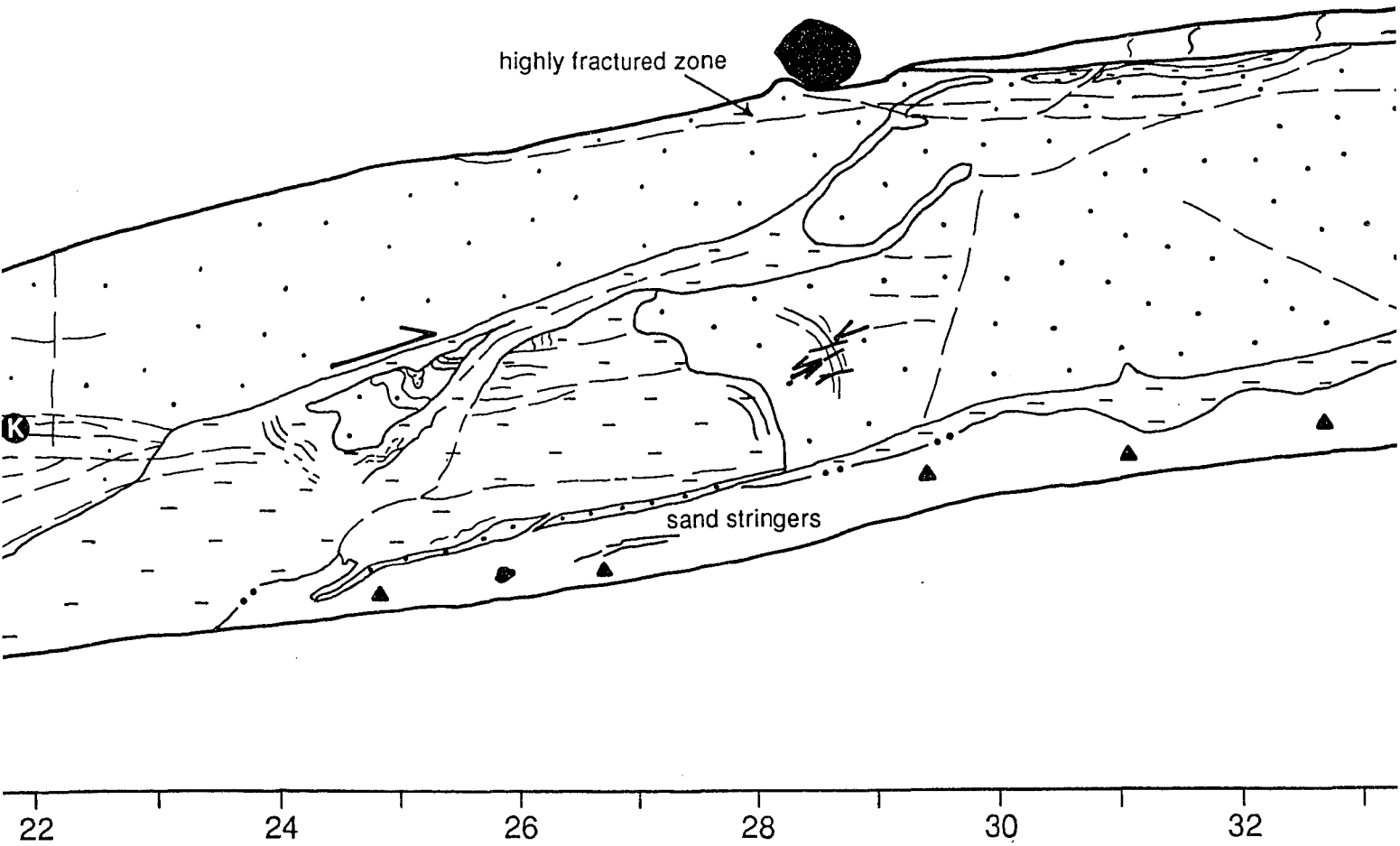

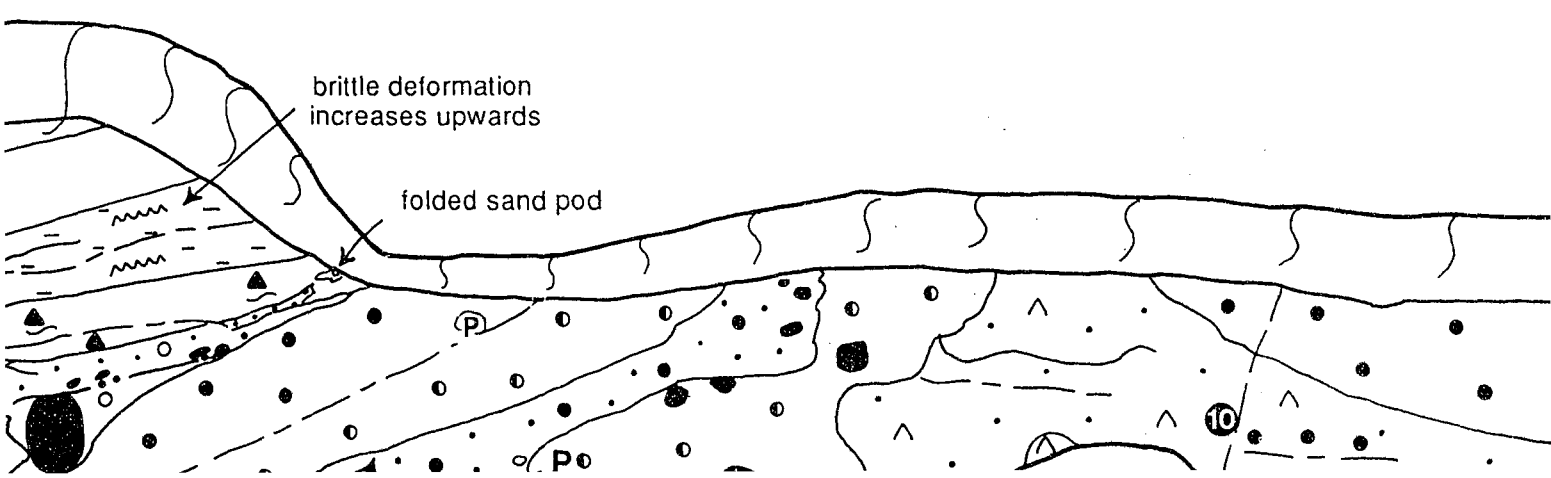

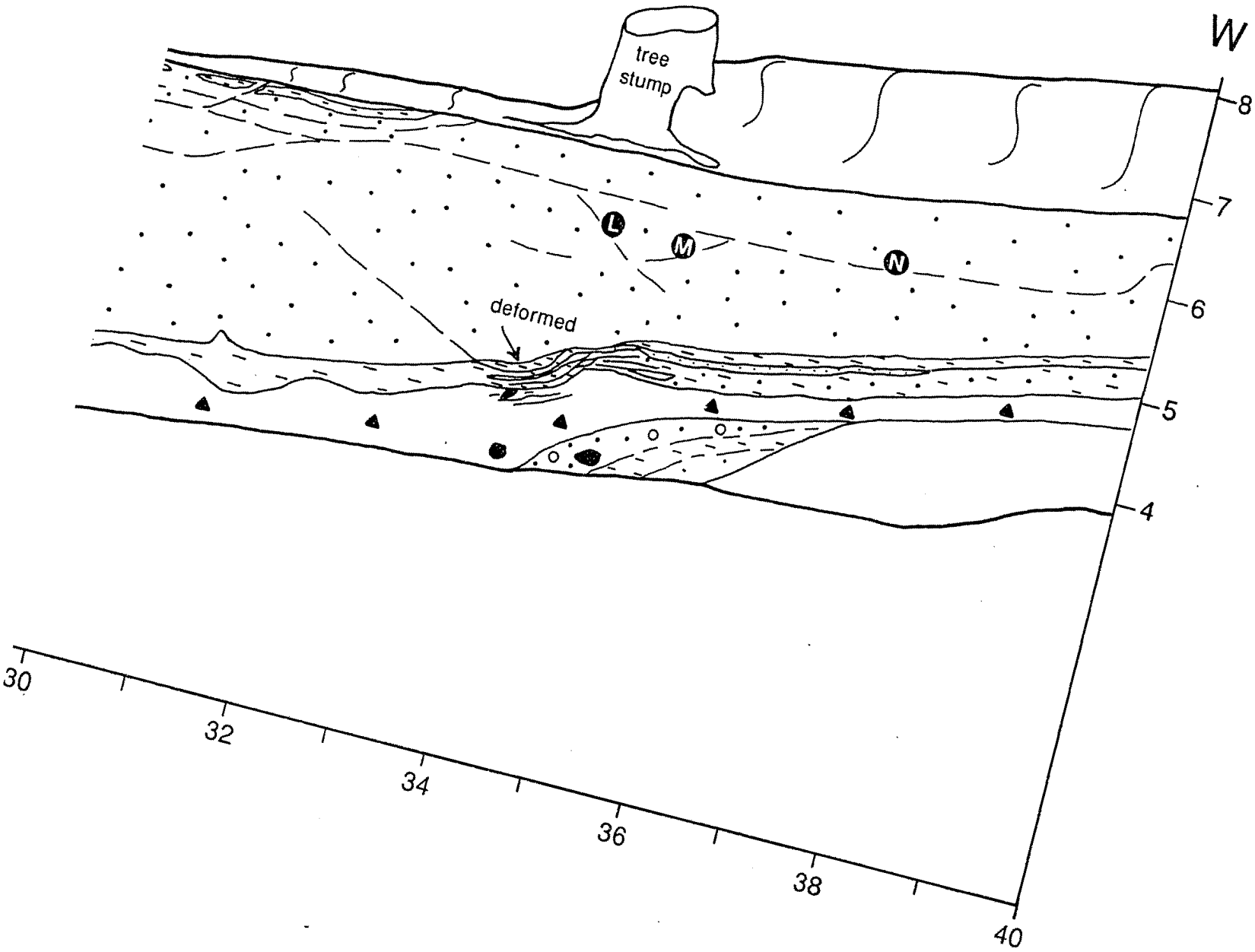

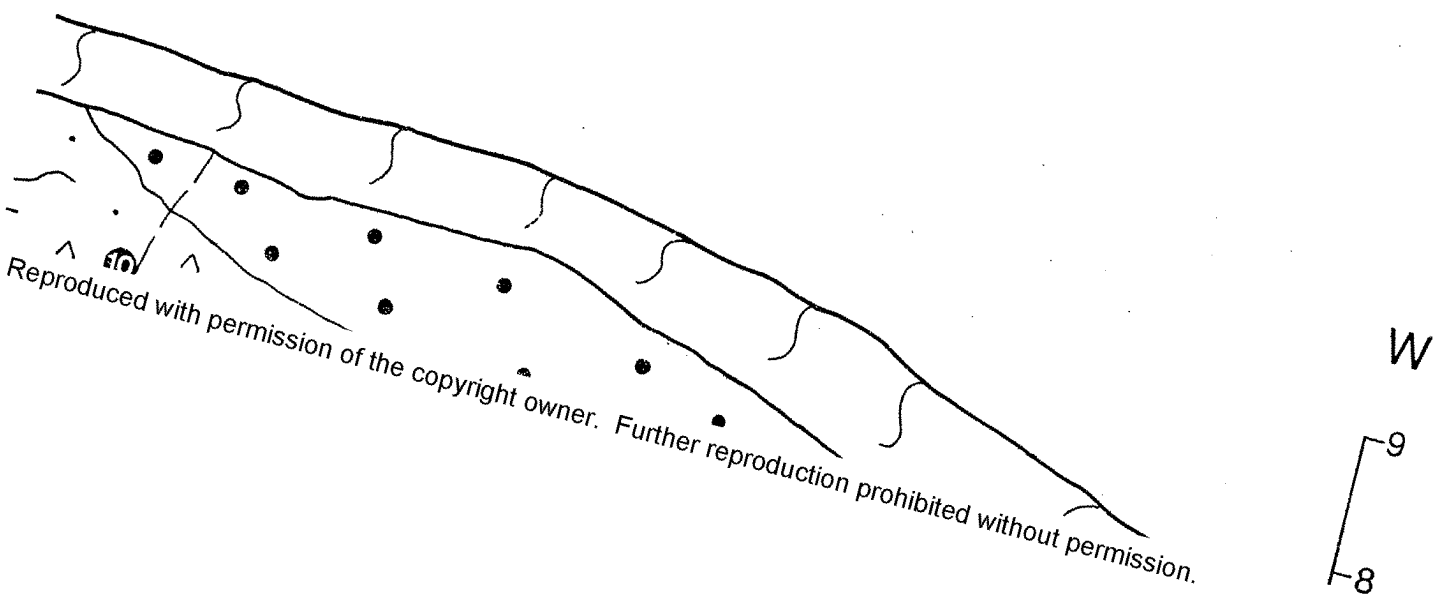

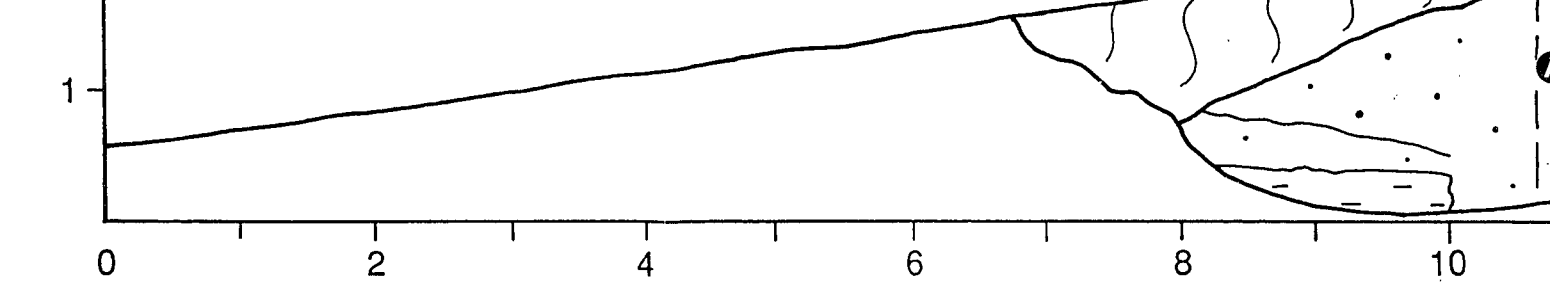

(B)

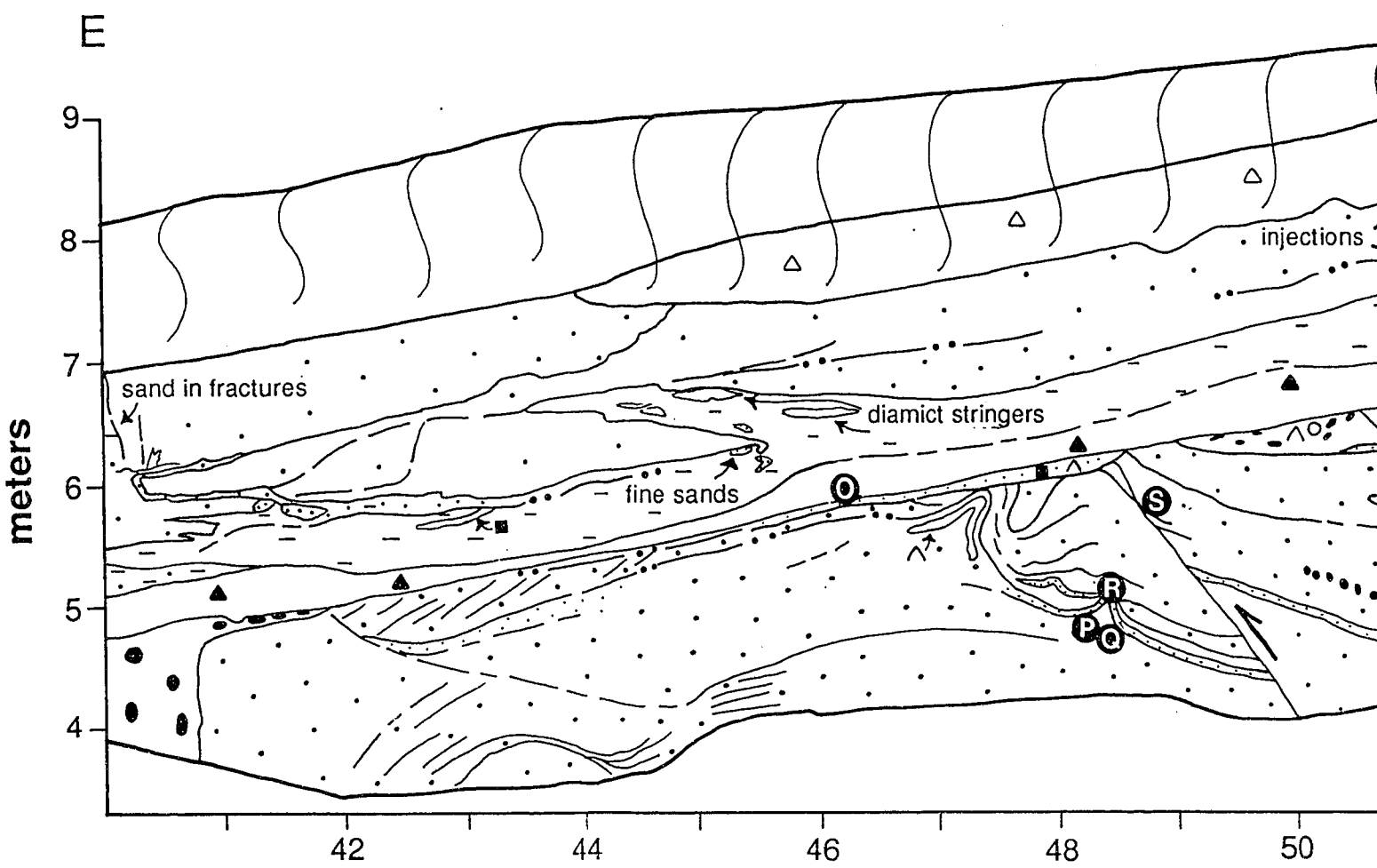

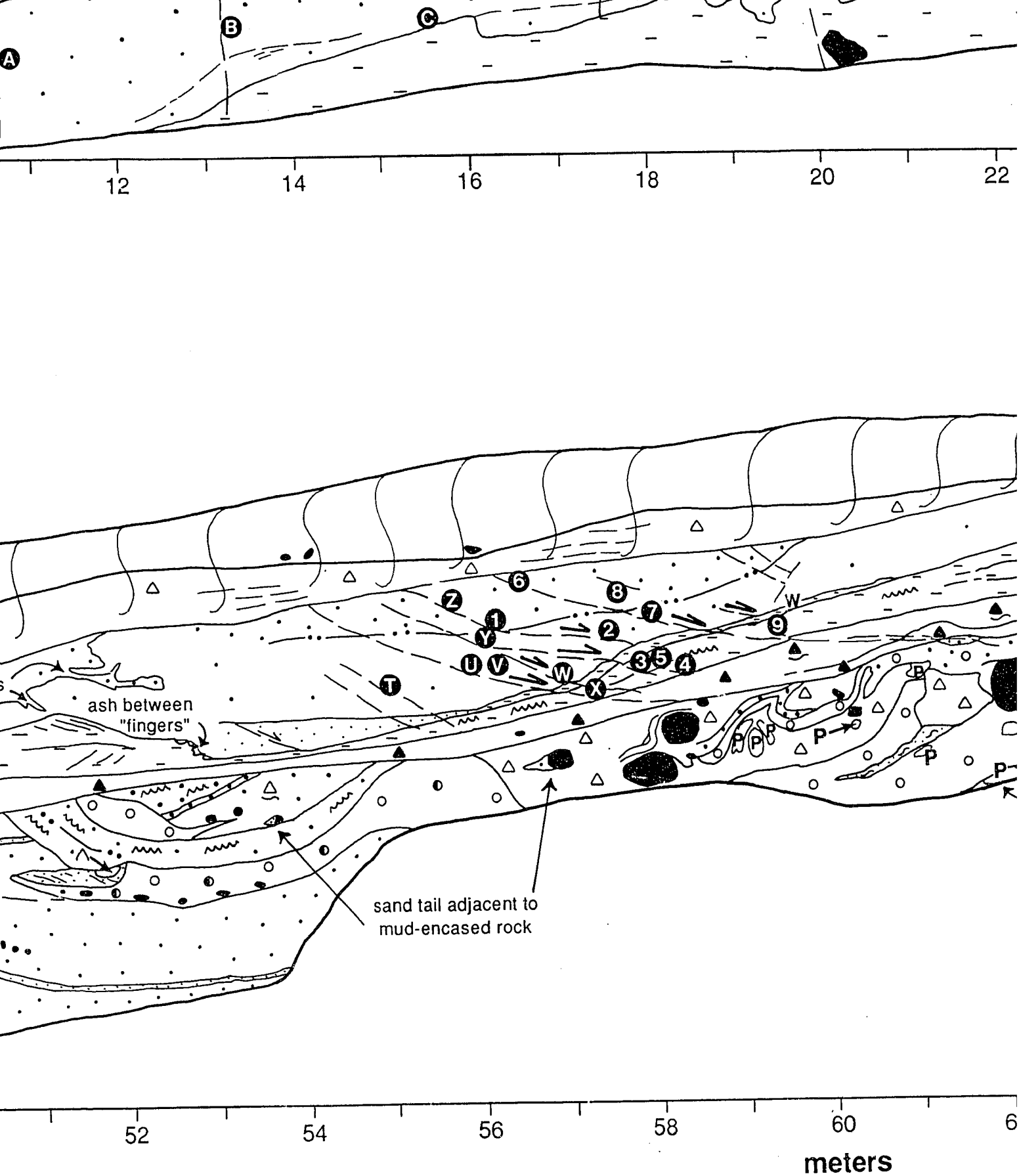

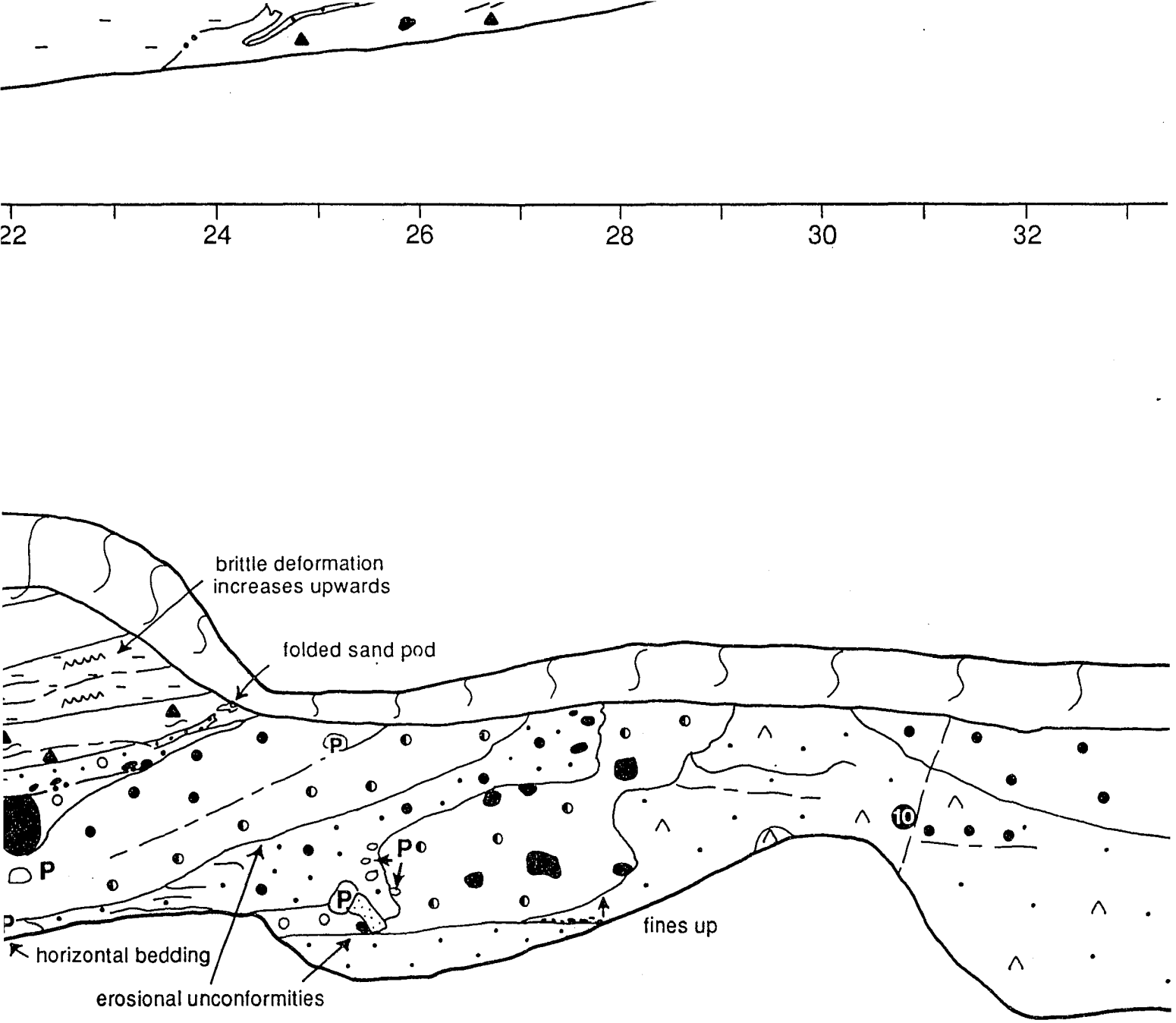

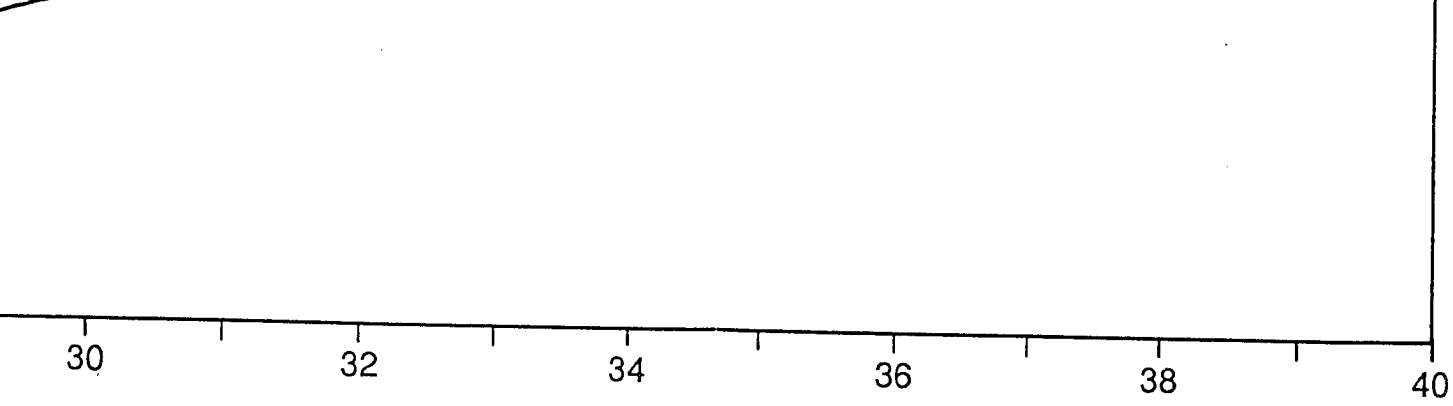

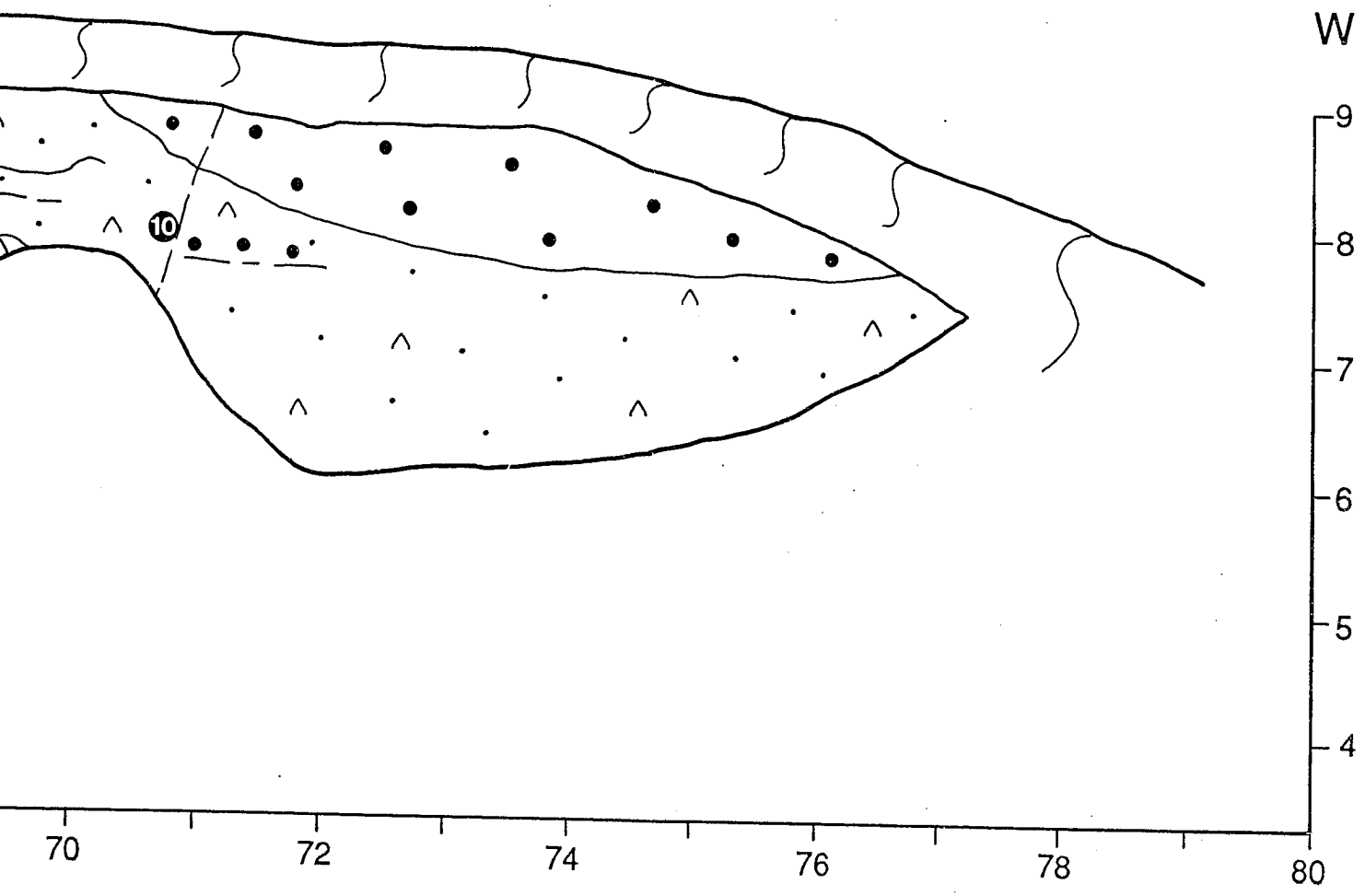

PLATE II
The Frutillar Alto Section